**UNIVERSITÉ DE STRASBOURG**

*ÉCOLE DOCTORALE DES SCIENCES DE LA VIE ET DE LA SANTÉ*
**IGBMC - CNRS UMR 7104 - Inserm U 1258**

# THÈSE présentée par :

## Kateřina JEŘÁBKOVÁ

soutenue le : **09 Octobre 2019**

pour obtenir le grade de : **Docteur de l'université de Strasbourg**

Discipline/ Spécialité : Aspects moléculaires et cellulaires de la biologie

---

# Les rôles de Trim15 et UCHL3 dans la régulation, médiée par l'ubiquitine, du cycle cellulaire.

The roles of Trim15 and UCHL3 in the ubiquitin-mediated cell cycle regulation.

---

**THÈSE dirigée par :**
  **Mme SUMARA Izabela**                              PhD, Université de Strasbourg
  **Mme CHAWENGSAKSOPHAK Kallayanee**   PhD, Charles University

**RAPPORTEURS :**
  **Mr LEON Sébastien**                                PhD, Institut Jacques Monod
  **Mr THORPE Peter**                                  PhD, Queen Mary University of London

**AUTRES MEMBRES DU JURY :**
  **Mr MENDOZA Manuel**                               PhD, Université de Strasbourg
  **Mr ŠOLC Petr**                                      PhD, Charles University
  **Mr SEDLÁČEK Radislav**                            PhD, Charles University

# CO-TUTELLE PhD THESIS

**between**

**Charles University (Czech Republic)**

Faculty of Science - Developmental and Cell Biology

**and**

**University of Strasbourg (France)**

École doctorale des sciences de la vie et de la santé - ED 414

## The roles of Trim15 and UCHL3 in the ubiquitin-mediated cell cycle regulation.

Author:

**Kateřina Jeřábková**

Co-supervised by:

Izabela Sumara, PhD
Kallayanee Chawengsaksophak, PhD
Assoc. Prof. Radislav Sedláček, PhD

Committee members:
Assoc. Prof. Petr Šolc, PhD
Peter Thorpe, PhD
Manuel Mendoza, PhD
Sebastien Leon, PhD

Strasbourg 2019

# DECLARATION

I declare that I wrote the thesis myself and that I cited all the information sources and literature. This work or a substantial part of it was not presented to obtain another academic degree or equivalent.

Prague ..........................

..........................................
Kateřina Jeřábková

# FINANCIAL SUPPORT

# Acknowledgements

# Contents

# ABSTRACT (ENGLISH)

Ubiquitin signaling is a key regulatory mechanism for many important cellular processes such as transcription, differentiation and cell division. Cell division requires duplication of all genetic material during S-phase followed by its precise partitioning between two daughter cells during mitosis. Misregulation of the complex mitotic machinery may lead to aneuploidy and genomic instability, known drivers of tumorigenesis. Indeed, systematic genetic analysis of many cancer tissues over the last decades, indicates the presence of severe chromosome abnormalities in thousands of cancer tissue samples. In this work, I investigated the function of two components of ubiquitin signaling, the deubiquitinating enzyme UCHL3 and the E3 ubiquitin ligase TRIM15. The hypothesized role of E3 ligase TRIM15 in the cell cycle regulation could not be confirmed by our experiments, but I observed an effect on cell adhesion and motility instead. UCHL3 was identified using high-content visual siRNA screen, as a critical factor controlling genome segregation and integrity. Interestingly, it has been previously reported that UCHL3 levels are altered in various cancer types, especially colon cancer. My data demonstrate that UCHL3 drives proper alignment of chromosomes at the metaphase plate by facilitating congression of polar chromosomes and by regulating recruitment of key kinetochore components necessary for formation of stable microtubule attachments. Depletion of UCHL3 leads to chromosome misalignment as well as defective kinetochore-microtubule attachments often leading to severe segregation errors such as lagging chromosomes. Using an unbiased proteomic approach, we identified a potential interactor and mediator of these phenotypes, the Aurora B kinase. I confirmed that UCHL3 interacts with Aurora B and I show that UCHL3 removes the non-proteolytic ubiquitin modifications of Aurora B. Since aneuploidy and the resulting genomic instability are hallmarks of many cancers, and cell adhesion plays an important role in tumor invasion and metastasis, our results suggest that both proteins could play a role in carcinogenesis.

# ABSTRAKT (CZECH)

Ubikvitinace patří k důležitým regulačním mechanismům buňky, které kontrolují různé biologické procesy mezi které patří diferenciace, transkripce a buněčné dělení. Buněčné dělení vyžaduje duplikaci celého genomu v průběhu S- fáze buněčného cyklu, která je následována rovnoměrným rozdělením genetické informace mezi dvě dceřiné buňky v průběhu mitózy. Nesprávná regulace buněčného dělení může vést k aneuploidii, tedy k abnormálnímu počtu chromozomů v buňce. Aneuploidie jsou známou příčinnou vzniku rakoviny. Systematická analýza genomu tisíců vzorků z rakovinných buněk ukázala, že většina nádorů má abnormální počet chromozomů. V mé dizertační práci jsem se zabývala studiem dvou proteinů, které jsou součástí ubikvitin- proteazomového systému, konkrétně deubikvitináza UCHL3 a ubikvitin ligáza Trim15. UCHL3 jsme identifikovali pomocí „high- throughput" testování, které bylo cíleno na rozpoznání dosud neznámých faktorů regulujících buněčné dělení. Předchozí studie ukazují, že zvýšenou expresi UCHL3 můžeme najít v buňkách některých nádorů a to především ve vzorcích rakoviny tlustého střeva. Můj výzkum ukázal, že UCHL3 reguluje správné seskupení chromozomů v metafázi a jejich následné rozdělení do dvou dceřiných buněk. Ztráta (delece) UCHL3 vede k nesprávnému uchycení chromozomů k dělícímu vřeténku a k následnému chybnému rozdělení chromozomů jehož častým důsledkem je aneuploidie. S využitím proteomiky se nám podařilo určit potenciální substrát UCHL3, kterým je kináza Aurora B jež je pro správný průběh mitózy nezbytná. Výsledky proteomické studie se mi podařilo ověřit a ukázat tak, že UCHL3 se váže na Auroru B a že ji deubikvitinuje v počáteční fázi mitózy. V rámci své doktorské práce jsem se zabývala také studiem ubikvitin ligázy Trim15 a jejím vlivem na regulaci buněčného cyklu, adhezi a motilitu buněk. Aneuploidie a genetická nestabilita jsou průvodními jevy většiny druhů rakovin a adhezivita buněk hraje důležitou roli v invazivitě nádorového onemocnění a jeho schopnosti metastazovat. Výsledky mé práce poukazují na to, že oba studované proteiny mohou mít významnou úlohu v karcinogenezi.

# SUMMARY (FRENCH)

J'ai effectué mon doctorat dans le cadre d'un programme de doctorat en co-tutelle entre l'Université de Strasbourg (France) et l'Université Charles de Prague (République tchèque). J'ai passé une partie de ma thèse à l'Institut de Génétique Moléculaire, AS CR (IMG) à Prague, sous la supervision de Kallayanee Chawengsaksophak, PhD et du Professeur associé Radislav Sedlacek, PhD. Le reste du temps, j'ai travaillé à l'Institut de Génétique et de Biologie Moléculaire et Cellulaire (IGBMC) à Strasbourg sous la supervision d'Izabela Sumara, PhD. Au cours de ma thèse, je me suis intéressée à comprendre le rôle de la signalisation de l'ubiquitine dans la régulation du cycle cellulaire tout en étudiant le rôle d'une ligase E3-ubiquitine, Trim15 et le rôle d'une enzyme de dé-ubiquitination (DUB), UCHL3.

## Introduction

La signalisation par l'ubiquitine (Ub) est un mécanisme de régulation clé impliqué dans divers processus biologiques. L'ubiquitination est une fixation covalente d'un fragment d'ubiquitine de 8 kDa à son substrat. Les modifications uniques par Ub ont généralement un rôle de signalisation, les substrats polyubiquinés sont souvent ciblés pour la dégradation des protéines. On sait également qu'il existe des chaînes Ub ramifiées et des chaînes mixtes avec d'autres molécules de type ubiquitine[1]. L'ubiquitination peut être inversée par les enzymes dé-ubiquitinantes (DUB) qui peuvent couper les chaînes d'ubiquitine des substrats et les transformer en monomères.

Les protéines à motif tripartite (TRIM) représentent une grande sous-famille des ligases d'ubiquitine RING-E3 comprenant plus de 70 de gènes chez l'homme[2]. Leurs rôles dans la catalyse de l'ubiquitination et l'assurance de la spécificité du transfert de l'ubiquitine à partir d'enzymes de conjugaison E2 sur diverses cibles impliquent les protéines TRIM dans la régulation de nombreuses activités cellulaires. Les protéines TRIM jouent également un rôle important dans d'autres fonctions cellulaires, telles que la prolifération cellulaire[3,4], la réparation de l'ADN[5], la pluripotence[6] et l'apoptose[7]. Cette large implication dans divers processus cellulaire est soulignée par l'association de nombreux gènes TRIM dans de nombreuses pathologies, comme les infections virales[8,9], les maladies cardiovasculaires[10], les troubles neuropsychiatriques[11], les maladies génétiques[12] et le cancer, soit comme oncogènes[13], soit comme suppresseurs de tumeurs[14]. Parmi de nombreux processus biologiques, qui sont régulés par la signalisation de l'ubiquitine, je me suis concentrée sur l'étude du rôle de

l'ubiquitination dans la division cellulaire, essentielle au maintien de l'intégrité du génome. La division cellulaire nécessite la duplication de tout le matériel génétique au cours de la phase S, suivie de sa répartition précise entre les deux cellules filles au cours de la mitose. Au cours de la prophase des cellules eucaryotes, l'enveloppe nucléaire est désassemblée et les chromosomes se condensent, permettant ainsi l'accès aux microtubules constituant le fuseau mitotique. Les centrosomes dupliqués continuent à se séparer pour former un fuseau mitotique symétrique, ce qui permet sa fixation aux kinétochores (attachement kinétochore-microtubule (KT-MT)) sur tous les chromosomes durant la prométaphase. Ce n'est que lorsque tous les kinétochores sont correctement fixés aux microtubules et que tous les chromosomes sont alignés au niveau de la plaque métaphasique que les cellules peuvent séparer leurs chromosomes. Après la ségrégation des chromosomes au cours de l'anaphase, l'anneau d'actinomyosine est formé et se contracte pour permettre la formation du sillon de division et l'abscission pendant la cytokinèse lorsque deux cellules filles sont prêtes. L'action coordonnée des protéines kinases et des phosphatases conduit à une correcte progression mitotique dans l'espace et dans le temps[15].

## PROJET 1 : IMPLICATION TRIM15 DANS LA PROGRESSION DU CYCLE CELLULAIRE ET LA MIGRATION

Dans ce projet, j'ai étudié le rôle de l'E3-ubiquitine ligase, Trim15 qui n'était pas bien compris à l'époque. Je me suis concentrée sur la détermination des profils d'expression de Trim15 chez la souris adulte ainsi que sur l'étude de lignées cellulaires knock-out dans le but de caractériser son importance dans la régulation du cycle cellulaire. En travaillant sur ce projet, plusieurs publications sur Trim15 ont paru, couvrant partiellement le travail que j'ai effectué, ce qui m'a amené à changer de projet. Dans ma thèse, j'ai résumé tous les résultats obtenus sur Trim15 dans le contexte des publications actuelles.

## PROJET 2 : UCHL3 CONTRÔLE LA SÉGRÉGATION DES CHROMOSES PENDANT LE MITOSE

Mon projet principal de thèse était d'étudier le rôle de l'UCHL3 dans la mitose. Par conséquent, je vais me concentrer sur sa description. Dans ce projet, je me suis particulièrement intéressée à l'étude de la régulation de la protéine motrice moléculaire CENP-E et de la kinase Aurora B. Parmi de nombreux rôles mitotiques, Aurora B assure la correction des attachements aberrants des kinétochores aux microtubules (KT-MT) et son activité est également indispensable pour l'activité motrice de CENP-E. Lorsqu'elle est active, la protéine CENP-E transporte les chromosomes polaires de la périphérie de la cellule vers la plaque métaphasique, facilitant ainsi

l'alignement des chromosomes. Une mauvaise régulation de la complexe machinerie mitotique conduit souvent à une aneuploïdie et à une instabilité génomique, caractéristiques de la tumorigenèse.

## PRINCIPALES QUESTIONS:

### 1.    Pouvons-nous identifier des acteurs mitotiques inconnus auparavant ?

Nous avons effectué un criblage de siRNA et régulait négativement toutes les protéines de liaison à l'ubiquitine et les enzymes de dé-ubiquitination (~ 500 gènes) connues et présumées. L'enzyme de dé-ubiquitination, UCHL3 est sortie en haut de la liste.

### 2.    Comment UCHL3 régule-t-il la progression de la mitose ?

Dans mon projet de thèse, je me suis concentrée sur la détermination du rôle de UCHL3 dans la progression du cycle cellulaire. D'après le criblage de siRNA, nous savons que l'inactivation de UCHL3 entraîne une division cellulaire aberrante conduisant à un phénotype de noyaux cellulaires polylobés. Le but de ma thèse était de comprendre le mécanisme sous-jacent à ce processus.

QU'EST-CE QUE UCHL3 ?

UCHL3 est une DUB de la famille de protéines hydrolase C-terminale. Sa structure est hautement conservée parmi les espèces et il existe une forte homologie avec d'autres protéines de la même famille, UCHL1 et UCHL5. UCHL3 contient trois sites catalytiques (Cys 95 étant le principal) et plusieurs domaines de liaison à l'ubiquitine (Ub)[16]. Récemment, il a été rapporté que UCHL3 régule la réparation des dommages de l'ADN par recombinaison homologue[17] et est également impliqué dans la réparation des ruptures chromosomiques induites par la topoisomérase[18]. Fait intéressant, les résultats à partir d'échantillons de patients atteints de tumeur indiquent que les taux d'expression de UCHL3 sont modifiés dans divers types de cancer, et en particulier dans le cancer du côlon. La participation de UCHL3 au cours de la mitose n'a pas été rapportée à ce jour.

Au cours de mon doctorat, je me suis concentrée sur la caractérisation détaillée du mécanisme par lequel UCHL3 contrôle la ségrégation des chromosomes, y compris l'identification du substrat de UCHL3. Mes données démontrent que UCHL3 détermine le bon alignement des chromosomes au niveau de la plaque métaphasique et la ségrégation des chromosomes lors de la mitose dans les cellules cancéreuses humaines ainsi que dans les cellules primaires.

## PRINCIPALES CONCLUSIONS

En confirmant les résultats du criblage siRNA, j'ai pu démontrer que la régulation négative de UCHL3 conduit à de graves défauts de la mitose.

Tout d'abord, j'ai utilisé un ensemble d'outils différents (inhibiteur de UCHL3, siRNA) pour démontrer que la régulation négative ou l'inhibition de UCHL3 entraine une augmentation du nombre de cellules avec des noyaux irréguliers. Les images ont été quantifiées avec Cell Profiler, en utilisant le facteur de forme comme critère de régularité du noyau. Les noyaux irréguliers résultent souvent de problèmes de ségrégation au cours de la mitose. Pour répondre à cette question, j'ai synchronisé les cellules en métaphase et observé l'alignement des chromosomes. L'appauvrissement en UCHL3 a entrainé de graves problèmes d'alignement. La surexpression de la protéine sauvage UCHL3 a rétabli le phénotype. Au contraire la surexpression du mutant avec les domaines catalytiques inactivés de UCHL3 (c / s) n'était pas suffisante pour rétablir ce phénotype. J'ai observé le même phénotype en utilisant l'inhibiteur de UCHL3 dans deux types de cellules différents : les cellules cancéreuses, HeLa et les fibroblastes primaires humains, IMR90. Il est important de noter que 90 minutes de traitement avec l'inhibiteur de UCHL3 suffisent pour promouvoir un nombre accru de chromosomes mal alignés, ce qui confirme le rôle de UCHL3 en particulier pendant la transition prométaphase-métaphase. Des expériences de vidéo en direct par microscopie ont montré un nombre accru de chromosomes à la traine au cours de l'anaphase, ce qui a confirmé l'hypothèse selon laquelle UCHL3 est indispensable a une progression mitotique appropriée. Les résultats pris tous ensemble démontrent que UCHL3 contrôle l'alignement des chromosomes pendant la métaphase et leur séparation dans les deux cellules filles et tout ceci dépend de son activité catalytique.

L'immunoprécipitation (IP) suivie par de la spectrométrie de masse a identifié Aurora B comme substrat potentiel de UCHL3. Jj'ai confirmé que UCHL3 interagissait avec Aurora B et était responsable de sa dé-ubiquitination. En utilisant la microscopie à super résolution, j'ai observé que UCHL3 contrôlait la localisation de CENP-E au cours de la métaphase, ce qui avait déjà été observé pour assurer un bon alignement des chromosomes[19],[20]. En l'absence de UCHL3, j'ai observé une diminution des niveaux de CENP-E au niveau des kinétochores, ce qui entraîne des problèmes de ségrégation. Comme l'aneuploïdie et l'instabilité génomique qui en résulte sont caractéristiques de nombreux cancers, nos résultats suggèrent un rôle important de UCHL3 dans la carcinogenèse.

## CONCLUSIONS ET PERSPECTIVES FUTURES

Dans mon projet de thèse, j'ai décrit un nouveau rôle pour l'enzyme de dé-ubiquitination, UCHL3 au cours de la mitose. En combinant les approches biochimiques, et la microscopie (vidéo en direct et super résolution), j'ai réussi à démontrer que UCHL3 contrôle spécifiquement l'alignement des chromosomes lors de la transition prométaphase-métaphase et que son absence entraine de graves problèmes de ségrégation, notamment des chromosomes à la traine ayant pour conséquence la formation de noyaux irréguliers. Je suppose qu'UCHL3 contrôle l'alignement des chromosomes en régulant l'activité d'Aurora B et le mouvement ultérieure des chromosomes à l'aide de CENP-E. Une régulation adéquate de la mitose est essentielle à la survie des cellules et une mitose aberrante conduit souvent à une aneuploïdie. Une compréhension approfondie des mécanismes contrôlant la correcte ségrégation des chromosomes est une clé pour le développement de traitements anticancéreux plus spécifiques.

# PROJECTS OUTLOOK

I have done my PhD in a study program 'doctorat en co-tutelle' between the University of Strasbourg, France and the Charles University in Prague, Czech Republic. I've spent part of my PhD study working at the Institute of Molecular Genetics, AS CR (IMG) in Prague under the supervision of Kallayanee Chawengsaksophak, PhD and Assoc. Prof. Radislav Sedláček, PhD and at the remaining time I was working at the Institute of Genetics and Molecular and Cellular Biology (IGBMC) in Strasbourg under the supervision of Izabela Sumara, PhD. During my PhD, I was interested in understanding the role of ubiquitin signaling in the regulation of cell cycle, in particular the specific functions of an E3-ubiquitin ligase Trim15 and a deubiquitinating enzyme (DUB) UCHL3. During my PhD I was mainly using human cultured cells as a model, therefore many mechanisms explained in my thesis are taken from perspective of human cells.

## TRIM15 IMPLICATION IN THE CELL CYCLE PROGRESSION AND MIGRATION

In this project I was studying the role of the E3-ubiquitin ligase Trim15, which at the time was not well understood. I focused on determining the expression profiles of Trim15 in adult mice as well as on studying knockout cell lines with the aim to characterize its importance for cell cycle regulation. I used mice as a model organism in combination with cultured human and mouse cells. While working on this project several publications about Trim15 appeared, which were partially covering the work I have done and it finally led me to change the project. In my thesis, I summarized the results that I obtained about Trim15 function and I discussed them in context of the recent publications.

## UCHL3 CONTROLS CHROMOSOME SEGREGATION DURING MITOSIS

Studying the role of UCHL3 in mitosis was the main project during my PhD and therefore in my thesis I dedicated more space to its description. In this project I have been particularly interested in studying the regulation of Aurora B kinase and CENP-E molecular motor protein during mitosis. Among many mitotic roles, Aurora B is ensuring correction of aberrant kinetochore- microtubule (KT-MT) attachments and its activity is also indispensable for CENP-E motor activity. When active, CENP-E is transporting polar chromosomes from the periphery of the cell to the metaphase plate, thus helping the correct chromosome alignment. Misregulation of the mitotic machinery often leads to aneuploidy and genomic instability, hallmarks of tumorigenesis.

# LIST OF ABBREVIATIONS

| | |
|---|---|
| AA | Amino acid |
| ADP | Adenosine 5′-diphosphate |
| APC/C | Anaphase- promoting complex/ cyclosome |
| APS | Ammonium persulfate |
| ATM | Ataxia telangiectasia mutated |
| ATP | Adenosine-5'-triphosphate |
| ATR | Ataxia telangiectasia mutated and rad3-related |
| Bp | Base pair |
| BSA | Bovine serum albumin |
| Bub1/3 | Budding uninhibited by benzimidazoles- 1 |
| BubR1 | Bub1- related protein-1 |
| CC | Coiled-coil domain |
| CCAN | Constitutive centromere- associated network |
| CDK | Cyclin- dependent kinase |
| CENP- | Centromere protein- |
| CEP55 | Centrosome protein of 55 kDa |
| CIN | Chromosomal instability |
| CKI | CDK inhibitor |
| CPC | Chromosome passenger complex |
| CRLs | Cullin-RING ligases |
| cDNA | Complementary DNA |
| CREST | Calcinosis, Raynaud's phenomenon, esophageal dysmotility, sclerodactyly, and telangiectasia (CREST syndrome autoimmune antibody) |
| DAPI | 4′,6-Diamidino-2-phenylindole dihydrochloride |
| DDR | DNA damage response |
| DNA | Deoxyribonucleic acid |
| DUB | Deubiquitinating enzyme |
| ECM | Extracellular matrix |
| EDTA | Ethylenediaminetetraacetic acid |
| FACS | Fluorescence-activated cell sorting |
| GFP | Green fluorescent protein |
| GPI | Glucose-6-phosphate isomerase |
| GTP | Guanosine-5'-triphosphate |

| | |
|---|---|
| H2A/ B | Histone 2A/ B |
| HASPIN | Histone H3 associated protein kinase |
| HECT | Homology to E6AP C terminus |
| HeLa K | Human cervix carcinoma cells, K stands for Kyoto |
| HIV-1 | Human immunodeficiency virus 1 |
| IF | Immunofluorescence |
| INCENP | Inner centromere protein |
| IP | Immunoprecipitation |
| JAMM | JAB1/ MPN/ MOV34 |
| K | Lysine |
| K-fiber | Kinetochore fiber |
| KD | Knockdown |
| KIF | Kinesin family |
| KMN | Kinetochore protein network |
| KO | Knockout |
| KT | Kinetochore |
| KT- MT | Kinetochore- microtubule |
| Live SR | Super resolution module |
| LUBAC | Linear ubiquitin chain assembly complex |
| M1 | Methionine |
| MAD2 | Mitotic arrest deficient-2 |
| MCAK | Mitotic centromere-associated kinesin |
| MDM2 | Mouse double minute 2 homolog |
| MEF | Mouse embryonic fibroblasts |
| MG132 | Proteasome inhibitor |
| MI | Mitotic index |
| MINDY | Motif interacting with ubiquitin (MIU)- containing novel DUB |
| mRNA | Messenger ribonucleic acid |
| MT | Microtubule |
| MTOC | Microtubule organizing center |
| Nedd8 | Neural precursor cell expressed developmentally down-regulated 8 |
| NHEJ | Non-homologous end joining |
| OTU | Ovarian tumor proteases |
| PBS | Phosphate buffered saline |
| PCM | Pericentriolar material |
| PFA | Paraformaldehyde |

| | |
|---|---|
| Plk1 | Polo- like kinase-1 |
| PP1/ 2A | Protein phosphatase-1/ 2A |
| PRC1 | Protein regulator of cytokinesis-1 |
| pH3T3 | Phospho histone 3 threonine 3 |
| qPCR | Quantitative real-time polymerase chain reaction |
| RBR | Ring between Ring |
| RING | Really Interesting New Gene |
| RNA | Ribonucleic acid |
| RT | Room temperature |
| RVD | Repeat variable domain |
| RZZ | Rod-Zwilch-ZW10 |
| SAC | Spindle assembly checkpoint |
| SAGA | Spt-Ada-Gcn5 acetyltransferase |
| SCF | Skip- Cullin- F-box |
| siRNA | Small interfering RNA |
| shRNA | Short hairpin RNA |
| SKAP | Small kinetochore-associated protein |
| STLC | S-trityl-L-cysteine (Eg5 kinesin inhibitor) |
| SUMO | Small ubiquitin modifier |
| TALEN | Transcription activator-like effector nuclease |
| TBE | Tris/ Borate/ EDTA |
| TBS | Tris-buffered saline |
| TCID | 4,5,6,7-tetrachlorodindan-1,3-dione (UCHL3 inhibitor) |
| TEMED | Tetramethylethylenediamine |
| TRIM | Tripartite motif |
| UBASH3B | Ubiquitin associated and SH3 domain containing B |
| UCH | ubiquitin C-terminal hydrolases |
| UCHL3 | Ubiquitin carboxyl-terminal esterase L3 (Ubiquitin Thiolesterase) |
| USP | Ubiquitin-specific proteases |
| WB | Western blotting |

# 1 INTRODUCTION

## 1.1 UBIQUITINATION

### 1.1.1 Mechanism of ubiquitination

Ubiquitin was first discovered by Gideon Goldstein in 1975 who described it as an ubiquitous small molecule that is highly conserved among different species, from yeast and plants to humans[21]. Since then, ubiquitin has been extensively studied and up to now, there are more than 60 000 publications about ubiquitin and recent study shows that 1.3 % of total cell proteome is modified by ubiquitin[22], emphasizing its relevance for most of the biological processes. Ubiquitin is synthesized *de novo* from four different genes (UBB, UBC, UBA52 and RPS27A), which are not functionally redundant as knocking out one of them results in severe phenotypes in mice[23]. Newly synthesized ubiquitin (ubiquitin precursor protein) is processed to monomers by deubiquitinating enzymes (DUBs)[24]. Free ubiquitin is covalently attached to different proteins by a complex cascade of reactions called ubiquitination.

Ubiquitination is a reversible posttranslational modification mediated by three different enzymes: the E1 activating enzyme, which activates the ubiquitin by ATP-dependent adenylation and transfers the ubiquitin to the active site of the next complex, the E2 conjugating enzyme which assists the E3 ubiquitin ligase to transfer the ubiquitin to the substrate, most commonly onto a lysine amino-group in the target protein. Ubiquitination can be repeated to attach more than one ubiquitin to the same substrate or to already attached ubiquitin molecule and at the same time ubiquitin or ubiquitin chains can be cleaved off at any point by different DUBs (Figure 1).

In humans, only two E1 enzymes have been described, UBE1[25] and UBA6[26,27] and around 40 E2 enzymes[28], which all bind E1 enzyme in addition to one or multiple of ~600 known E3 ligases[29]. Based on their structural properties, E3 ubiquitin ligases are divided into three subfamilies: Really Interesting New Gene (RING) which can directly transfer ubiquitin from E2 enzyme to the substrate, Homology to E6AP C terminus (HECT) and Ring between Ring (RBR) which transfer ubiquitin in two steps, first to one of their domains and after to the substrate[30]. This multistep organization of ubiquitin transfer ensures high substrate specificity of the ubiquitination process.
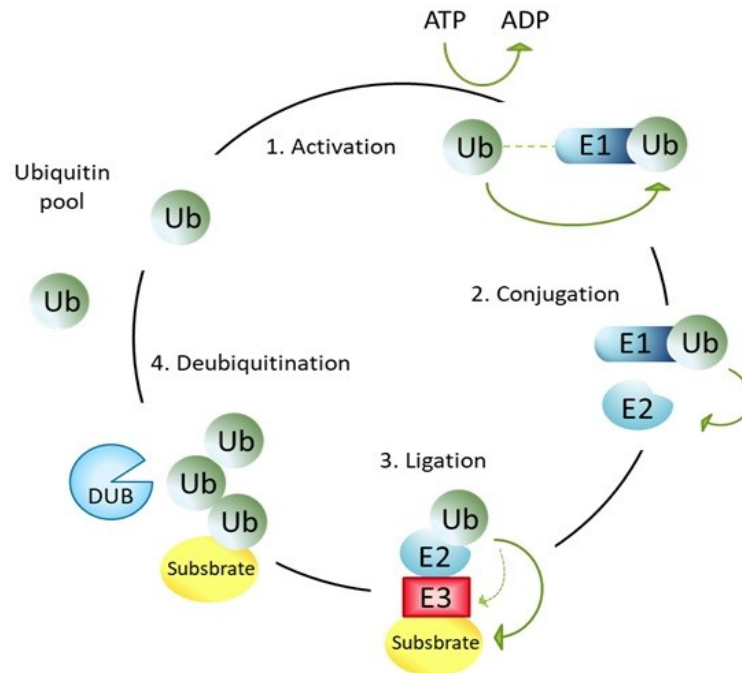
**Figure 1 Mechanism of ubiquitination**

There are three subsequent steps of ubiquitination which can be reverted by DUB mediated deubiquitination.

Green circle – ubiquitin, E1 – activating enzyme, E2 – conjugating enzyme, E3 – ubiquitin ligase, DUB – deubiquitnating enzyme. Arrows indicate ubiquitin movement during each step.

(Adapted from Heaton et al., DOI: 10.1084/jem.20151531)

## 1.1.2     Types of ubiquitin modifications

Ubiquitin is a small 8.6 kDa protein, which is most commonly attached to a protein lysine residue (K), but other sites such as thiol groups of cysteine, hydroxyl group of serine and threonine residues or even the α-amino group of protein N-terminus have been also described[31-34]. The diversity of ubiquitin modifications lies in the different abilities of ubiquitin ligases to conjugate ubiquitin to the substrates which can result in mono-, multi-mono- and polyubiquitination. Mono-ubiquitination is the attachment of a single ubiquitin molecule to the substrate which can be further ubiquitinated to produce polyubiquitin chains. Any of the seven lysine residues (K6, K11, K27, K29, K33, K48, K63) or the N-terminal methionine (M1) of ubiquitin can be used for further ubiquitination forming polyubiquitin chains of different topologies. Typically, homotypic chains linked by one particular lysine residue are formed, heterotypic (mixed) chains linked by a combination of K sites[35] and branched chains[36] have

been also observed. Additional regulation level of the complexity is given by post-translational modifications of ubiquitin itself by phosphorylation[37,38], acetylation[39], ADP-ribosylation[40] or SUMOylation[41]. Mixed chains combined with ubiquitin-like modifiers (SUMO, Nedd8) also exist. This immense variety of ubiquitin modifications is referred to as 'The ubiquitin code' (Figure 2). Different chain topologies are specifically recognized by the effector proteins (ubiquitin receptors or ubiquitin-binding proteins), which can transfer modified substrates to the distinct cellular compartments or to the downstream signaling components, thereby determining substrates' fate[42,43].
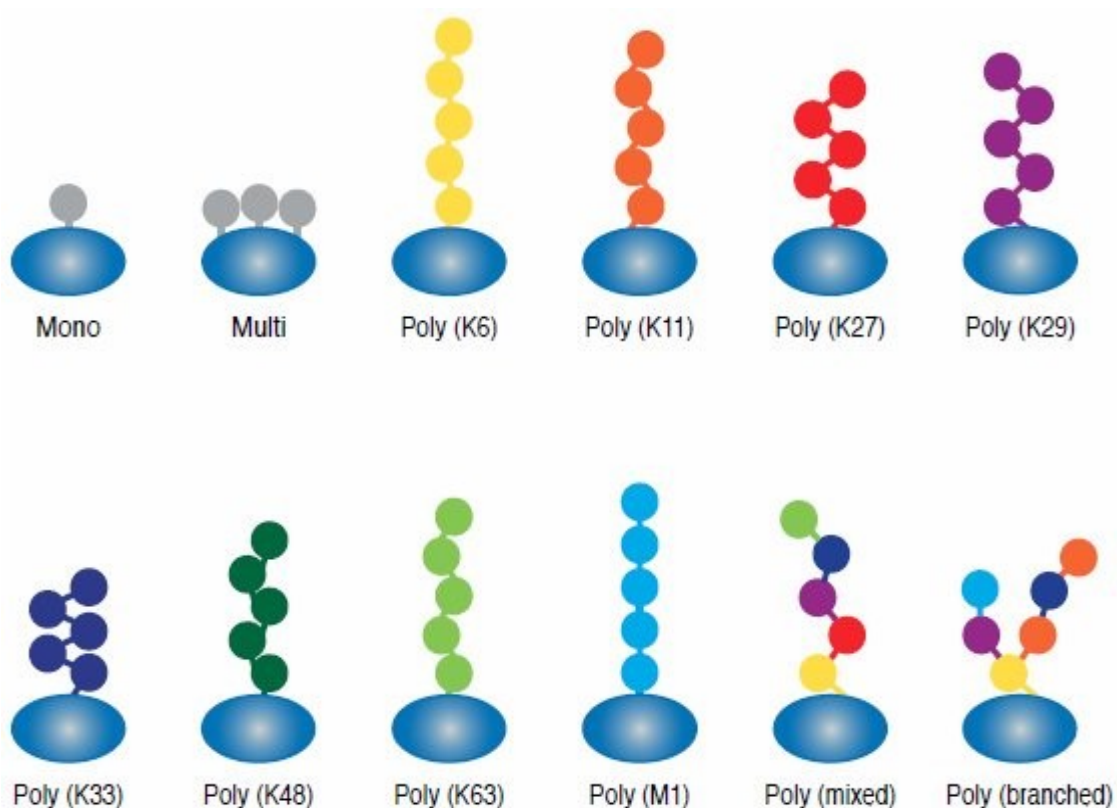


**Figure 2 The ubiquitin code**

A schematic representation of possible ubiquitylation modifications occurring in cells. Each type of ubiquitylation is depicted by a different color: mono- and multi-ubiquitylation, polyubiquitylation linked through any of seven Lysine (K) residues or N-terminal Methionine (M1) as well as mixed and branched polyubiquitylation. Additional level of complexity is provided by posttranslational modifications on ubiquitin molecules (not depicted in the scheme). Based on the steric positioning of the used residues, the polyubiquitin chains may adopt distinct conformations (depicted in a schematic, inaccurate manner) ranging from more compact (K27, 29, 33, 48, branched, mixed) to more linear (K6, K11, K63 and M1) topologies.

Source: Jerabkova, Sumara, DOI: 10.1016/j.semcdb.2018.12.007

# 1.2 BIOLOGICAL ROLES OF DIFFERENT UBIQUITIN MODIFICATIONS

Initially, it was thought that ubiquitination is solely a signal for protein degradation and that protein has to be modified by at least four K48-linked ubiquitin molecules in order to be recognized by the large protease 26S proteasome. The first evidence of the non-proteolytic ubiquitination came in the 90s, when the role of K63 linkage has been connected to the DNA repair process[44]. It is now well accepted that the proteasome-mediated proteolytic degradation is not the only possible outcomes and that ubiquitination can regulate many different molecular events including activation of enzymes, protein-protein interactions or subcellular localization. K48 linkage is the most studied modification mediating degradation of substrates by the 26S proteasome[45] and it is largely involved in cell cycle progression[46–48], development[49], cell differentiation[50] and DNA damage response[51]. K11 linked chains promote proteasomal degradation of Cyclin B which is key for proper mitotic progression[52,53]. Mass Spectrometry studies revealed the also K6, K27 and K29 linked chains can target proteins for degradation[54]. Interestingly, degradation signal is not restricted to polyubiquitin chains, since single ubiquitin is sufficient to degrade proteins involved in muscle differentiation[55], and a multiple mono-ubiquitination is necessary for the proteasomal processing of precursor protein to generate active transcription complex[56] and it can serve as an alternative degradation signal driving mitotic progression[57]. Lysosomal K63 chain-mediated protein degradation has been implicated in the immune response[58] and lipoprotein uptake[59]. K63-linked and phosphorylated K6-linked chains are important for mitochondrial quality control by promoting mitophagy[60].

Next to K48-, the K63-linked chains are the second most abundant polyubiquitin modifications in the cells[54] and, except for few cases, they most commonly have non-degradative signaling roles in protein-protein interactions[61,62], protein sorting and trafficking[63,64], kinase and transcription factors activation[65,66] and during DNA damage response[67,68] often functioning as a scaffold to facilitate recruitment of other proteins [69].

Mono-ubiquitination is a wide spread protein modification, as more than a half of all ubiquitin-modified proteins are mono-ubiquitinated[70]. It is largely involved in protein localization[71,72], protein-protein interaction[73] and complex formation[74], DNA damage response[75] and in epigenetic pathways[76].

So far the only described E3-ligase complex able to synthesize M1-linked linear ubiquitin chains is the linear ubiquitin chain assembly complex (LUBAC)[77] which has been shown to

regulate the immune and inflammatory responses by NFκB activation[78,79] and it is involved in cell death[80,81] and in the regulation of mitotic progression[19].

# 1.3    DEUBIQUITINATING ENZYMES

The complexity of the ubiquitin code demands a highly sophisticated system to counteract it. DUBs are directly opposing the action of E3-ubiquitin ligases by catalyzing a proteolytic reaction that cleaves ubiquitin/s from the substrate proteins creating a counterbalance and a possibility to quickly correct the signal based on the current cellular conditions or environmental inputs.

There are approximately 100 DUBs encoded by the human genome, which belong to two major groups, the thiol proteases with a cysteine residue in their catalytic site and the metalloproteases with coordinated zinc ion ($Zn^{2+}$). The two groups can be further divided into six structurally and evolutionary distinct families[82,83]. There are five cysteine families, the ubiquitin-specific proteases (USP), the ubiquitin C-terminal hydrolases (UCH), the ovarian tumor proteases (OTU), the Josephin family, the newly discovered motif interacting with ubiquitin (MIU)-containing novel DUB (MINDY)[84] family and one metalloprotease family JAB1/ MPN/ MOV34 (JAMM)[83].

DUBs interact with ubiquitin hydrophobic patches which ensures specificity to the ubiquitin over the ubiquitin-like modifications[83], but some UCH, USP and JAMM family members are also able to cleave NEDD8[85–87].

The most abundant cellular DUBs are part of the proteasome system (Rpn11, UCHL5, USP14), the DUBs involved in ubiquitin processing during *de novo* synthesis and during ubiquitin recycling (USP5, Otulin), the DUBs associated with the linear ubiquitin chain assembly complex (LUBAC) and the DUBs regulating the translation initiation machinery associated with the Spt-Ada-Gcn5 acetyltransferase (SAGA) complex[70].

## 1.3.1 The substrate recognition patterns and the catalytic activity

The ability of DUBs to cleave ubiquitin depends on their binding properties. They can bind to the ubiquitinated protein or to the ubiquitin molecule with different levels of specificity. Depending on the DUB activity, single ubiquitin molecule or the whole ubiquitin chain can be cleaved off during one proteolytic reaction. DUBs from the USP family often recognize and bind the target protein[88] and they cleave ubiquitin non-specifically, precisely modulating signaling pathways and cellular processes.

Another abundant group consist of DUBs binding the ubiquitin chains. These DUBs have different levels of specificity. They can bind a single ubiquitin molecule and process the chain non-specifically (exo-cleavage activity) or they can bind two ubiquitin molecules and based on the chain geometry they distinguish among different linkages (endo-cleavage activity). The DUBs from the OTU family show high linkage specificity towards specific homotypic chains[89–91]. Members of the JAMM family are often K63-linkage specific[92,93] and the DUBs from MINDY family are K48-linkage specific[84,94]. In contrast, members of the UCH family bind ubiquitin close to its C-terminal region with only a little contact to the ubiquitin molecule increasing the possibility to cleave different types of chains[17,95].

A single DUB can have different activities, for example USP21 has endo-cleavage activity towards K63-linked chains[96], but due to steric properties it has exo-cleavage activity towards K6-linked chains and can process them only from the distal end[97]. Branched chains or modified ubiquitin can reduce the binding affinity of certain DUBs[98] and their activity is also regulated by a number of posttranslational modifications[83]. Some DUBs work as a part of bigger complexes, as in the 26S proteasome (RPN11, USP14, UCHL5) where substrate recognition is given by other members of the complex[99,100]. The different DUBs' recognition patterns and activities are summarized in Figure 3.

-32-
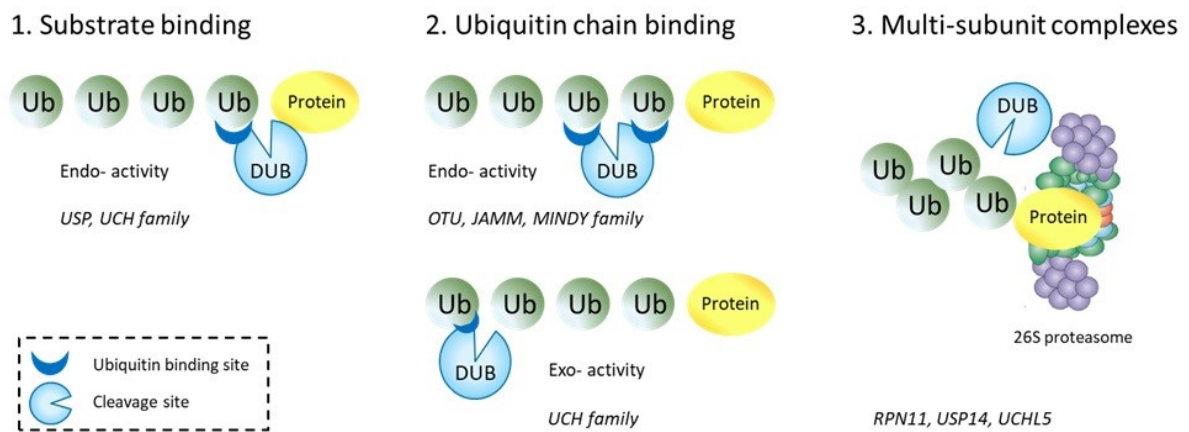


**Figure 3 The DUB activity is based on their recognition pattern.**

Different recognition and binding properties of DUBs and their cleavage activity with examples. A single DUB can have more than one activity depending on the substrate.

Blue crescent – ubiquitin binding site, light blue circle – DUB, notch shows the cleavage site, green circle – ubiquitin, yellow oval – ubiquitinated protein

# 1.4   UBIQUITIN SIGNALING IN CELL CYCLE REGULATION

## 1.4.1   The cell cycle progression and its checkpoints

Cell cycle is a complex set of events that precedes and follows the cell division and it is driven by CDK activity. Proper CDK activation depends on the ubiquitin-mediated oscillation in protein levels of cyclins and kinase inhibitors that dictate the progression through different phases. In the first growth phase (G1) cell increases its mass and synthesizes necessary proteins until it reaches a restriction point (in mammals, START in yeast), where it either commits to the next cell cycle or it stops dividing and enters quiescence (G$_0$). Decision to enter the cell cycle is irreversible, it starts with duplication of the genetic material during DNA synthesis phase (S), followed by a second growth phase (G2) and by equal distribution of the duplicated chromosomes during mitosis (M) which is completed by the cell separation during cytokinesis. Uncontrolled cell division often gives rise to the malignant tumor growth and the cancer progression. In order to prevent malignancies, cell activates checkpoints to delay the cell cycle progression and to gain time for error correction. The G1/S, G2/M and M checkpoints can be recognized which are largely regulated by the balanced activity of ubiquitin ligases and deubiquitinating enzymes.

In addition to the phase transition checkpoints, the DNA damage checkpoint controls the genome integrity and prevents proliferation of cells with damaged DNA by cell cycle arrest. DNA damage happens continuously as a result of environmental stress, therefore the cell needs a robust mechanism of DNA damage detection and DNA repair. In presence of DNA breaks or damage associated with replication, cell initiates a cascade of signaling events, the DNA damage response (DDR) mediated by ATM/ATR kinases, respectively[101,102]. The DDR includes a number of phosphorylation and ubiquitination events which result in reversible cell cycle arrest giving time for DNA repair. When the DNA damage checkpoint is activated it results in ATM dependent recruitment of repair factors, degradation of cyclins and stabilization of the tumor suppressor protein p53, further promoted by several DUBs (USP10[103], USP11[104], OTUD5[105]). The G1 DNA damage checkpoint can not only slow down the cell cycle progression, but it can also irreversibly stop the cell cycle if the DNA damage is not repaired, resulting in apoptosis or in cellular senescence. Components of the DNA damage checkpoint and the DDR pathway are often mutated or deregulated in many cancers.

# 1.5  MITOSIS

Mitosis is the last phase of the cell cycle during which one cell is divided into two. Cell division poses a potential risk for the cell, because the genetic information needs to be divided between the two daughter cells. Errors in this process or damage to the genetic material are deleterious for the cell, resulting often in a cell death. A tight control of mitosis is necessary for the normal cell growth. Mitosis has fascinated scientists since the 19th century and it was named by W. Flemming who derived the name from Greek word for thread (*mitos*) and he was one of the first scientists who published the illustration of human chromosomes as seen during mitosis (Figure 4)[106].
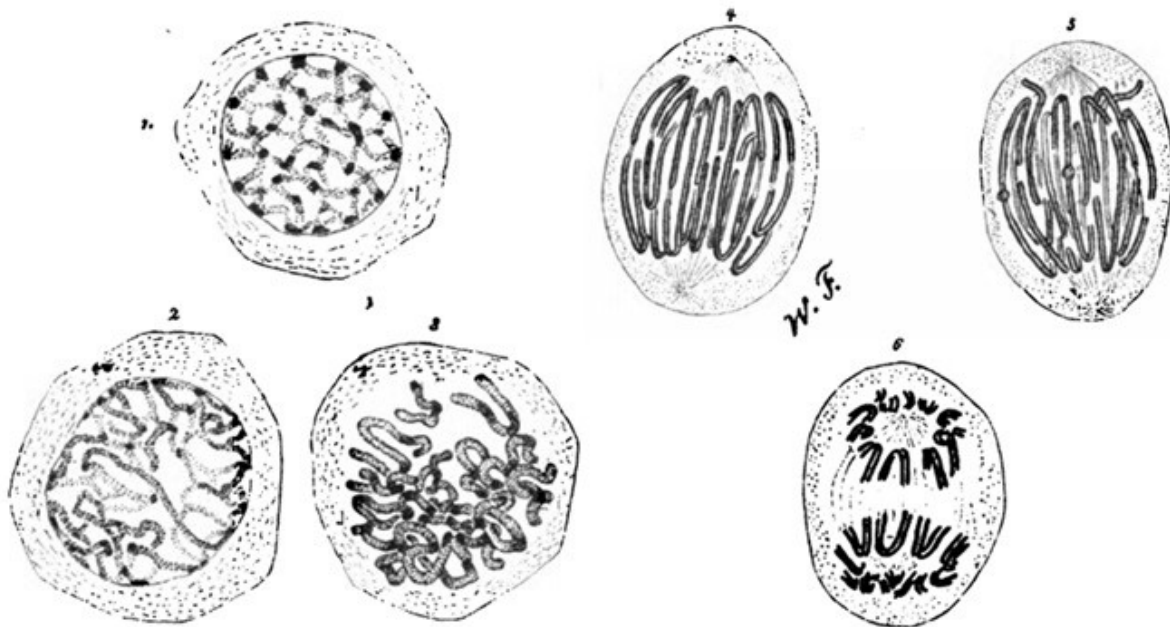


**Figure 4 Different stages of mitosis**

Illustration of different phases of mitosis as seen by Walther Flemming using the newly discovered anilin dyes. Zellsubstanz, Kern und Zelltheilung, published 1882 by F.C.W. Vogel in Leipzig.

The human cells, in contrast to some yeast, undergo an open mitosis, which means that the nuclear envelope is disassembled in the beginning of the process. The nuclear envelope dissolves in prophase when the chromosomes condense and microtubules start to form the mitotic spindle. It is followed by the centrosome separation, the attachment of spindle microtubules to the kinetochores (the protein structures assembled around the centromeric

region of the two sister chromatids) and the formation of bipolar spindle during prometaphase, until all chromosomes are aligned in the equatorial zone of the cell in metaphase. The fidelity of chromosome attachment and alignment is controlled by the Spindle Assembly Checkpoint (SAC) also known as the mitotic checkpoint. Upon alignment of all chromosomes, the anaphase starts and the two sister chromatids of each chromosome are pulled apart and segregated to the opposite spindle poles. In telophase the chromosomes decondense, the nuclear envelope is reassembled and the ingressing cleavage furrow leads to the physical separation of cytoplasm giving rise to the two daughter cells in the last step of cell division called cytokinesis.

## 1.5.1    Mitotic structures

Mitosis is a very dynamic process and a lot of structural rearrangements need to be done. The whole cell changes its appearance for the duration of mitosis. In this following chapter I will describe the main structures typical for mitosis, their assembly, regulation and function.

### Mitotic chromosomes

To ensure proper division of the replicated DNA mass, chromosomes need to change their structural properties from relaxed chromatin to a highly compacted state (condensed chromosomes). Mitotic chromosomes have the typical X shape as visible on the scanning electron microscope image[107] (Figure 5A) and the simplified drawing (Figure 5 B) showing the two sister chromatids of each chromosome connected in their centromeric regions onto which the multi-subunit protein complexes called kinetochores are assembled. The first images of mitotic chromosomes by electron microscope were taken at the end of 70s, but it took 20 years, until discovery of a heteromeric complex Condensin, in *Xenopus laevis* egg extracts[108] which shed a light on how the DNA is compacted. Several models were proposed since then, but the mechanism still remains unclear[109]. The condensation process starts in prophase and is triggered by CDK1 activity[110]. Vertebrates have two condensin complexes, first condensin II interacts with DNA in the nucleus, condensin I binds to DNA after nuclear envelope breakdown and they are distributed along the chromosome arms. Loop exclusion model[111,112], proposes the existence of condensin generated DNA loops (Figure 5D) that are held together in a dynamically moving system resulting in tightly packed mass with very low structural reproducibility, suggesting a rather stochastic mechanism[113]. Condensins are necessary for structural integrity of chromosomes and for successful completion of mitosis[114]. In addition,

Topoisomerase II activity is needed for decatenation of entangled DNA as inhibition of its activity showed increased number of chromosome bridges in anaphase[115].

Cohesin complex is structurally very similar to condensin (Figure 5C), yet it has a distinct role. After DNA replication, cohesin holds two sister chromatids together along the whole chromosome arms. In prophase, Plk1 and Aurora B activity triggers cleavage-independent dissociation of cohesin from chromosome arms resulting[116,117] in resolution of sister chromatids that are still held together by cohesin in the centromeric region. It is the cohesin cleavage by separase that triggers anaphase onset and allows for segregation of the sister chromatids to the two daughter cells. Proper timing of cohesin cleavage is a key for error-free chromosome segregation and is tightly controlled by the mitotic checkpoint[118].
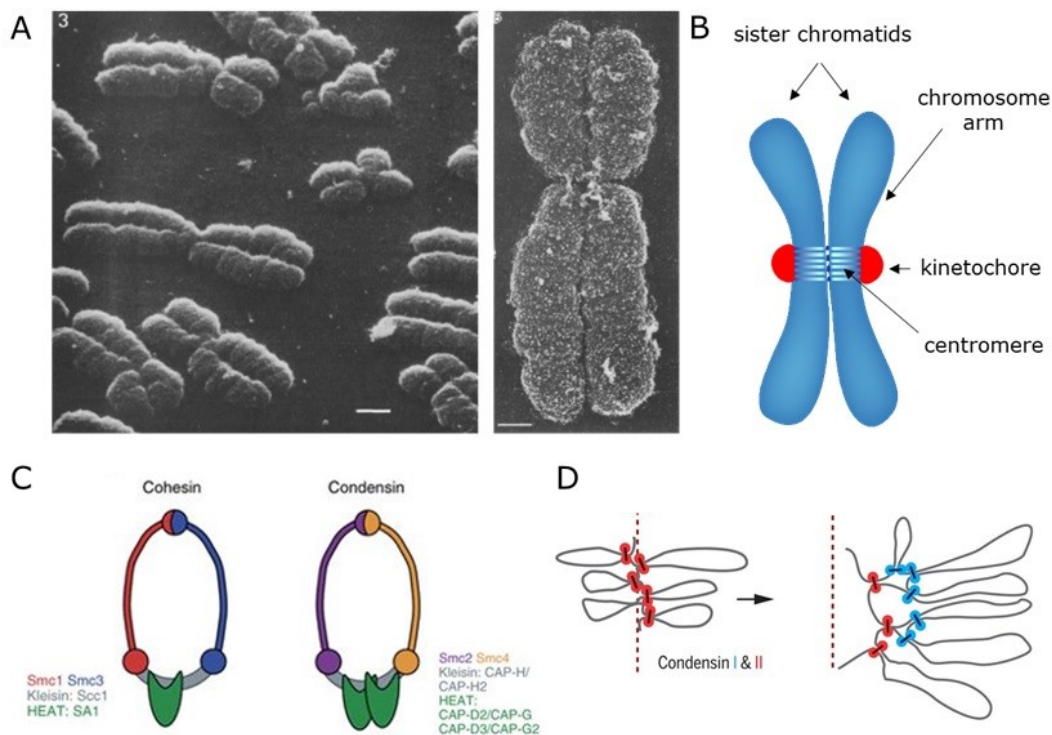


**Figure 5 Cromosome structure and condensation**

(A) Mitotic chromosome under scanning electron microscope, scale bar 1µm, zoom 0.5µm. PMID: 7166573 (B) cartoon depicting different regions of chromosome (C) Color-coded structure of human cohesin and condensin with their subunits. DOI: 10.1038/nsmb.3507 (D) Loop organisation of DNA by Condensin I and Condensin II. DOI: 10.1126/science.aao6135

The **centromere** is essential for chromosome segregation since it is a building platform for the kinetochore complex, the place where spindle microtubules attach. Different organisms have centromeres of various sizes, from point centromere (very short region) in budding yeast to holocentromere in C. elegans (whole chromosome)[119]. Human cells possess regional centromere, a specific region of DNA with cohesion of sister chromatids that can be seen under a microscope as a thin part of the condensed chromosome (Figure 5A, B). It has high structural elasticity therefore it can bend without causing damage to the chromosomal DNA[120]. Centromere is a constitutive heterochromatin region defined by zones of short repetitive sequences (α-satellites) with a typical nucleosome composition containing histone H3 variant Centromere Protein-A (CENP-A).

**Kinetochore** is the place where spindle microtubules attach to the chromosome and therefore it is crucial for proper chromosome segregation. It is not only a place of attachment, but also a residing site of many molecular motors that are the driving force for chromosome movement around the cell, important for chromosome alignment and their segregation during anaphase. Human kinetochores bind around 30 microtubules[121] in contrast to 7 in mice and 1 in the budding yeast. Kinetochores are assembled *de novo* every cell division, from prophase to prometaphase, when spindle microtubules start to make first contacts with the chromosomes. CENP-A is indispensable for kinetochore assembly, since its deletion has a lethal phenotype in mice[122]. Based on the proximity to the centromere the inner and the outer kinetochore can be distinguished (Figure 6).

In prophase, CENP-A directly binds and recruits CENP-C and CENP-N, creating a necessary structural base for kinetochore formation[123]. CENP-C links centromere with the kinetochore and recruits 14 different CENP- (-C, -H, -I, -K to -U) proteins forming the constitutive centromere-associated network (CCAN)[124] and the inner kinetochore.

The outer kinetochore is a multi-subunit complex interacting with microtubules and forming the stable attachments. It consists of three main complexes (KNL1, Mis12, Ndc80) which is often referred to as the kinetochore protein network (KMN)[125]. Ndc80 is a tetrameric complex that binds microtubules[126] through its two N-terminal domains, also known as Hec1 subunits. Mis12 complex (MIS12, PMF1, Nsl1, Dsn1) connects the KMN to the inner kinetochore via CENP-C and CENP-T binding. KNL1 is the largest subunit and is mostly disorganized, serving as a scaffold for protein binding. Kinetochore recruits many different proteins regulating either microtubule attachment (MCAK, Kif2b, Astrin-SKAP complex), SAC response (Bub1, MAD1, MAD2) or chromosome movement (motor proteins dynein and CENP-E).

**Dynein** is targeted to kinetochores by the adaptor complex Rod-Zwilch-ZW10 (RZZ) and is responsible for chromosome movement towards the (-) microtubule end as well as for removal of mitotic checkpoint components, when the SAC response is being attenuated.

**CENP-E** is a kinesin motor protein mediating microtubule (+) end movement of chromosomes and it is also known to help microtubule capture[127] and it is involved in maintenance of stable microtubule attachment. CENP-E inhibition disrupts proper chromosome alignment at metaphase.

**MCAK** belongs to the Kin I group of kinesins which is not primarily involved in movement along MTs, but it depolymerizes them. MCAK activity is important for correction of merotelic attachments and for chromosome congression[128].
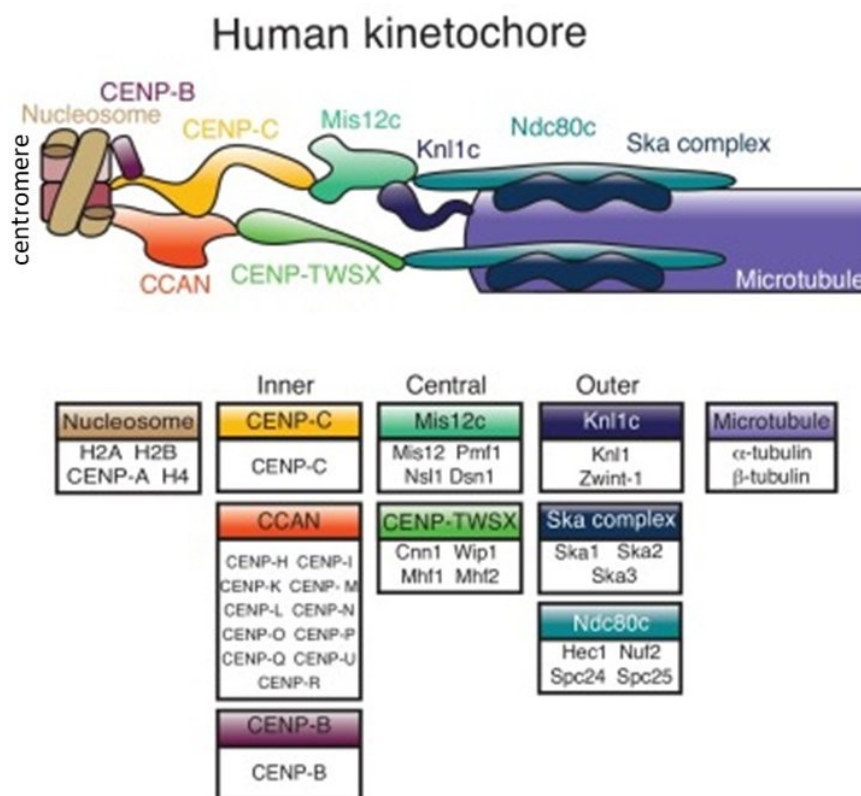


**Figure 6 Kinetochore structure**

A color-coded scheme depicting the individual protein complexes forming human kinetochore and their special position from centromere (left) towards the microtubule (right). Source: DOI: 10.1016/j.ceb.2019.03.016

## Centrosomes

Centrosomes are cellular organelles important for spindle formation and spindle geometry functioning as the microtubule organizing centers (MTOC). Mature centrosome consists of two centrioles that are surrounded by pericentriolar material (PCM) with high level of structural organization[129]. Each centriole is composed of nine microtubule triplets forming the typical barrel-like structure. PCM consists of different proteins which recruit γ-tubulin necessary for formation of new microtubule fibers (MT nucleation) emanating from the pole[130]. Centrosomes are replicated in a cell cycle dependent manner. In G1/S transition, centrioles are separated followed by duplication and elongation of the daughter centriole in S phase. Centrosome maturation is finished at the mitotic entry and the two centrosomes are separated and positioned in the cell by Eg5 (kinesin-5, KIF11) movement resulting in a bipolar spindle formation[131].

## Mitotic spindle

Microtubules are tubular structures composed of α- and β-tubulin heterodimers in a highly organized manner. Microtubule protofilaments (linear chains of tubulin) form a planar sheet that is closed by α, β subunit binding and forms a polarized tubule in which α-subunits mark the (-) end and β-subunits mark the (+) end. Microtubules are very dynamic structures, they are constantly growing and depolymerizing in and ATP dependent manner (Figure 7) which can happen on any of the MT ends.

During prometaphase, mitotic spindle is formed by microtubules growing from the two centrosomes that are positioned at the opposite poles of the cell, forming a bipolar spindle. Different types of microtubules can be identified within the spindle (Figure 8A), such as non-kinetochore microtubules which are not stably attached or the kinetochore fibers (K-fibers) which are stably binding to the kinetochores. K-fibers are bundles of parallel microtubules which are further stabilized by clathrin containing inter-microtubule bridges[132,133] which are part of the mesh network (proteins connecting and stabilizing K-fibres)[134]. Nucleation of microtubules can be initiated from the spindle poles (most common) or from the kinetochores and they are incorporated in the spindle by sliding of antiparallel MTs[135–137], but these events are rather rare in normal conditions. Spindle microtubules have stable orientation, their (-) ends are directed towards the poles and their (+) ends are facing the equator or cell cortex.
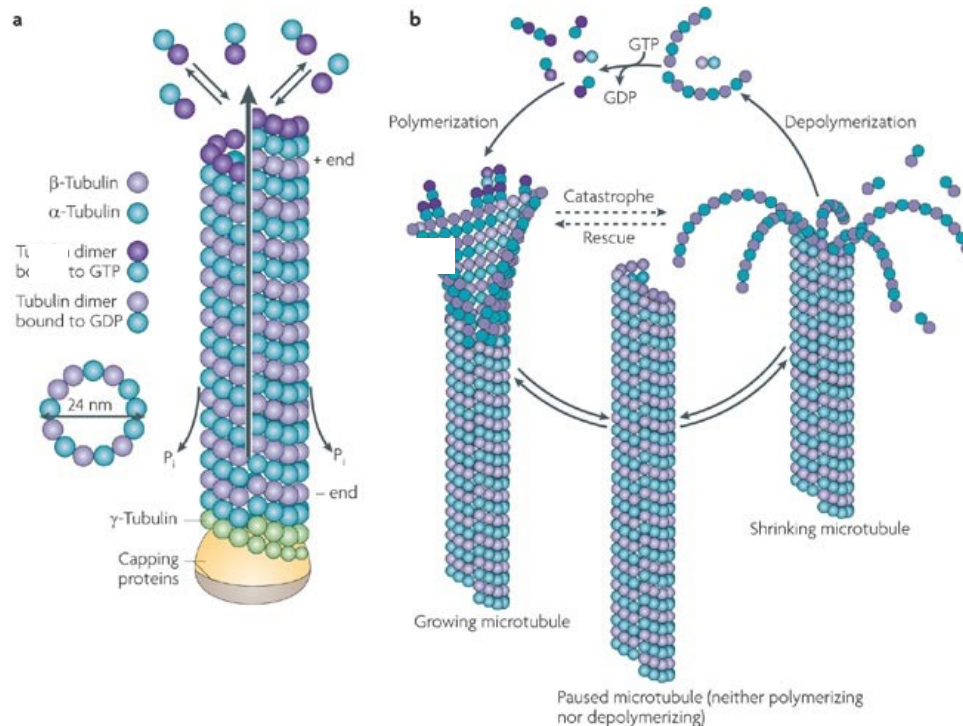
**Figure 7 Microtubule dynamics**

Left: mechanism of γ-tubulin mediated microtubule nucleation from centrosomes.

Right: GTP dependent microtubule polymerization and depolymerisation dynamics.

Green circle- γ-tubulin, blue circle- α-tubulin, violet circle- β-tubulin

Source: DOI, 10.1038/nrn2631

Inter-polar microtubules are important for stability of the spindle and for chromosome segregation. They emanate from spindle poles and grow towards the equatorial zone where they meet with microtubules from the opposite pole and form antiparallel microtubule bundles crosslinked with Protein regulator of cytokinesis-1 (PRC1) and other proteins, referred to as the 'mesh network'. The antiparallel microtubules can grow and slide along each other resulting in spindle elongation which is important for segregation of sister chromatids during anaphase, but it also determines the spindle length in metaphase[138]. Sliding of anti-paralel microtubules is regulated by activity of (+) and (-) end directed motor proteins KLP61F and Ncd, respectively[139,140]. Recent studies propose an existence of bridging fibers connecting the K-fibers of both sister chromatids which helps to withstand the tension and contributes to the curved spindle shape[141,142].

The Kinetochore-microtubule (KT-MT) attachment is a stochastic process which happens in prometaphase and is prone to errors therefore a reliable correction mechanism is needed to

achieve error-free chromosome segregation. The desired bipolar (amphitelic) attachments are formed when the kinetochores are attached to the microtubules emanating from the opposite poles, monotelic and syntelic attachments result from binding of one or both kinetochores to MTs from a single pole. Merotelic attachments are similar to bipolar attachment, but one kinetochore is attached to both spindle poles (Figure 8B). If these attachments persist until anaphase, the chromosomes are not segregated properly and result in lagging chromosomes. The merotelic attachments are the most frequent cause of aneuploidy (loss or gain of chromosome) in mammalian cells[143] and greatly increase the chromosomal instability (CIN)[144].
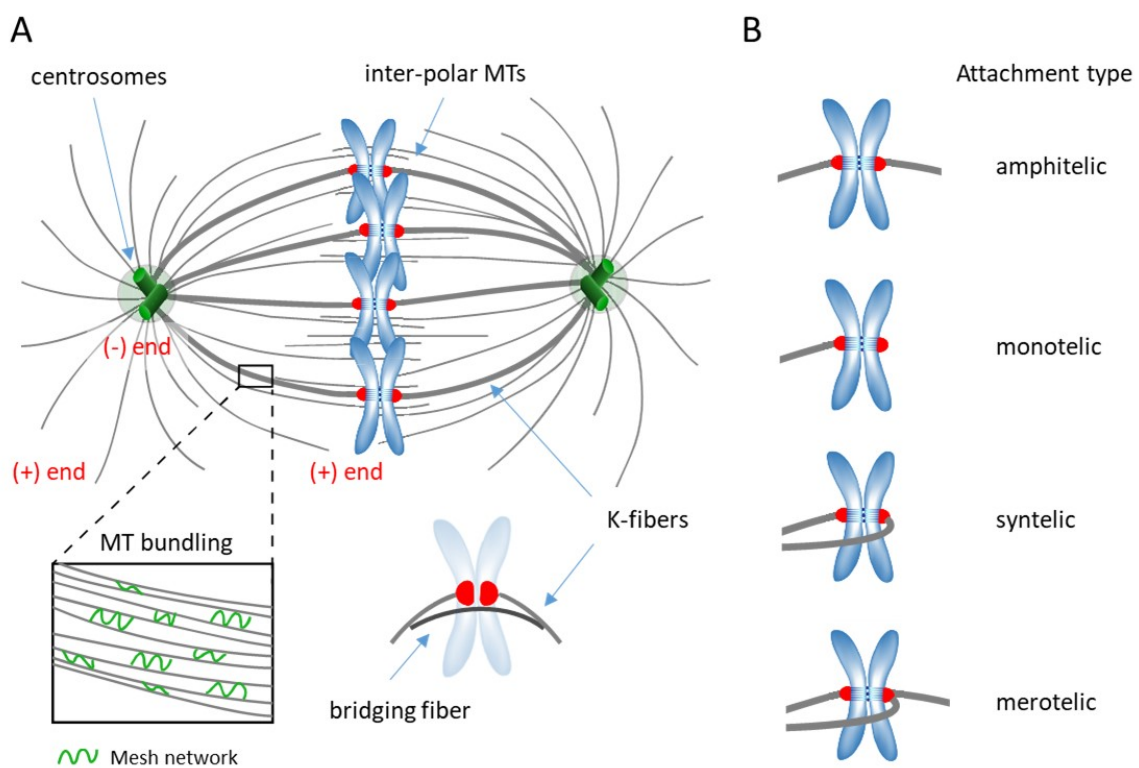


**Figure 8 Structure of mitotic spindle**

(A) Drawing showing the main components of mitotic spindle and the different types of microtubules forming mitotic spindle. (B) Types of kinetochore- microtubule attachments.

MT – microtubule, K-fiber – kinetochore microtubules

# 1.5.2 Mitotic regulators

Cell cycle regulation depends mainly on ubiquitination and phosphorylation events, which are frequently interconnected. In this chapter I want to provide an overview of the most important kinases and ubiquitin-related factors for mitotic progression. Their activity needs to be properly coordinated in time and space by restricting their localization to specific cell compartments or by recruitment of phosphatases or DUBs that oppose their role (Figure 9).

## Mitotic kinases

**Cdk1** (cdc2 in yeast) belongs to Ser/Thr protein kinase family and it is highly conserved among species. Protein levels of Cdk1are stable during the cell cycle and its activity is regulated by association with mitotic cyclins (cyclin A and B) that function as regulatory subunits. Cdk1 is an important regulator of mitotic progression, it is activated by cyclin B at the G2/M transition, its activity peaks in prometaphase and it is inactivated at anaphase onset by APC/C mediated cyclin B degradation. Cdk1 promotes mitotic entry and its activity is necessary for many structural changes typical for mitosis, such as nuclear envelope breakdown, centrosome separation, chromosome condensation, kinetochore assembly and cytoskeleton rearrangement, which are all necessary for spindle formation and separation of the two daughter cells. A high-throughput search for Cdk1 substrates in mitosis identified more than 400 potential substrates including proteins associated with nuclear envelope (Lamin A/B/C, NUP133, RANBP2), centromere and kinetochore (INCENP, CENP-C, DSN1) and cytoskeleton (TPX2, KIF20A, KIF18B, MAP 4/7) further underlying Cdk1 importance[145]. Interestingly, Cdk1 also phosphorylates other mitotic kinases (Aurora B, Haspin) and phosphatases (PP1) to regulate their activity[146].

The family of Aurora Ser/ Thr protein kinases contain three members: Aurora A, Aurora B and Aurora C. They are structurally very simmilar, yet they have distinct functions. Aurora C expression is restricted to germ cells that undergo meiosis, therefore high Aurora C levels can be found in testis and oocytes[147,148]. In contrast, Aurora A and B are expressed ubiquitously and they are important regulators of mitosis.

Together with Cdk1 and Plk1, **Aurora A** activity is necessary for the Cdk1 dependent mitotic entry and deletion of Aurora A results in G2 arrest. Aurora A localizes to the centrosomes and contributes to their maturation by recruitment of PCM components (centrosomin, γ-tubulin). In addition, Aurora A phosphorylates CDC25 phosphatase and the level of phosphorylation is

proportional to cyclin B translocation to the nucleus and to the subsequent activation of Cdk1[149]. This step is tightly controlled by the DNA damage checkpoint preventing premature onset of mitosis. Aurora A strenhtens cohesion of sister chromatids by phosphorylation of histone variant CENP-A (Ser7) which prevents the chromosomes from 'cohesion fatigue' (loss of cohesion)[150]. Aurora A participates in spindle organization during prometaphase and is also necessary for the formation of the central spindle during anaphase where it promotes MT nucleation in the midzone[151]. Despite their different roles, Aurora A and Aurora B have some common substrates important for chromosome movement and microtubule stability and spindle dynamics including MCAK, KIF2b, KIF18 and CENP-E[20,152,153].

**Aurora B** is the catalytic subunit of the Chromosome passenger complex (CPC), consisting of inner centromere protein (INCENP), Survivin, Borealin (known as Dasra B) and Aurora B kinase[154]. The CPC has dynamic localization during mitosis and controls many important processes including chromosome condensation, SAC activation, correction of KT-MT attachments and cytokinesis[155].

In early mitosis, CPC is targeted to inner centromere by phosphorylation of two histones, H2A (Thr120), H3 (Thr3) by Bub1 and Haspin kinases which creates the docking sites for Borealin and Survivin subunits of CPC[156]. CPC binding to pH3T3 is further promoted by Aurora B activation of Haspin, generating a positive feedback loop stimulating CPC recruitment to the inner centromere[157]. Aurora B is activated by INCENP binding which triggers autophosphorylation at Thr232 residue resulting in full activation. In prophase, Aurora B contributes to chromosome condensation by promoting condensin I association with mitotic chromosomes[158]. Aurora B is the main kinase involved in the correction of erroneous KT-MT attachments (syntelic, merotelic)[159]. In prometaphase, Aurora B phosphorylates kinetochore proteins including Ndc80, KNL-1 and Mis12 resulting in decreased affinity of KMN towards microtubules leading to destabilization of KT-MT attachments. This mechanism increases the MT turnover at KTs and increases the chance that correct, amphitelic attachments will be made[160,161]. Aurora B activity negatively regulates Astrin-SKAP complex further weakening the KT-MT attachments during prometaphase. Another important substrate of Aurora B is MCAK (KIF2C) which has a MT- depolymerizing activity. Aurora B phosphorylation inhibits MCAK activity and retains it at the centromere. Upon dephosphorylation it is relocalized to KTs where it promotes MT disassembly and thus correction of improper attachments[162]. This probably serves as an additional mechanism to correct erroneous attachments even after Aurora B activity is attenuated. Aurora B is also an important mediator of the SAC response (see

chapter about SAC). Upon chromosome alignment, before the anaphase onset, ubiquitin ligase Cul3-mediated mono-ubiquitination triggers Aurora B relocalization to the microtubules by UBASH3B ubiquitin receptor and MKLP2 (kinesin-6) motor protein[163]. In telophase, Aurora B localizes to the midbody and contributes to timely regulation of abscission and cytokinesis in order to prevent cells from chromosome breakage by cytokinetic machinery[164].

Polo-like kinase 1 (**Plk1**) belongs to the family of Ser/Thr kinases and contains two polo-box domains that are important for regulating its activity and the dynamic subcellular localization. Plk1 activity is necessary for duration of the whole mitosis. It promotes mitotic entry and regulates centrosome dynamics, KT-MT attachments, SAC signaling and mitotic exit. In G2, Plk1 localizes to centrosomes and contributes to the centrosome maturation by phosphorylation of pericentrin, promoting the recruitment of γ-tubulin and Aurora A to centrosomes[165]. In addition, Plk1 contributes to centrosome separation by two distinct mechanisms: phosphorylation of Mst2-Nek2A[166] kinase module and by phosphorylation of kinesin Eg5 leading to centrosome positioning by a Cdk1-independent mechanism[167]. In prometaphase, Plk1 localizes to kinetochores and contributes to stability of KT-MT attachments by recruitment of the protein phosphatase 2A (PP2A) which opposes the role of Aurora B[168,169]. In metaphase, Plk1 is removed from kinetochores which contributes to SAC silencing[170]. In telophase and during cytokinesis, Plk1 localizes to the midbody and negatively regulates recruitment of the abscission factor CEP55 which complements the Aurora B mediated control of timely abscission and cytokinesis[171]. At mitotic exit, Plk1 is polyubiquitinated by APC/C$^{Cdh1}$ and degraded by proteasome.
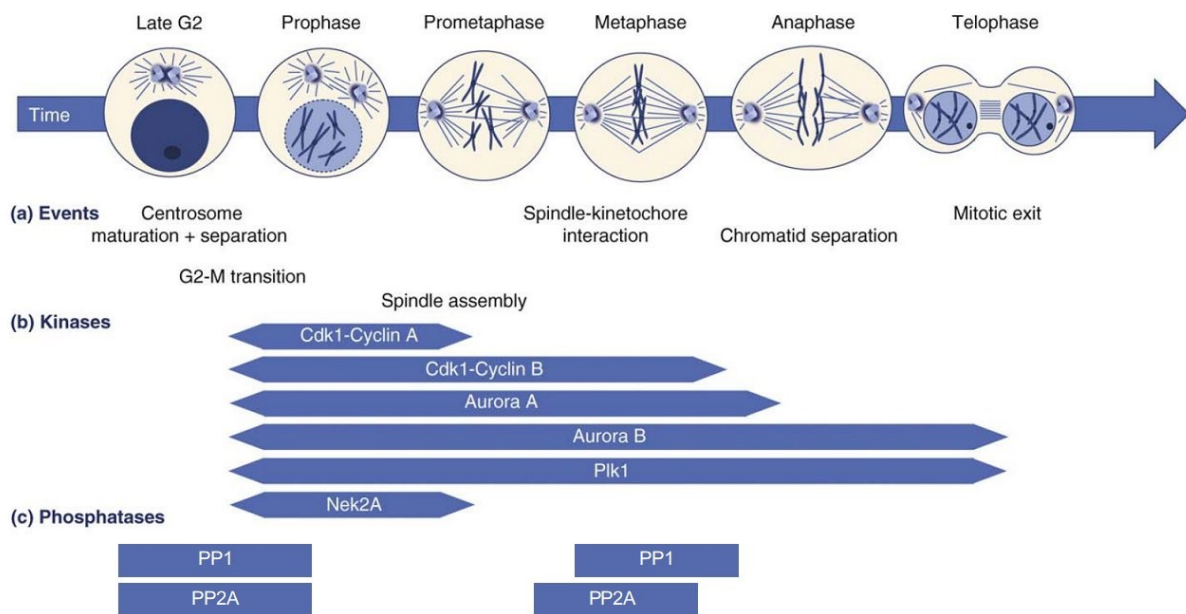
**Figure 9 Overview of the main kinases and phosphatases regulating mitotic progression.**

Left to right: different phases of mitosis ordered chronologically together with important structural changes of the cell (a). (b) List of kinases important for regulation of mitosis and (c) the phosphatases counterbalancing kinase activity. Length of the purple rectangle corresponds to the time they are activated in mitosis.
Adapted from: doi:10.1016/j.tcb.2009.06.005

## The mitotic ubiquitin- related factors

The most studied E3 ligases regulating cell cycle progression are SCF and APC/C. They are both Cullin-RING ligases (CRLs) and they form multi-subunit complexes with different cofactors and adaptor proteins which further tune their substrate specificity (Figure 10). Mitotic entry is regulated by SCF$^{\beta\text{-}Tcrp}$ complex which controls protein levels of negative regulators of CDK1 (Wee1, Emi1) and is counteracted by USP50 deubiquitinase[172]. CDK1 and Aurora A activity is necessary for the mitotic entry and is controlled by USP7 which indirectly promotes Aurora A degradation resulting in G2 arrest[173]. Error- free mitotic progression is under the control of the mitotic checkpoint (also called SAC), which prevents chromosome segregation prior their proper alignment at metaphase plate by inhibiting the APC/C ubiquitin ligase. USP44 further stabilizes the mitotic checkpoint complex and inhibits anaphase onset[174] while USP16 promotes chromosome alignment by targeting Plk1 to kinetochores[175]. The USP39 and USP9X DUBs have been implicated in the control of proper chromosome alignment by regulating the transcription and localization of the key mitotic kinase Aurora B[176,177].

Additionally, USP4 indirectly contributes to SAC activation by control of mRNA splicing of important SAC components[178]. Upon chromosome alignment, APC/C$^{cdc20}$ promotes proteasomal degradation of Cyclin B by K11-linked polyubiquitination[179] and results in cytokinesis and mitotic exit. Several DUBs have been shown to control cytokinesis, CYLD which negatively regulates cytokinesis by increasing the stability of microtubules[180] and USP8 and AMSH promote the scission by deubiquitination of ESCRT machinery components at the central spindle and the midbody[181]. Mitotic exit is further promoted by APC/C$^{cdh1}$ mediated ubiquitination and degradation of mitotic cyclins (cyclin A, cyclin B) and mitotic kinases (Plk1, Aurora A, Aurora B)[48,182]. USP35 is so far the only DUB described to oppose the APC/C$^{cdh1}$ by deubiquitinating and stabilizing Aurora B kinase[183] (Figure 10).

Until now, several DUBs have been identified to regulate mitotic progression as discussed in this chapter, but the list is by far incomplete and further studies are necessary to fully understand how DUBs are regulating mitotic progression.
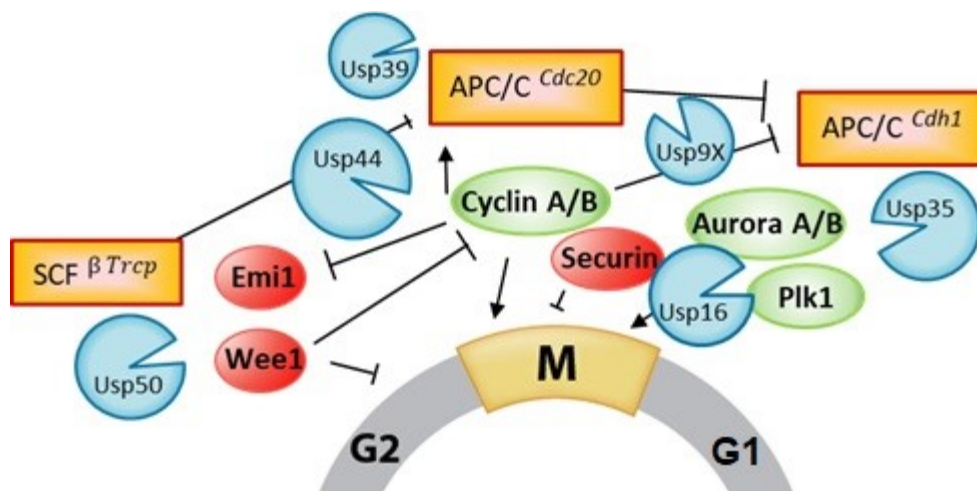


**Figure 10 Regulation of mitosis by ubiquitin- related factors**

Orange rectangle – ubiquitin ligase, blue circle – DUB, green circle – positive cell cycle regulator, red circle – negative cell cycle regulator.

Adapted from: DOI: 10.1146/annurev-biochem-060410-105307

## 1.5.3 Mechanism of the spindle attachment and the chromosome congression

To achieve proper chromosome alignment, kinetochores first need to be attached to the spindle microtubules and after, chromosomes need to be transported to the equatorial zone of the cell (chromosome congression) by combination of pushing and pulling forces of molecular motors and by polymerization and depolymerization of the spindle microtubules.

KT-MT attachment is a stochastic process, described by the 'search and capture' model. Polar microtubules elongate and search for kinetochores, exploring the space as they grow. Interestingly, fission yeast use the microtubule pivoting around the polar body (human centrosome) to quickly capture kinetochores along the whole length of MT[184]. Mitotic spindle nucleates from centrosomes and many temporary and unstable attachments are made, before the bi-oriented state is achieved. In the beginning, kinetochores often bind to the side of microtubules (lateral attachments) and they are pulled towards the MT (+) end to form the stable end-on attachments in a conversion process[185].

It remained a big question in the field what is the mechanism of chromosome congression, which factors are the key players and how the pulling forces are generated. It is now clear that more than one mechanism contributes fast and efficient chromosome alignment.

Different congression mechanisms apply depending on the position of chromosome in the cell and its attachment status. When the chromosome is captured by the spindle microtubule at the cell periphery, it is transported by a dynein mediated movement to the pole[186], a microtubule dense region, where it has a higher chance to be bound by microtubules from the opposite pole (Figure 11A). Chromosomes with the monotelic attachment can be transported to the equatorial zone by a CENP-E dependent movement along an already established K-fiber (Figure 11B). Chromosomes with bipolar attachments need to be transported to the equatorial zone to complete their alignment (Figure 11C). This chromosome has more MTs attached from the near pole, but yet it is moving away from this pole. We can distinguish the leading kinetochore (closer to the equatorial zone) and the trailing kinetochore (facing the pole). The mechanism regulating this chromosome movement has long been discussed and it was proposed that the force is proportional to the length of the microtubule, resulting in a movement away from pole[187]. Both, plus and minus end directed motors are present at the kinetochore and their activity is regulated by phosphorylation, therefore chromosome can be moved in both directions, depending on the surrounding signals[188]. Laser ablation studies showed, that the

pulling force is generated only on the leading kinetochore ensuring movement to the center of the cell[189] during which MTs at the leading KT are shortening and MTs at the trailing KT are growing. This is possible due to the ability of kinetochores to stay attached to microtubules even when they are polymerizing/ depolymerizing (Figure 11D) and results in chromosome alignment. In metaphase, all chromosomes are attached to the spindle, but despite its static look it is a highly dynamic structure. K-fibers are constantly growing from their (+) ends and they are shrinking at the poles from their (-) ends. This shrinkage happens at a higher pace than the growth, resulting in pulling forces towards the poles and it also causes a constant polar movement of tubulin subunits in the spindle, so called 'poleward microtubule flux'[190]. Poleward flux has been observed by photoactivation and photobleaching experiments, where patches of tubulin were seen to move to the poles[190,191] (Figure 11E). It serves as an additional mechanism for protein removal from kinetochores and it was shown to contribute to chromosome movement during anaphase[192,193].
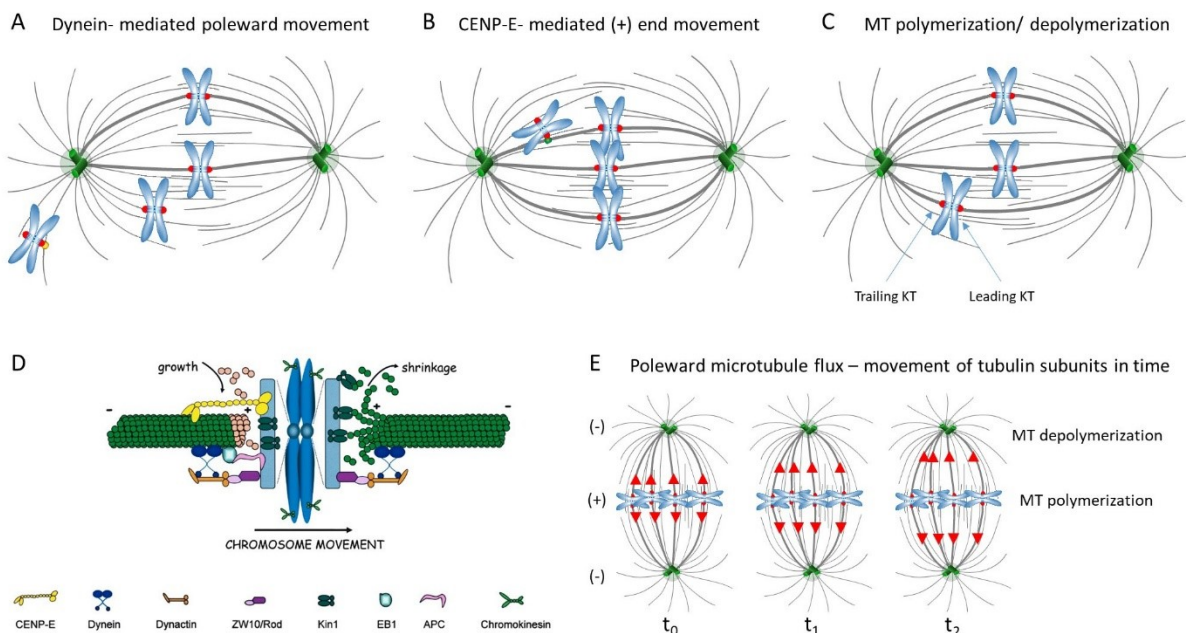


**Figure 11 Mechanisms of chromosome congression and properties of the bi-oriented spindle.**
(A-C) Different mechanisms of chromosome transport from the cell periphery to the equatorial zone. (D) The kinetochore- microtubule interface showing the mechanism by which kinetochores bind growing and shrinking microtubules. Adapted from: DOI: 10.1016/S0092-8674(03)00115-6 (E) The poleward flux established upon chromosome biorientation at metaphase. Red triangle – fluorescently labelled tubulin.

# 1.5.4    Spindle assembly checkpoint (SAC)

SAC senses the occupancy of kinetochores by microtubules and is regulated by activity of different kinases and phosphatases. When there are no MTs attached to KTs, the activity of mitotic kinases is dominant and the SAC response is high. Upon formation of bipolar attachment, the activity of mitotic phosphatases becomes dominant and SAC is silenced. Interestingly, the SAC response is potentiated by presence of unattached KTs and therefore it is not efficient in sensing merotelic attachments, because the kinetochores are bi-oriented and fully occupied by MTs[143]. Aurora B activity is necessary for correction of erroneous (merotelic, syntelic) attachments[161]. SAC prevents premature anaphase onset by inhibiting the activity of APC/C ligase, which ubiquitinates separase inhibitor securin and the CDK cofactor cyclin B and targets them for proteasomal degradation. Cohesin cleavage by separase triggers anaphase and subsequent drop in CDK activity results in mitotic exit. APC/C activity is dependent on the cdc20 cofactor, which is the target of the SAC generated mitotic complex (cdc20, MAD2, Bub3 and BubR1)[194]. Aurora B activity promotes localization of SAC components to the kinetochores[195] by targeting Mps1 kinase to KTs and by potentiating its activity[196]. Mps1 phosphorylation promotes recruitment of Bub1 kinase to KTs, amplifying the SAC response. Aurora B inhibition results in weak SAC signaling and premature mitotic exit[197].

SAC signal is generated at the kinetochore and it is diffused in the cell by cascade of events. First, unattached kinetochores recruit Mad1 which interacts with MAD2 dimer and is able to change the conformation of cytoplasmic 'open' MAD2 (o-MAD2) to 'closed' MAD2 (c-MAD2) which has a high binding affinity to cdc20 cofactor, activator of APC/C ligase[198]. Complex of c-MAD2 and cdc20 can diffuse to cytoplasm and another MAD2 can be 'activated' leading to fast amplification of the signal (Figure 12A). The APC/C-cdc20-c-MAD2 complex is inactive and cells remain arrested in metaphase.

After KT attachment and chromosome alignment, the SAC signaling needs to be silenced, which is achieved by combination of poleward microtubule flux and dynein dependent removal of SAC components from kinetochores[199] in addition to high activity of PP1 phosphatase which opposes Aurora B and dephosphorylates its substrates[200]. Upon SAC silencing, Bub1 stays localized to kinetochores but MAD1 and MAD2 dissociate from KTs leading to physical separation of the kinase and its substrates, stopping further generation of SAC signal[201]. Interesting protein is p31[Comet] which is structurally very similar to MAD2. It binds to MAD1-MAD2 core complex at kinetochores and sterically blocks the site for O-MAD2

binding, which subsequently blocks O-MAD2 activation and stops generation of SAC response[202]. In addition, p31[Comet] binds to soluble MAD2 forming APC/C-cdc20-Mad2-p31[Comet] complex, which can partially activate APC/C resulting in auto-ubiquitination and dissociation of MAD2 cdc20 complex, further contributing to the APC/C activation[203] (Figure 12B). Combination of these mechanisms leads to SAC silencing and timing of these events needs to be tightly controlled since it results in irreversible sister chromatid separation by cohesin cleavage and to the anaphase onset.

Defects in SAC signaling or in the correction machinery result in segregation errors. The most frequent causes are weak SAC response (premature anaphase entry) and aberrant KT- MT attachments (merotely) which both lead to lagging chromosomes and aneuploidy. At certain rate, aneuploid cells are present in normal tissues[204], but they are quickly eliminated. Lagging chromosomes can result in micronuclei or they can cause chromosomal damage by the cytokinetic machinery which is detrimental for the cell and induces a global stress and activation of the DNA damage response pathway which leads to cell cycle arrest, apoptosis or senescence[205–207]. In some cases, cells adapt and manage to tolerate aneuploidy either by inhibition of the DNA damage response pathway (p53 mutation) or by transcriptional adaptation (increased gene transcription, higher copy number) leading to upregulation of the compensatory mechanisms[208,209]. This constant adaptation of the cancer cells to tolerate aneuploidy is what makes the development of anti-cancer drugs so challenging.
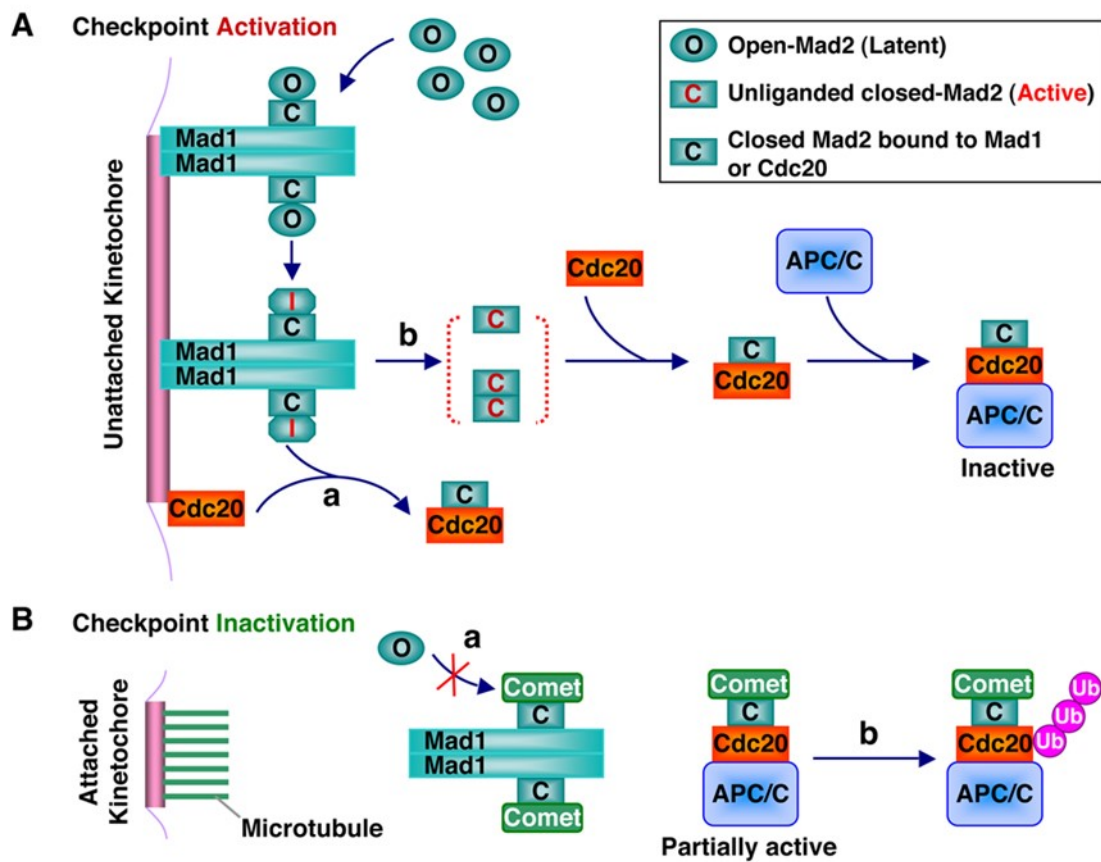
**Figure 12 Spindle assembly checkpoint activation and deactivation**

(A) In presence of unattached kinetochores, MAD1 binds to kinetochores and catalyses conformational chance of o-MAD2 to c-MAD2 which forms complex with cdc20 and inhibits APC/C ligase activity.

(B) Upon attachment of all kinetochores to microtubules the SAC is silenced, mitotic checkpoint components are removed from kinetochores and p31[comet] inhibits the conformational change of MAD2 stopping the SAC signal from propagation. Polyubiquitination of cdc20-MAD2 leads to dissociation of the mitotic checkpoint complex and to full activation of APC/C.

Source: DOI: 10.1016/j.str.2008.10.002

# AIMS OF THE STUDY

Mitosis is one of the cell cycle phases and it is the step of physical cell division. During this process the duplicated genetic content is divided into two daughter cells and therefore it needs to be tightly regulated. Defects in the cell division are highly detrimental for the cell and for the whole organism and they often lead to cell death or to aneuploidy, a known driver of tumorigenesis.

**Main aim**: The main aim of this project was to identify novel factors of the ubiquitin signaling that are important for regulation of the cell cycle progression and mitosis.

**Aim 1**: Describe the function of ubiquitin ligase Trim15 and assess its ability to regulate the cell cycle progression.

**Aim 2**: Characterize the deubiquitinase UCHL3 and confirm its involvement in the regulation of mitosis.

**Aim 3**: Characterize the phenotype of UCHL3 downregulation and its relevance for the human primary cells.

**Aim 4:** Investigate the mechanism by which UCHL3 regulates mitotic progression and identify the potential substrates of UCHL3 enzymatic activity.

# PROJECTS

## 2 UCHL3 CONTROLS THE CHROMOSOME SEGREGATION DURING MITOSIS

### 2.1 BACKGROUND

UCHL3 is a deubiquitinating enzyme belonging to the family of ubiquitin C- terminal hydrolases and it catalyzes the removal of ubiquitin molecule from its substrates.

UCH protein family consists of four members: UCHL1, UCHL3, UCHL5 and BAP1[210] which have high structural similarity. UCHL3 is well conserved throughout the evolution. There is a high homology of UCHL3 proteins among species, from Arabidopsis and Drosophila to mouse and human[211]. UCHL3 is a small protein of 27 kDa encoded by a 9 exon gene of ~1000 bp which is located on the human chromosome 13. The mRNA of UCHL3 can be alternatively spliced producing three putative transcript variants. Until now, only the longest transcript has been well described to produce the UCHL3 protein of 230 amino acid (AA)[212]. UCHL3 protein has several ubiquitin binding domains and multiple catalytic sites among which the cysteine 95 residue is the main one[213,214] (Figure 13). The UCHL3 gene has about 50% homology to the UCHL1 gene, but despite their similar function in the ubiquitin cleavage, it was shown that they regulate distinct biological processes. Unlike UCHL3, UCHL1 possesses also ubiquitin ligase activity and its expression is restricted to the brain, testes and ovary while UCHL3 is expressed ubiquitously[215]. Interestingly, UCHL3 has a capacity to cleave the ubiquitin- like molecule Nedd8[86] which regulates the activity of Cullin ring ligases[216]. UCHL3 also has an established role in the processing of the ubiquitin precursor proteins during *de novo* ubiquitin synthesis[24]. Several *in vitro* studies described UCHL3 as a protease capable of hydrolyzing only small ubiquitin conjugates and peptides, due to the structural properties of UCHL3 suggesting that bigger substrates would not fit into the catalytic site[214,217–221]. These findings have been recently challenged by the growing number of *in vivo* studies describing the role of UCHL3 in protein deubiquitination.

UCHL3 knockout mice are viable, but they show degeneration of skeletal muscles and retina[222]. Other studies with UCHL3 knockout mice show involvement of UCHL3 in spatial learning and working memory[223] as well as in insulin signaling and obesity[224,225]. Recently a number of publications appeared describing the role of UCHL3 in DNA repair pathway by homologous recombination (HR)[17] and non-homologous end-joining (NHEJ)[226] as well as in the DNA repair of topoisomerase-induced breaks[95]. In addition, some studies described upregulation of UCHL3 in the invasive breast cancer, in cervical carcinoma and in the progression of prostate cancer metastasis[227–229]. Those studies collectively show involvement of UCHL3 in various biological processes by catalyzing the removal of different ubiquitin modifications from its substrates and thus opposing proteolytic as well as non-proteolytic ubiquitination.
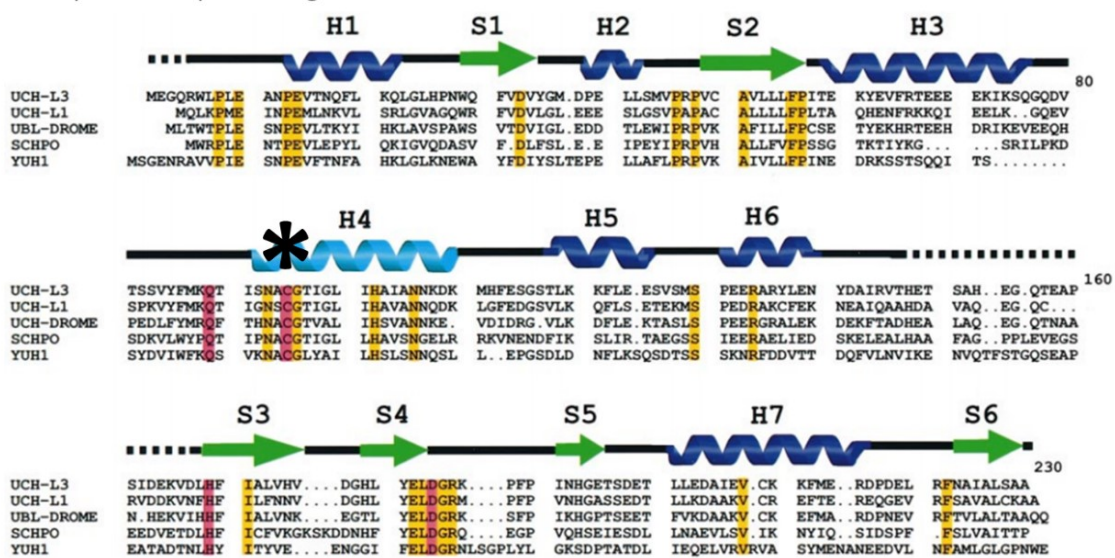


**Figure 13 UCHL3 protein is highly conserved among species**

The sequence alignment of UCHL3 protein from different species: UCH-L3 (human), UCH-L1 (human), UBL-DROME (D.melanogaster), SCHPO (Schizosaccharomyces pombe), YUH1 (S.cerevisiae). Yellow color: ubiquitin binding sites, red color: catalytic site, black asterisk: C95.

Source: doi: 10.1093/emboj/16.13.3787

# 2.2   MATERIALS AND METHODS

## 2.2.1      Reagents and antibodies

TCID (4,5,6,7-tetrachlorodindan-1,3-dione) UCHL3 inhibitor (Ref. 27720-1), C9H2Cl4O2, CAS #: 30675-13-9, Tebu-Bio. UCHL3 inhibitor which was published previously to successfully inhibit the catalytic activity of UCHL3. TCID inhibits also UCHL1 (IC=75µM), I used TCID at 2µM working concentration to ensure specificity for UCHL3[215,230,231]. Monastrol (Ref. M8515) and 4′,6-Diamidino-2-phenylindole dihydrochloride (DAPI) (Ref. D8417) were purchased from Sigma-Aldrich. S-Trityl-L-cysteine (STLC), (Ref. ALX-105-011-M500) was purchased from Enzo Life Sciences and the proteasomal inhibitor MG132 was purchased from Tocris bioscience (No. 1748). Protease inhibitors (cOmplete EDTA-free Protease Inhibitor Cocktail) were purchased from Roche, 1 tablet was diluted to final volume 10 ml lysis buffer.

UCHL3 antibody was produced by IGBMC antibody facility using immunized rabbits and I purified the serum with SulfoLink resins according to the manufacturer's protocol. The Astrin polyclonar rabbit antibody was a kind gift from Ulrike Gruneberg (Cancer Research UK). Following commercial antibodies were used: Mouse monoclonal BubR1 (BD Biosciences, 612502 clone 9/BubR1), mouse monoclonal α-tubulin (Sigma Aldrich, T5168), human polyclonal CREST[232] (Antibodies Incorporated, 15-234), rabbit polyclonal Aurora B (Abcam ab2254), mouse monoclonal UCHL3 (Sigma Aldrich, clone H7171), mouse monoclonal CENP-E (Thermo Scientific, MA1-5758), rabbit polyclonal GFP (Abcam, ab290)

## 2.2.2      Plasmids

All GFP plasmids used were cloned into pEGFP-N1 plasmid (Clontech) generating different expression vectors: pEGFP-N1, pEGFP-N1-UCHL3-WT, pEGFP-N1-UCHL3-C/S. For UCHL3 cloning the longest transcript variant (NCBI, variant2 NM_006002.4) was used to design specific primers for amplification of UCHL3 from human cDNA. To generate the catalytic dead mutant of UCHL3, cysteine 95 residue was mutated to serine by G > C base exchange in the cysteine codon (Appendix Table 8).

## 2.2.3    Cell culture

### Cell lines and medium

All cell lines were purchased from ATCC and cultured at 37 °C in 5% CO2 humidified incubator, if not stated otherwise. I used several different cell lines of human origin and cultured them as listed below.

HeLa Kyoto (HeLa K) human cervix carcinoma cells were cultured in high glucose DMEM-GlutaMAX (4.5 g/L glucose) supplemented with 10% fetal calf serum (#9150), 1% penicillin and streptomycin. HeLa K cells stably expressing Tubulin-GFP-H2B-mCherry were purchased from Ellenberg laboratory and a standard medium for HeLa K cells was used to culture them. Human primary lung fibroblasts (IMR90) were cultured in EMEM containing non-essential AA, 2 mM L-glutamine, 1 mM sodium pyruvate, 1500 mg/L sodium bicarbonate, 10% fetal calf serum and gentamycin. Dld1-mCherry cell line was a kind gift from Don Cleveland and it was cultured in RPMI-1640 medium containing 2 mM L-glutamine, 10 mM HEPES, 1 mM sodium pyruvate, 4500 mg/L glucose, 1500 mg/L sodium bicarbonate, 10% fetal calf serum and gentamycin.

### Cell seeding

I trypsinized cells and counted them in Neubauer chamber (5-10 squares) and calculated the concentration. For all immunofluorescence experiments I was seeding cells on 9-15 mm glass coverslips (Menzel-Glaser) in 24-well plates at a density 15 000 cells per well.

### Cell cycle synchronization

**1. STLC (prometaphase)**

I diluted STLC in DMSO to produce 50 mM stock and I treated cells for 16 hours with STLC containing medium at 5 µM working concentration.

**2. Monastrol (prometaphase)**

I used 100 mM stock of Monastrol in DMSO and I incubated cells for 16 hours in Monastrol containing medium at final concentration 100 µM.

**3. Monastrol washout (different mitotic phases)**

I incubated cells for 16 hours in Monastrol containing medium at final concentration 100 µM, washed them five times with warm medium and released them in fresh culture medium for

different time intervals, aproximately 30 minutes to reach metaphase and 45 minutes to reach anaphase.

**4. Monastrol release (metaphase)**

For all Monastrol release experiments, I used 100mM Monastrol stock in DMSO and 50 mM stock of proteasome inhibitor (MG132) in DMSO. For each experiment I diluted both drugs in culture medium and used them at following working concentrations: Monastrol 100 μM and MG132 50 μM and I used the same protocol for all cell types. I treated cells with 500 μl of Monastrol containing medium for 16 hours and after I washed them five times with 2 ml of warm medium and released them for 90 minutes to fresh medium containing proteasome inhibitor to arrest the cells in metaphase.

## 2.2.4 Stable UCHL3-GFP cell lines

Stable cell lines were generated in HeLa Kyoto cells by random integration of GFP-UCHL3 plasmids (section Plasmids). Three lines were generated: GFP-HeLa expressing empty GFP plasmid as a control, GFP-WT-UCHL3 expressing wild-type sequence of UCHL3 and GFP-C/S-UCHL3 expressing catalytic dead mutant of UCHL3. Expression levels of different proteins were estimated by western blot and for my experiments I chose the cell lines which were expressing near endogenous levels of those proteins.

## 2.2.5 UCHL3 shRNA virus production and generation of the HeLa K and Dld1 cell lines

For retroviral mediated silencing of genes induced by stable expression of short hairpin RNA (shRNA), four sequences targeting UCHL3 and one control sequence (targeting Firefly luciferase) was cloned into an LMP backbone[233] (Appendix Table 1). This plasmid contains long terminal repeats and retroviral packaging signal necessary for the virus production and PKG promoter driven expression of a cassette coding for puromycin resistance and GFP. Furthermore, for improved production of the shRNA, it contains a cassette with U6 promoter driven expression of miR30 microRNA context into which the designed shRNA sequences are cloned.

Retrovirus was produced by transiently transfecting the Phoenix packaging cell line (G. Nolan, Stanford University, Stanford, CA) with the prepared plasmids. Supernatant was collected, filtered to remove cellular debris, polybrene was added and the supernatant was used to infect

HeLa cells or Dld1 cells overnight. After 2 days, cells were selected using puromycin for 48 hours. After the selection, the presence of replicatively competent retrovirus was excluded using qPCR. Knockdown of UCHL3 was validated using qPCR.

## 2.2.6    UCHL3 silencing by siRNA

Cells were transfected by Oligofectamine at the final concentration 30 nM of the siRNA. I used different siRNAs (sequences are listed in Appendix Table 2). Transfection reaction was based on the manufacturer's instructions and I downscaled it to use of smaller volumes (Appendix Table 3). For rescue experiments with UCHL3 GFP plasmids, I used Lipofectamine 2000 according to manufacturer's instructions to transfect both, cDNA and siRNA at the same time.

## 2.2.7    Immunoprecipitation

For IP experiments, I used HeLa K cells stably expressing GFP-UCHL3 proteins. I prepared cell extracts from cells in 1ml of lysis buffer (10 mM Tris HCl pH 7.5, 150 mM NaCl, 0.5 mM EDTA, 0.5% NP-40, protease inhibitor cocktail) per four 10 cm dishes in each condition. To capture the proteins I used GFP-trap agarose beads (Chromotek) which I blocked overnight in 3% BSA diluted in wash buffer (10 mM Tris HCl pH 7.5, 150 mM NaCl, 0.5 mM EDTA, protease inhibitor cocktail). After blocking beads, I washed them three times in lysis buffer and incubated them with 10 mg of cell extracts overnight, rotating at 4 degrees. Before elution, I washed the beads 5 times for 5 minutes with 1 ml washing buffer (centrifugation 500g, 2 minutes) and after I boiled them in 2x Laemmli SDS sample buffer (BioRad) for 15 minutes and loaded the samples on SDS-PAGE followed by western blotting (WB).

## 2.2.8    Western blot analysis

To isolate proteins from the cells, I scraped them from the culture dish, pelleted them by centrifugation at 4ºC and washed them twice with PBS. I lysed them using RIPA buffer (50 mM Tris-HCl pH7.5, 150 mM NaCl, 1% Triton X-100, 1 mM EDTA) supplemented with 1 mM NaF, 1 mM DTT and protease inhibitor cocktail Complete. I lysed the cells on ice by mechanical disruption with a needle (26G brown) 10 times up and down. After, I centrifuged the samples at 10 000g for 30 minutes at 4ºC, transferred the supernatant to a clean tube and measured protein concentration using Bradford assay (Biorad) in 1 mL cuvettes. Samples were boiled 10 minutes in Leamli buffer with β-Mercaptoethanol (BioRad), resolved on 10%

polyacrylamide gels or pre-cast gradient gels (Thermo Scientific, NW04120BOX) and transferred to PVDF membrane (Millipore) using semi-dry transfer unit (Amersham). I used 5% non-fat milk for blocking the membranes and for antibody dilution and TBS-T (25mM Tris-HCl, pH 7.5, 150mM NaCl, 0.05% Tween) for washing the membranes.

## 2.2.9    RNA isolation and cDNA preparation

To isolate RNA from cells I used the RNA isolation kit from Machery Nagel according to their protocol. I used at least 300 000 cells per one reaction. For cDNA preparation I used SuperScript II Kit from Invitrogen and 2500 ng of RNA per reaction with 10mM dNTPs mix from Sigma and Oligo_dT anchor (Appendix Table 4).

## 2.2.10    Quantitative PCR analysis

I used 20 ng of cDNA as a template, SybrGreen I master mix from Roche (04 887 352 001) and 1μM primers in final volume of 10 μl per reaction as listed in primer sequences (Appendix Table 4). I normalized the UCHL3 expression to a combination of three housekeeping genes (GAPDH, HPRT, PO) and I run them at 62ºC annealing temperature. I used the software from Roche (LightCycler® 480 SW 1.5.1) to analyze my data. I determined the efficiency (E) for all primer pairs using large dilutions of template cDNA (50x – 3000x) and I calculated the relative expression using this formula: $R = E\wedge[C_P \text{ sample} - C_P \text{ control}]$. If not calculated otherwise, I assumed that E= 2.

## 2.2.11    Immunofluorescence

### Motor proteins

 I removed medium and incubated cells in extraction buffer (PHEM, 1 mM PMSF, 1 mM ATP, 0.5% Triton X-100) for 3 minutes at 37 ºC and after I fixed the cells in 4% PFA for 2 minutes at 37 ºC followed by two times 5 minutes incubation with 0,5% Triton in PBS at 37 ºC. Next, I blocked the cells in 3% BSA in PBS-T and I followed the normal protocol from this step onwards. PHEM buffer (pH 6.9, PIPES 45mM, HEPES 45mM, EGTA 10mM, $MgCl_2$ 5mM).

### Standard protocol

I used this protocol for all my experiments if not stated otherwise. I washed the cells once in PBS and fixed them in 4% PFA for 17 minutes at room temperature, washed them three times

in PBS and permeabilized them in 0.5% NP-40 for five minutes. Next, I washed them three times in PBS-T and blocked them in 3% BSA in PBS-T for either 90 minutes at room temperature (RT) or at 4 degrees overnight. I diluted primary antibodies in the blocking buffer and incubated them for 2 hours at RT, I washed the cells 3 times five minutes in PBS-T and incubated them with secondary antibodies at 1:500 dilution for one hour at RT in the dark. I washed the cells 3 times 10 minutes with PBS-T and incubated them with DAPI diluted in PBS at final concentration 1 µg/ml for 10 minutes at RT. I washed them 2 times in PBS-T and mounted them on glass slides using Mowiol and dried them overnight at RT in dark.

For all the samples I took high resolution images using Leica spinning disc confocal microscope at 100x magnification with Live SR module and I processed the pictures in Image J followed by the analysis in Cell Profiler as described later.

## 2.2.12    Mitotic index quantification

I used HeLa cells stably expressing the shRNA against either Luciferase (control) or UCHL3 (sh2 UCHL3), I synchronized them by monastrol and after 16 hours of treatment I took photographs of living cells in multiple randomly chosen regions of the culture dish. I calculated the mitotic index (MI) for each condition as a ratio of the mitotic cells number divided by the total number of cells. I determined the mitotic cells by their characteristic round shape.

## 2.2.13    Live video imaging

To film the cells, I used glass bottom dish, 30 mm diameter with four compartments. I used two wells per each treatment/ cell line. For acquisition, I used Leica CSU-W1 spinning disc, 63x objective, oil. Time frame 5 min, z step= 2µm. I placed the cells into a humid heated chamber with 5% $CO_2$ and 80% humidity in the microscope and I rinsed the cells five times with warm medium to wash the monastrol out. I selected eight positions for each condition and I was acquiring pictures for four hours. After acquisition, I processed the files using ImageJ and I created maximum projections for all positions in all time points.

## 2.2.14    Quantification: the percentage of cells with misaligned chromosomes

To quantify cells with misaligned chromosomes I stained the cells with DAPI to visualize DNA. To eliminate biased counting, I always used a blinded approach and I revealed the

sample IDs only in the end of each experiment. I counted the cells directly at the microscope. I was counting the number of cells with aligned chromosomes and the number of cells with misaligned chromosomes and I calculated the percentage of each from the total number of cells counted. In each experiment I counted between 200-800 cells per condition depending on the seeding density.

## 2.2.15    Cell Profiler data analysis

To analyze the immunofluorescent images I used Cell Profiler 3.1.8 and I created different pipelines according to the question I was asking, which is described in detail in the following paragraphs.

### 1. Irregular nuclei quantification

In my experiments I was determining the shape of nuclei in different conditions and I wanted to find an unbiased way how to quantify this parameter. For this purpose, I decided to use the form factor as a criteria. In Cell Profiler, the form factor is calculated as $4*\pi*Area/Perimeter^2$, where area is the number of pixels in the region and perimeter is the total number of pixels around the boundary of each region in the image [234]. Objects that are perfectly round have their form factor equal to 1. For each set of experiments, I identified the primary objects (nuclei) based on the DAPI channel, I measured the form factor for each nucleus in the given treatment group and I set a threshold to discriminate between regular and irregular nuclei. I considered all nuclei above the threshold as regular and all nuclei below it as irregular. I calculated the percentage of irregular nuclei per each condition. All nuclei were numbered to be able to trace back the form factor values to the individual nuclei. (For examples, see Appendix Figure 33)

### 2. The relative intensity on kinetochores

To quantify relative intensity of the proteins of interest (POI) on kinetochores I generated a pipeline that automatically recognizes single kinetochores based on the CREST immunofluorescence image. I used thresholding to make the image clearer for automated recognition, but this thresholding served only for recognition, all quantifications were made from the raw images (Appendix Figure 34A). The software recognized objects of different sizes and shapes (Appendix Figure 34B), but I estimated that all kinetochores are approximately of the same size and those differences are a result of focus plane position and the signal quality. To make the size of kinetochores uniform, I added a step in which the program drew circles

around the centers of the objects, which allowed for having all kinetochores of the same size (8 pixels in diameter) (Appendix Figure 34C). Next, the program measured intensity of the CREST signal and the intensity of POI (BubR1 or CENP-E) within the circle area. Following the measurements, the program exported several overlay images in a tiff format with numbered kinetochores so I was be able to track back the position of each kinetochore and its number (Appendix Figure 34E). In the end, the program exported all the intensity measurements to an Excel file which contained among other parameters the Mean Intensity value of each kinetochore region. After processing all the images in Cell Profiler, I went through the exported overlay images manually to check the quality of the recognition. In Excel I calculated the ratio of the POI intensity to the CREST intensity (POI/ CREST) and I normalized these results to the control (control = 1). All values are shown relative to the control, which allows for comparison of the results from different experiments.

In case of the Astrin intensity quantification, I enlarged the circle determining the region of kinetochore in all the conditions to 16 pixels in diameter, because the CREST and Astrin signals do not have exact overlap (Appendix Figure 34D). After I calculated the Astrin to CREST ratio and normalized the relative intensity to the control as previously.

For most of my experiments I was interested to know the intensity value relative to the kinetochore spatial position in the cell. To get this information, I went through the exported overlay images and I manually assigned the spatial attributes directly to the Excel file, based on the kinetochore numbering (A- aligned, M- misaligned).

## 2.2.16 Statistics

To statistically evaluate my data I used parametric t-test, One-Sample T-test for samples normalized to the control and Two-sample T-test for the rest of the conditions. I considered the values significantly different when P value was smaller than 0.05 and I assigned stars according to P values as follows: P<0.05 *, P<0.01 **, P<0.001 *** P< 0.0001 ****. In all graphs I show my results as Mean ± SEM (or SD) of minimum three independent experiments or more. Details for each result are listed in figure legends.

## 2.2.17 High-throughput siRNA screen

Description taken from Methods section of manuscript 'Ubiquitin Receptor Protein UBASH3B Drives Aurora B Recruitment to Mitotic Microtubules' published previously by the lab[163].

## siRNA-based libraries and visual high-content screening

For the siRNA screens, custom-made libraries were purchased from Dharmacon. 20 nM of siRNA SMARTpools with 4 different siRNAs for each gene (siGENOME for the primary screen and ON-TARGETplus for the secondary screen) were transfected into HeLa cell lines (obtained from the German Cancer Research Centre DKFZ, Heidelberg, Germany) grown in Greiner µClear 96-well microplates using a high-throughput (HT) reverse chemical transfection with the INTERFERin delivery reagent (Polyplus-transfection SA, Illkirch France). The HT transfection protocol was optimized for reaching 90-95% transfection efficiency with minimal toxicity on a TECAN Freedom EVO liquid handling workstation. The screens were performed in technical triplicates. To limit biological variability, cell passage (n=3 after thawing), serum batch, transfection agent batch were strictly determined. Internal controls such as positive and negative siRNA controls (Table S1), transfection efficiency control ("PLK1" siRNA that leads to mitotic cell death), were added to each microplate to determine parameters for inter-plate and day-to-day variability. Three days post-transfection, the cells were fixed and subjected to immunofluorescence with anti-α-Tubulin antibody (Sigma T5169) allowing labeling of the cytoplasmic ("cell") compartment. Secondary detection was performed with Alexa fluor-488-labeled secondary antibodies (Molecular Probes) and nuclei were stained with DAPI (labeling nucleus compartment "Nuclei"). High-throughput cell imaging was carried out with the INCELL1000 HCS epi-fluorescent microscope to collect an average of ~1,000 cells per microwell.

## Analysis of the high-content siRNA screening data

Multi Target Analysis parameters measuring nuclei and cell morphology for the non-targeting, control siRNA and for the Aurora kinase B siRNA-treated cells were extracted using the Multi Target Analysis module of the INCELL1000. These parameters describe the DAPI nuclei stain and the cytoplasmic α-Tubulin stain of the two assay conditions. The Principle Component Analysis (PCA) was used to identify parameters that maximize the dynamic range between positive and negative controls.

# 2.3 RESULTS

## 2.3.1 High-content siRNA screen identifies novel human DUBs required for faithful mitosis.

In order to identify novel components of the ubiquitin system controlling mitotic division, we performed high-content visual siRNA screens in human cells. We were particularly interested in screening the ubiquitin factors from the family of deubiquitinating and ubiquitin binding proteins. The ubiquitin siRNA library targeting about 500 genes including about 100 known or predicted DUBs and other ubiquitin factors was used. To silence selected candidate genes a pool of four different siRNAs was used (Appendix Table 9).

It was shown previously that defects in mitosis lead to formation of irregular nuclei in the daughter cells[235,236]. We took the nuclear shape as a readout for our screen and considered the top hits as potential mitotic regulators. Cells were fixed and automatically analyzed by multi-parameter software for 40 different visual parameters including number of nuclei per single cell as well as shape of the nuclei (indicating possible defects in chromosome segregation), based on Principle Component Analysis (PCA). This novel approach allowed generating a hit-list of the ubiquitination system-related genes that may play a role in the regulation of cell division. Importantly, all our positive controls, such as Aurora B and Cullin 3 which roles in mitosis are already well described, scored high on the list. Notably, the hit-list contained also other proteins with established roles in chromosome segregation and cytokinesis, including APC, CUL4B and others, suggesting the relevance of the selected approach. Interestingly, a number of putative candidates for novel regulators of chromosome segregation and cytokinesis were identified using this approach. Among them, the DUB, Ubiquitin carboxyl-terminal esterase L3 (ubiquitin thiol-esterase), UCHL3, scored as the strongest hit in this analysis.

## 2.3.2    UCHL3 is important for maintenance of a proper nuclear shape.

To validate the results from the siRNA screen the silencing of UCHL3 was repeated using two single siRNAs from the pool. Additionally, we used siRNA to silence UCHL1, another member of the C-terminal hydrolase family to address the whether this is a common phenotype for all the members or whether it is specific to UCHL3. We observed that silencing of UCHL3 resulted in an increase of irregular and polylobed nuclei, but despite the high homology of UCHL1 to UCHL3, the nuclear shape was not affected by UCHL1 silencing. This led us to a conclusion that only UCHL3 plays a role in irregular nuclei maintenance (Figure 14A). We confirmed the efficiency of single siRNAs in depleting the target gene by western blot analysis (Figure 14B). Quantification of cells with irregular nuclei revealed that about 45 % of UCHL3 depleted cells display irregular nuclei compared to 18 % of control cells (Figure 14C).

In the beginning of my project, I wanted to further confirm the results from the siRNA screen using a different set of tools to rule out a possibility of the off-target effect of the siRNAs used. I silenced UCHL3 in unsynchronized HeLa cells by treatment with a different siRNA targeting the 3'UTR region of the UCHL3 mRNA (UCHL3 3'UTR) for 48 hours. Additionally, I inhibited UCHL3 hydrolase activity with a commercially available inhibitor (TCID) for 24 hours. As TCID has been shown to inhibit also UCHL1 at higher concentrations (IC=75μM), I used 2μM working concentration for the TCID inhibitor, to ensure specificity for UCHL3[215,230]. To quantify the effect of UCHL3 inhibition on the nuclear shape I took form factor as a criterion for regularity of the nucleus and I quantified it using Cell Profiler as described in the methods section. Both treatments (siRNA, TCID) lead to increased number of cells displaying irregular nuclei phenotype (Figure 15A, D). Upon treatment with 3'UTR siRNA I could see an increase in the irregular nuclei phenotype from 18 % in the control cells to 42 % in UCHL3 depleted cells (Figure 15B). The efficiency of the UCHL3 knockdown was confirmed by using western blot (Figure 15C). The effect of UCHL3 inhibitor was less pronounced, but I could still see an increased number of cells with irregular nuclei, from 19 % in the control cells to 29 % in TCID treated cells (Figure 15E).

-69-

A



B

C

Irregular nuclei
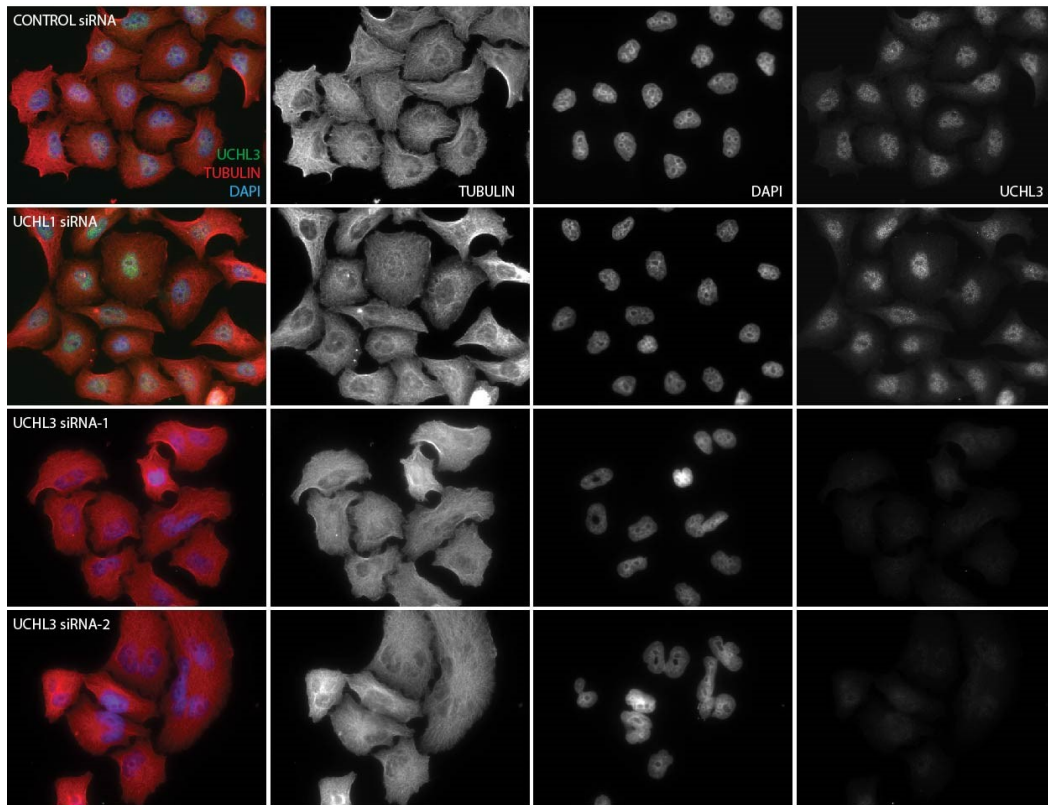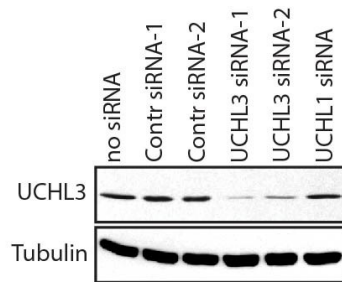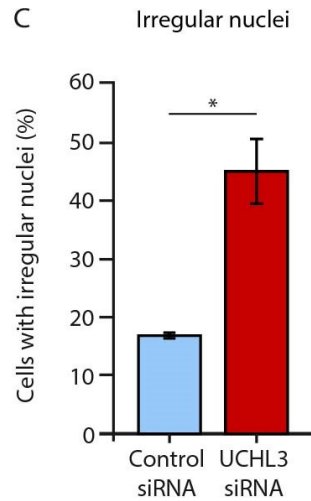


**Figure 14 Validation of the siRNA screen.**

(A) HeLa cells were transfected with control, UCHL1 and UCHL3 siRNA-1 and siRNA-2. After 48 hours cells were fixed and stained for tubulin (red), DAPI (blue) and UCHL3 (green).

(B) Western blot showing the efficiency of different siRNAs to downregulate UCHL3.

(C) Quantification of A. Graph shows percentage of cells displaying irregular nuclei phenotype.
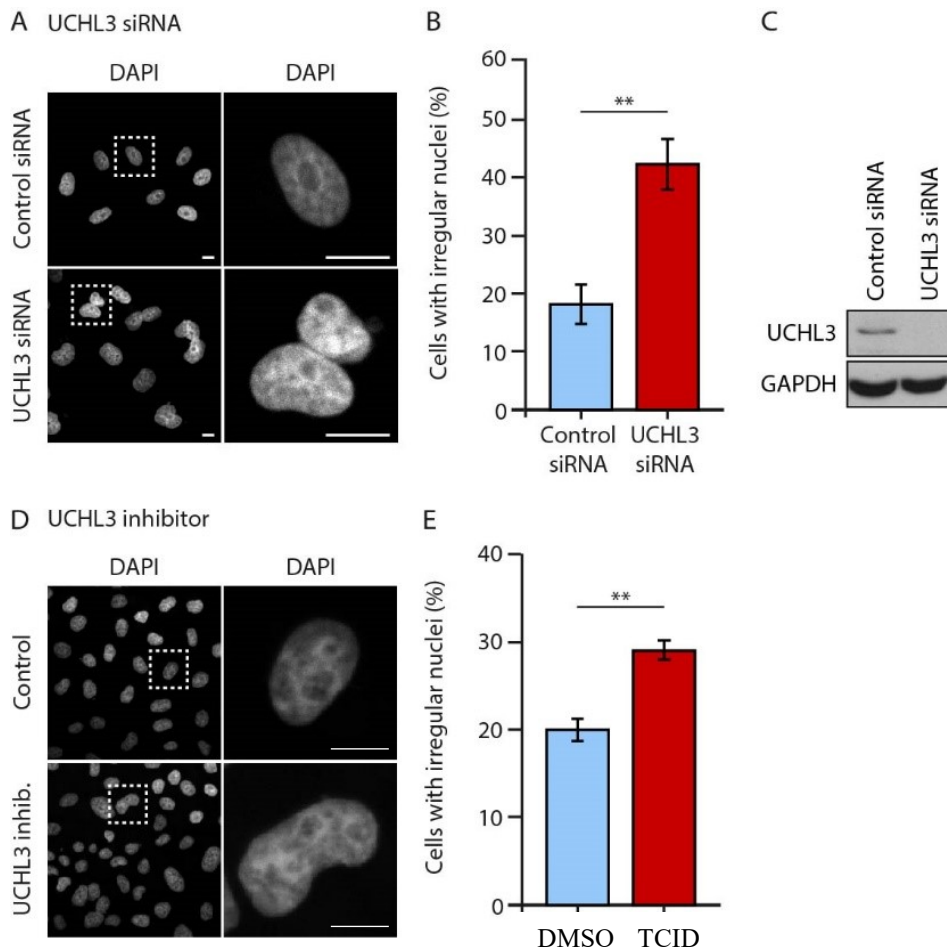
**Figure 15 UCHL3 downregulation or inhibition leads to irregular nuclei phenotype.**
(A) Representative image of HeLa cells treated for 48 hours with UCHL3 3'UTR siRNA. (B) Quantification of irregular nuclei phenotype using Cell Profiler. Control siRNA 18.3 % ± SEM 3.3 % and 3'UTR siRNA 42.3 % ± SEM 4.3 % cells with irregular nuclei, P= 0.0043. Graph represents four experiments with total number of analysed cells 886 in control and 828 in siRNA treated cells. (C) Western blot confirmation of the UCHL3 knockdown. (D) Representative image of HeLa cells treated for 24 hours with UCHL3 inhibitor (TCID). (E) Quantification of irregular nuclei phenotype using Cell Profiler. Control (DMSO) 19.5 % ± SEM 1.1 % and TCID 28.6 % ± SEM 1.1 % cells with irregular nuclei, P= 0.0012. Graph represents four experiments with total number of analysed cells 2110 in control and 2230 in siRNA treated cells. Scale bar represents 10 μm.

### 2.3.3 UCHL3 controls proper chromosome alignment during metaphase.

Since irregular nuclei are often observed due to segregation problems during mitosis, I hypothesized that UCHL3 could be a factor controlling chromosome alignment and their segregation. To answer my question whether UCHL3 regulates the early steps of mitosis, I needed to have a closer look at the mitotic progression in UCHL3 depleted cells. For my experiments I used HeLa cells transfected with 3'UTR siRNA against UCHL3. I synchronized the cells using monastrol release protocol. Monastrol inhibits Eg5, a motor protein necessary for centrosome separation and spindle formation, thereby arresting cells in prometaphase. Cells were synchronized by 16 hours of monastrol treatment, followed by wash and release into a proteasome inhibitor for 90 minutes. Degradation of securin and cyclin B is the key step necessary for the onset of anaphase, therefore the cells stayed arrested in the metaphase upon the inhibition of proteasome. This protocol (Figure 16A) enabled me to observe the chromosome alignment process during the 90 minute time-window as cells align their chromosomes and proceed from prometaphase to metaphase. After 90 minutes, I fixed the cells and counted the percentage of cells with aligned or misaligned chromosomes (Figure 16B). In the control situation, majority of the cells had no defects, up to 75 % of the cells aligned their chromosomes properly with only 25 % of cells displaying misalignment phenotype. After knockdown of UCHL3 there was a strong increase in cells showing misaligned chromosomes, as 45 % of cells did not manage to form a proper metaphase plate (Figure 16C). In contrast, UCHL3 depletion did not affect the formation of the bipolar mitotic spindle (Figure 16B). To our knowledge, these results present a first evidence that UCHL3 can regulate mitotic progression in human cells.
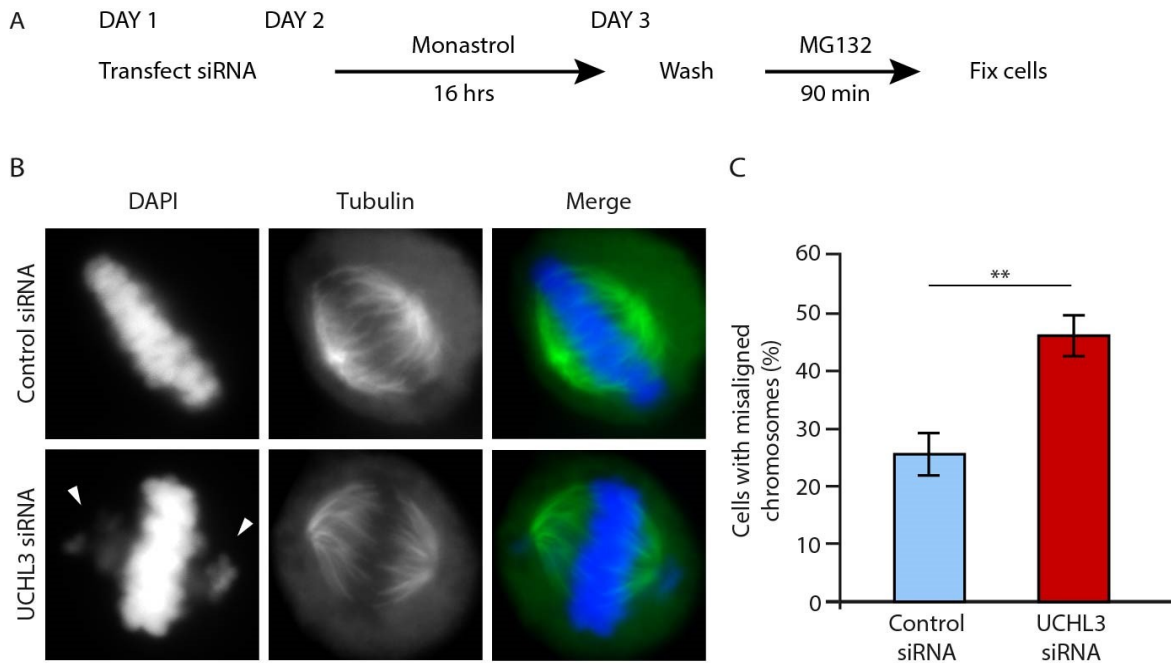
**Figure 16 UCHL3 controls chromosome alignment during metaphase plate formation.**

(A) Experimental setup: cells were transfected with control and 3'UTR UCHL3 siRNA 48 hours prior fixing.

(B) Representative images of HeLa cells treated for 48 hours with UCHL3 3'UTR or control siRNA and synchronized to metaphase according to the protocol in A. Cells were fixed and stained, α-tubulin (green), DNA (blue). (C) Quantification of B. Percentage of cells having at least one misaligned chromosome were counted in both categories. Graph represents results from seven experiments with total number of analysed cells 2356 in control and 2801 in siRNA treated cells. Control siRNA 25.2 % ± SEM 3.7 % and 3'UTR siRNA 45.4 % ± SEM 4.2 % cells with misaligned chromosomes, P= 0.0034.

## 2.3.4 UCHL3's catalytic activity is necessary for proper chromosome alignment.

To confirm that the observed phenotype is specific to downregulation of UCHL3 and to exclude a possible off-target effect of the siRNA, I performed rescue experiments with overexpression of UCHL3 cDNA from a plasmid. Additionally, I wanted to assess whether the UCHL3 catalytic activity is important for chromosome alignment. To this purpose I used two different N-terminal GFP-labelled UCHL3 protein expression constructs: 'UCHL3-WT', which contains a wild type cDNA sequence of UCHL3 and 'UCHL3-C/S' which has a mutation in the catalytic center of the protein (Cysteine 95 to Serine). This mutation renders the catalytic center inactive and abolishes the hydrolase activity of UCHL3. GFP expressing construct was used as a negative control. I transfected HeLa cells with 3'UTR siRNA together with GFP control or UCHL3-WT or UCHL3-C/S plasmid. I synchronized the cells to metaphase using monastrol release protocol (as shown in Figure 16A) and after fixing the cells I stained DNA with DAPI (Figure 17A). In parallel, I isolated proteins from a fraction of the cells for western blot analysis to confirm the expression levels of the introduced proteins. All ectopic proteins were expressed equally and on a level similar to the expression of the endogenous UCHL3 (Figure 17B). In each condition I counted the number of cells that had misaligned chromosomes. To avoid any bias, I quantified all my experiments in a blinded setup. In the cells transfected with empty-GFP plasmid, UCHL3 knockdown led again to increased number of cells showing misaligned chromosomes, this was rescued in cells expressing the GFP-UCHL3-WT protein. Interestingly, the expression of the catalytically dead mutant GFP-UCHL3-C/S did not rescue the phenotype and cells showed higher number of alignment defects compared to their controls (Figure 17C). Interestingly, catalytically dead version GFP-UCHL3-C/S did not affect chromosome alignment in WT cells, suggesting that this form cannot act as dominant negative mutant. From these experiments I conclude that UCHL3 specifically controls proper chromosome alignment at the metaphase plate and its catalytic activity is necessary for this process.
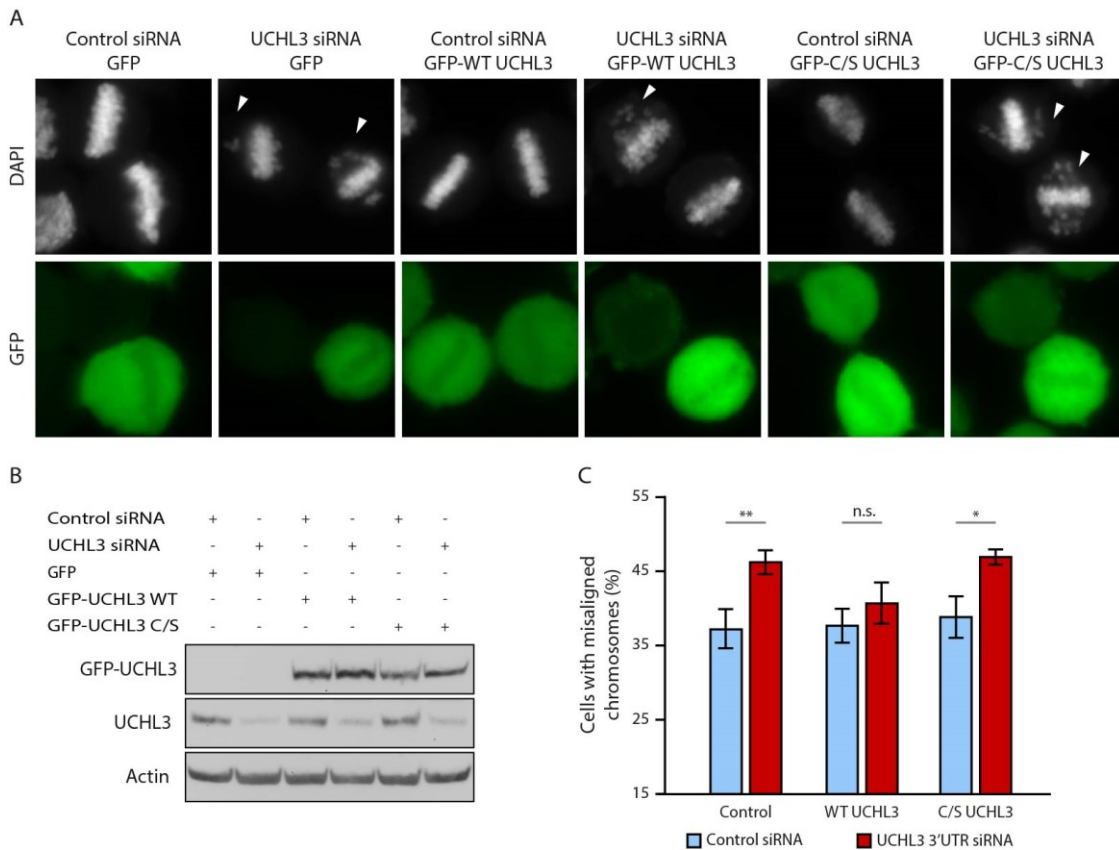
**Figure 17 Catalytic activity of UCHL3 is important for proper chromosome alignment.**

HeLa cells were transfected with control and 3'UTR UCHL3 siRNA 48 hours prior fixing the cells and synchronized to metaphase according to the protocol in Figure 16A. (A) Representative images showing chromosome alignment in different conditions. Arrowheads point to misaligned chromosomes. Cells transfected with GFP plasmids are shown in green. (B) Western blot showing expression levels of different UCHL3 proteins, probed with UCHL3 antibody with Actin as a loading control. (C) Quantification of A. Percentages of cells having at least one misaligned chromosome were counted in all categories (Appendix Table 5). Graph represents results from four individual experiments with average number of 2000 analysed cells per each condition. P values are P= 0.0242, P= 0.4306, P= 0.0366, respectively.

## 2.3.5 UCHL3 does not regulate Spindle assembly checkpoint (SAC) response in human cells.

The observed phenotypes of UCHL3 downregulation, the formation of irregular nuclei and chromosomal misalignment in metaphase are indicative of defects in chromosome segregation. Segregation errors, such as lagging chromosomes are deleterious for the cell and as such can have fatal consequences, therefore the cell strictly controls the alignment status prior to anaphase onset. This raised the question whether the UCHL3-depleted cells can properly activate SAC. To answer this, I focused mainly on two parameters: the ability of cells to maintain mitotic arrest induced by drugs perturbing proper spindle assembly and second, the ability to recruit checkpoint components to the kinetochores.

To address the first point, I treated cells with monastrol in which presence the bipolar spindle cannot be formed, resulting in increased number of attachment errors. This subsequently leads to a number of unattached or partially attached kinetochores, which activate the SAC and arrest the cells in prometaphase. To this purpose I used HeLa K cells where UCHL3 was silenced by stable expression of shRNAs (see Methods) and after 16 hours of monastrol synchronization I took photographs of living cells (Figure 18A) and I quantified the mitotic index (MI) for each condition. The average mitotic index was MI= 0.7 for both control and UCHL3 depleted cells showing no significant change between the two conditions (Figure 18B). Taken together, UCHL3 downregulation does not change the ability of cells to maintain the mitotic arrest.

Next, I measured the kinetochore intensity of BubR1, which is a key component of the mitotic checkpoint and is recruited to unattached kinetochores during prometaphase. I quantified the fluorescent signal of BubR1 and CREST in HeLa cells transfected with either control or UCHL3 siRNA, after synchronization to prometaphase by monastrol. I did not see any difference in BubR1 recruitment to kinetochores in control and UCHL3 depleted cells (Figure 18C, D), suggesting that UCHL3 is not directly involved in BubR1 recruitment to kinetochores. In conclusion, upon UCHL3 downregulation, the mitotic checkpoint is not affected during prometaphase, because cells are able to maintain mitotic arrest and to recruit mitotic checkpoint component BubR1 to kinetochores normally. These results indicate that UCHL3 is not involved in the spindle assembly checkpoint response.

-83-
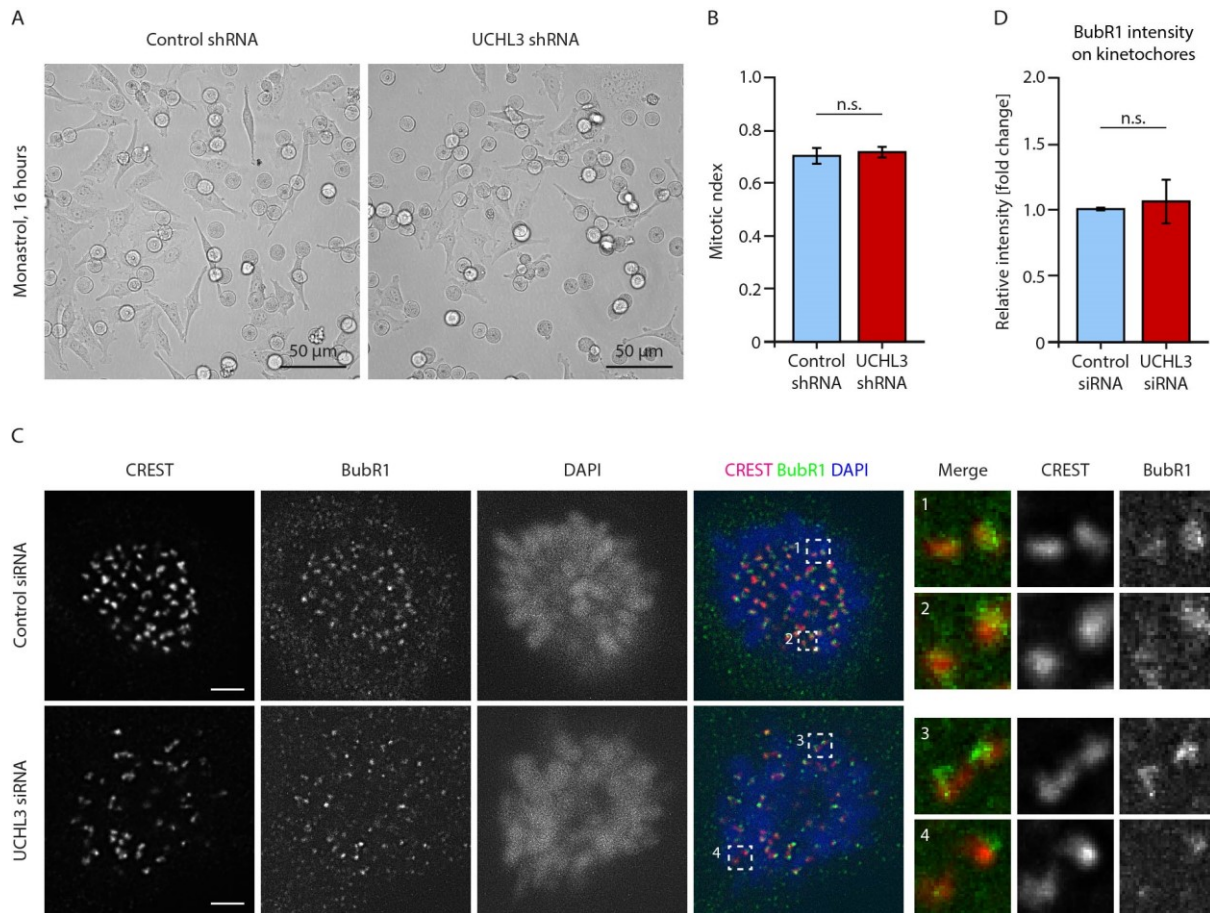
**Figure 18 UCHL3 does not regulate SAC response.**

(A) Representative phase contrast images of control (shLuc) and UCHL3 depleted cells (sh2 UCHL3). (B) Quantification of A, data from three different experiments, total number of cells counted: control n= 1384, sh2 UCHL3 n= 1288. Mitotic index, Mean ± SEM: control MI= 0.707 ± 0.018, sh UCHL3 MI= 0.718 ± 0.013, Statistical analysis by T-test, P= 0.6571. (C) HeLa K cells transfected with control or 3'UTR UCHL3 siRNA, scale bar= 2 μm. Left: IF images with antibodies against BubR1 (green) and CREST (red), co-stained with DAPI (blue). Right: Enlarged kinetochore regions showing co-localization of BubR1 (green) and kinetochore (red) signals. (D) Quantification of relative BubR1 intensity on kinetochores normalized to the control shown as Mean ± SEM, data from three different experiments. Control = 1, n= 2740 kinetochores, UCHL3 siRNA 1.06 ± 0.18, n= 2831 kinetochores. Statistical analysis by One-sample T-test, P= 0.7765.

-85-

## 2.3.6 UCHL3 regulates the chromosome alignment during prometaphase to metaphase transition.

To better understand the mechanism by which UCHL3 controls mitosis, it is important to understand the timing of these events. In my previous experiments, I was using siRNA for UCHL3 downregulation. This is a long treatment and cells undergo at least one division in the absence of UCHL3. Due to this fact, I could not exclude the possibility that UCHL3 acts during interphase and the resulting phenotype is just a consequence of earlier events. To rule out this scenario, I established a protocol where, instead of siRNA, I used TCID to inhibit UCHL3 for two different time-periods, and I employed the previously established protocol for monastrol release to assess the alignment of chromosomes at the metaphase plate. First, I added the UCHL3 inhibitor together with monastrol for 16 hours and subsequently after the washout for 90 minutes. In the second condition, I added the UCHL3 inhibitor only after the washout and incubated cells for 90 minutes (Figure 19A). Using this approach, I could distinguish whether UCHL3 acts directly in prometaphase to metaphase or earlier in the cell cycle. To better visualize the positions of individual chromosomes, I performed the experiment in HeLa cells stably expressing GFP labelled CENP-A kinetochore protein and after fixing the cells, I stained DNA using DAPI (Figure 19B) and for each condition I counted the number of cells that had misaligned chromosomes. Data are presented as a fold increase relative to the control. In the first group, labelled 'Long-term treatment', I could observe 50% increase of cells that did not align their chromosomes properly, fold change from 1.0 to 1.5, which corresponds to 25 % and 38 % cells with misalignments in DMSO and TCID treatment, respectively (Figure 19C). These results are very similar to the results obtained with UCHL3 siRNA where I also observed about 50% increase in cells having misaligned chromosomes (fold change from 1.0 to 1.55). Interestingly, after the 90 minutes treatment with UCHL3 inhibitor, labelled 'Short-term treatment', I could observe about 40% increase of cells that did not align their chromosomes properly. Fold change from 1 to 1.39, representing an increase from 35 % to 47 % cells with alignment problems in control and UCHL3 inhibition, respectively (Figure 19D). Taken together, 90 minutes of UCHL3 inhibition is sufficient to induce the misaligned chromosomes phenotype and this short treatment has a similar effect as 17.5 hours treatment with UCHL3 inhibitor or 48 hours of siRNA-mediated downregulation of UCHL3. This result confirms the initial hypothesis that UCHL3 regulates chromosome alignment during prometaphase to metaphase transition.
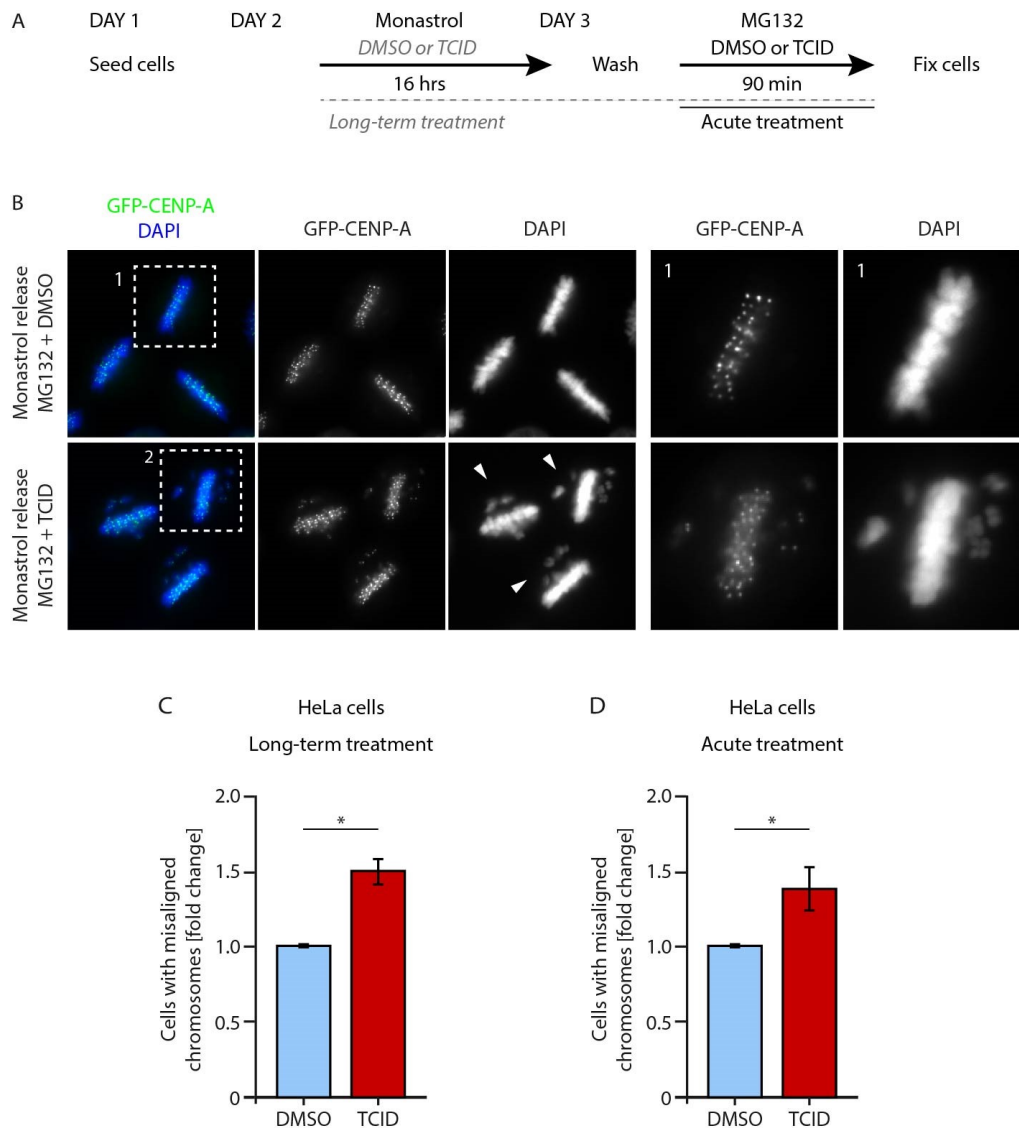
**Figure 19 UCHL3 acts specifically during prometaphase to metaphase transition.**

All experiments were done using HeLa cells stably expressing GFP-CENP-A. (A) Experimental design for cell synchronization and UCHL3 inhibition. (B) Representative images showing chromosome alignment after 17.5 hours of treatment with UCHL3 inhibitor. GFP-CENP-A (green), DNA stained with DAPI (blue). (C) Quantification of B – Long term treatment. The graph represents three different experiments and shows the fold increase of cells having misaligned chromosomes. Control (DMSO) 1.0, UCHL3 inhibition (TCID) $1.50 \pm$ SEM 0.06, P= 0.0157, total number of analyzed cells: 830 in control and 1090 upon UCHL3 inhibition. (D) Quantification of Short-term treatment. The graph represents five different experiments and shows the fold increase of cells having misaligned chromosomes. Control (DMSO) 1.0, UCHL3 inhibition (TCID) $1.39 \pm$ SEM 0.13, P= 0.0394, total number of analyzed cells: 1260 in control and 1541 upon UCHL3 inhibition.

-89-

## 2.3.7 UCHL3 is indispensable for the chromosome alignment in human primary cells.

I wanted to investigate if the mechanism of UCHL3 action is also relevant for human primary cells. Until now, I was using HeLa cells for my experiments, which are of cancer origin and therefore I wanted to understand whether this is a unique feature of cancer cells or whether UCHL3 is also important for division of primary cells. To address this question, I selected IMR90 (human primary lung fibroblasts) as a new model to study the UCHL3 function. I used the standardized protocol for monastrol release (Figure 20A) and I treated the cells with UCHL3 inhibitor (TCID). After releasing cells from monastrol, I fixed them using PFA and stained with antibodies against CREST and tubulin and co-stained DNA with DAPI (Figure 20B). In all conditions I quantified the number of cells displaying at least one misaligned chromosome and normalized the results to their respective controls. In the long-term treatment, I observed 34% increase in cells having alignment defects which corresponded to increase from 42 % in the control to 54% in UCHL3 inhibited cells (Figure 20C). In the short-term treatment, after 90 minutes with UCHL3 inhibitor, I observed 43% increase in cells having misaligned chromosomes, which represents increase from 38 % in controls to 53 % in UCHL3 inhibited cells (Figure 20D).

Thus, 90 min treatment with UCHL3 inhibitor is sufficient to induce the same phenotype as long-term treatment, confirming the hypothesis that UCHL3 activity is needed during the prometaphase to metaphase transition. Taken together, UCHL3 controls chromosome alignment not only in cancer cells, but also in human primary fibroblast, suggesting a fundamental role of UCHL3 in the control of chromosome segregation in human cells.
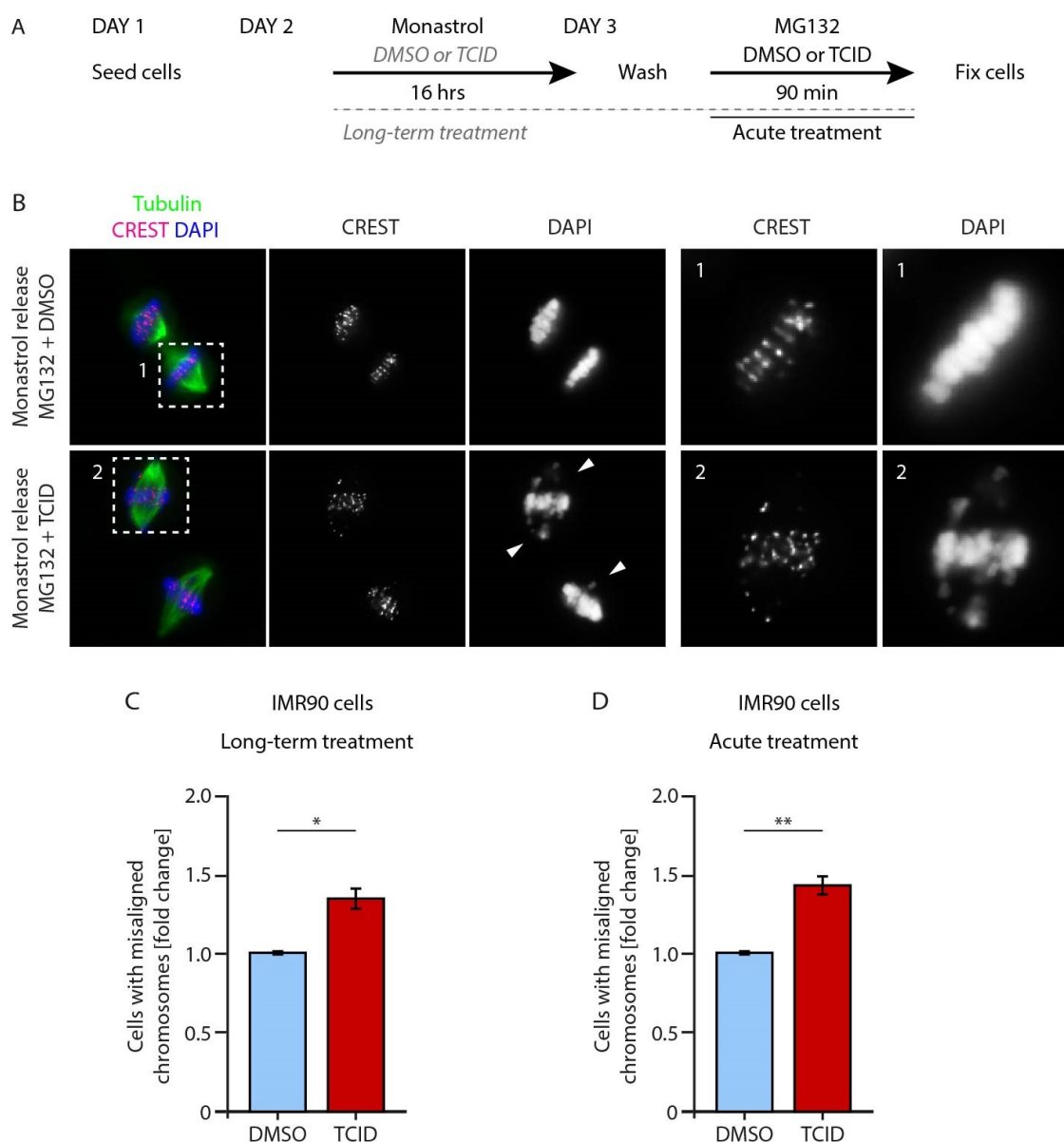
**Figure 20 UCHL3 controls chromosome alignment in human primary fibroblasts, IMR90.**
All experiments were done using IMR90 cells. (A) Experimental design for cell synchronization and UCHL3 inhibition. (B) Representative images showing chromosome alignment after 17.5 hours of treatment with UCHL3 inhibitor. Cells were fixed and stained, α-tubulin (green), CREST (red), DNA stained with DAPI (blue). (C) Quantification of B – Long term treatment. The graph represents three different experiments and shows the fold increase of cells having misaligned chromosomes. Control (DMSO) 1.0, UCHL3 inhibition (TCID) 1.34 ± SEM 0.07, P= 0.0190, total number of analyzed cells: 1378 in control and 1541 upon UCHL3 inhibition. (D) Quantification of Short-term treatment. The graph represents five different experiments and shows the fold increase of cells having misaligned chromosomes. Control (DMSO) 1.0, UCHL3 inhibition (TCID) 1.43 ± SEM 0.06, P= 0.0055, total number of analyzed cells: 951 in control and 994 upon UCHL3 inhibition.

## 2.3.8 UCHL3 protein is indispensable for proper chromosome segregation.

In my previous experiments, I have confirmed that UCHL3 plays an important role in proper chromosome alignment at the metaphase plate. Next, I wanted to understand if this has a functional consequence and the alignment problems result in segregation errors later during the anaphase. To answer this question, I used live-video microscopy to be able to follow individual cells in time. First, I used HeLa cells stably expressing GFP-tubulin to visualize the spindle and mCherry-Histone H2B (mCherry-H2B) to follow the chromosomes. I used control and 3'UTR UCHL3 siRNA for 48 hours to downregulate UCHL3 and I determined the efficiency of the knockdown by qPCR which showed that the levels of UCHL3 mRNA dropped to 20% upon siRNA treatment (Figure 21E).

I synchronized the cells into prometaphase by adding monastrol for 16 hours and after the monastrol washout I acquired time-lapse images every five minutes for four hours. Representative time frames are shown in Figure 21A, where the presence of polar chromosomes can again be observed in the UCHL3 knockdown, similar to my previous results with siRNA and the UCHL3 inhibitor. In these live video experiments, I was quantifying two main parameters: presence of segregation errors and time the cells needed to transit from prometaphase to anaphase onset. In control situation, cells could divide normally, they aligned their chromosomes at the metaphase plate and segregated them equally to the two daughter cells. In the cells depleted of UCHL3, I could observe, in addition to the alignment defects, frequent segregation errors, mainly lagging chromosomes. Examples of segregation errors are shown in Figure 21B. I counted the total number of cells showing lagging chromosomes in both conditions and I could see a significant increase in cells with segregation errors upon UCHL3 downregulation, from 17 % in the control to 39 % in the knockdown (Figure 21C). These results further confirm that UCHL3 controls chromosome alignment during metaphase plate formation as well as their subsequent segregation to the two daughter cells.

Next, I measured the time the cells needed to proceed from prometaphase (time of the release was set as time = 0) to anaphase. I did not observe any significant difference in the timing between the control and UCHL3 knockdown, but there was a non-significant tendency for UCHL3 depleted cells to take longer time to reach anaphase. Control cells needed on average 64 minutes to reach anaphase compared to UCHL3 depleted cell which needed on average 70 minutes (Figure 21D, Figure 22F). These results further confirmed my initial observation that

UCHL3 controls chromosome alignment. Furthermore, I was able to show that the alignment problems are followed by segregation errors in UCHL3 depleted cells and therefore UCHL3 is indispensable for proper chromosome segregation.
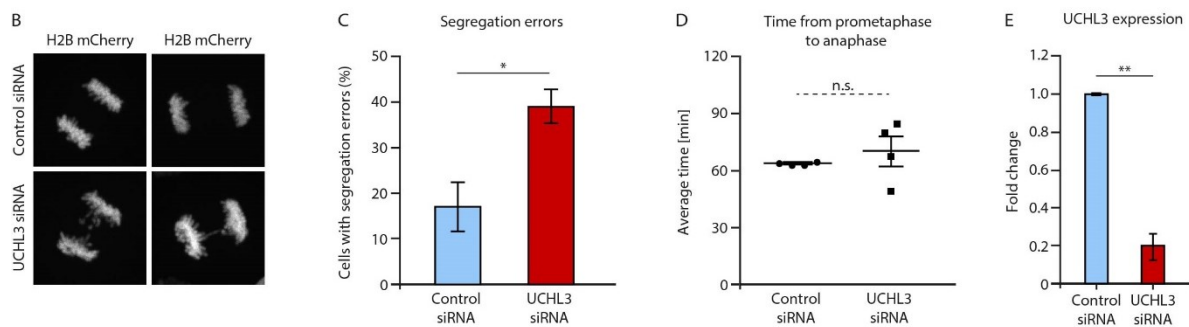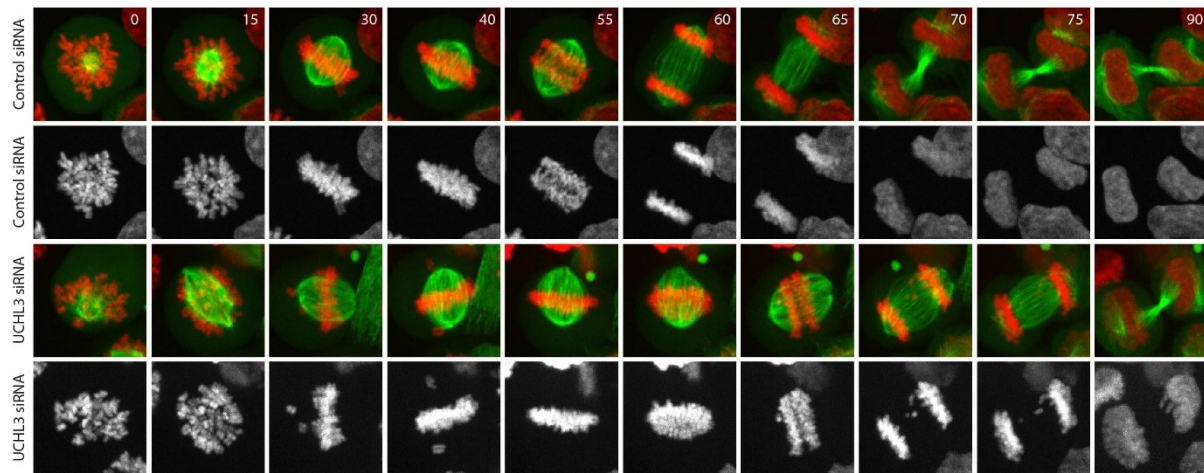
**Figure 21 Live video experiments show that UCHL3 depletion leads to segregation errors.**

Live video experiment using HeLa K cells stably expressing Tubulin-GFP and H2B-mCherry synchronised to prometaphase by monastrol and released in fresh culture medium at t=0 of the acquisition. (A) Selected time-frames of control and UCHL3 depleted cells showing merge of Tubulin (green) and DNA (red) signal and DNA single channel (grey). (B) Examples of segregation errors often observed upon UCHL3 KD. (C) Quantification of segregation errors shown as mean percentage of cells with errors ± SEM of four different experiments. Control 17.07 % ±5.92 % n= 127 cells, UCHL3 KD 39.01 % ± 3.78 % n= 198 cells. Statistical analysis by Student's t-test, p= 0.0354. (D) Quantification of the average time the cells needed to proceed from prometaphase to anaphase shown as mean time ± SEM. Control 63.8 min ± 0.4 min, UCHL3 KD 70.4 min ± 7.0 min. Statistical analysis by Student's t-test, P= 0.4450. (E) qPCR analysis of cells transfected with siRNA to estimate the knockdown efficiency.

In order to confirm the results obtained with HeLa cells in a different experimental model, I used the colorectal adenocarcinoma cells (Dld1) that stably express histone H2B-mCherry and control or UCHL3 shRNA (see Methods and Appendix Table 1). I verified the UCHL3 knockdown using qPCR and I chose UCHL3 shRNA2 for my further studies (Figure 22E). The advantage of this approach is that the cells expressing the shRNA express GFP at the same time, so it is possible to distinguish the cells with the knockdown from the wild type ones.

To synchronize the cells, I used the monastrol washout protocol and I was acquiring images every five minutes during four hours. Representative time frames are shown in Figure 22A, where we can see the polar misaligned chromosomes in UCHL3 depleted cells in prometaphase and the lagging chromosomes during anaphase. I quantified the same parameters as for HeLa cells: the number of segregation errors and the time that cells needed to go from prometaphase to anaphase. Interestingly, the results were very similar to the ones obtained with HeLa, I could observe increase in cells showing segregation errors upon knockdown of UCHL3 (Figure 22B). I quantified the number of cells displaying segregation errors and I could see a significant increase of lagging chromosomes from 26 % in controls to 51 % in UCHL3 depleted cells (Figure 22C). I also counted the time the cells needed to proceed from prometaphase to anaphase, but despite a strong tendency of the UCHL3 depleted cells to take longer time to reach anaphase (59 min in control vs. 69 minutes in UCHL3 knockdown), the difference of duration did not reach statistical significance (Figure 22D). When I plotted the values from all experimental replicates together, in both cell lines I could see a strong tendency for the UCHL3 depleted cells to take longer time before reaching anaphase. In wild type situation the majority of cells divides within 75 minutes, therefore I set the threshold at 75 minutes and calculated the percentage of cells that did not manage to divide within this time period. In HeLa K as well as in Dld1 cells I could see a higher percentage of cells that did not divide within 75 minutes upon UCHL3 downregulation. In UCHL3 depleted HeLa cells 31 % cells did not divide before the 75 minutes compared to 21 % cells in control (Figure 22F) and in Dld1 cells 47 % of cells did not divide before 75 minutes compared to only 15 % of cells in the control (Figure 22G). Taken together, the results from the two different experimental approaches show that UCHL3 controls chromosome alignment as well as chromosome segregation during mitosis and that UCHL3 downregulation does not lead to significant changes in the duration of mitosis.
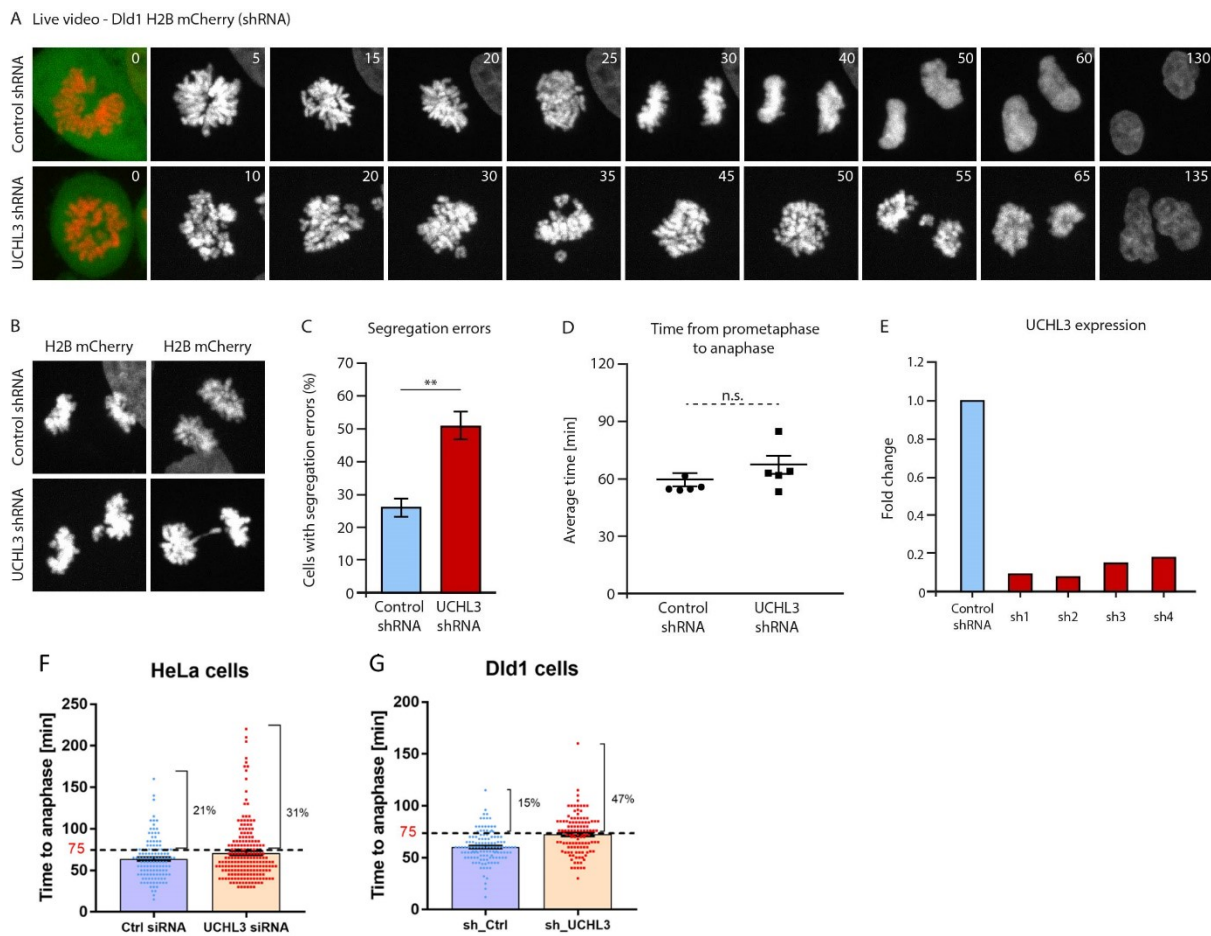
**Figure 22 UCHL3 controls chromosome segregation in human Dld1 cells.**

Live video experiment using Dld1 cells stably expressing H2B-mCherry and either control GFP-shRNA (shLuc) or UCHL3 GFP-shRNA (sh2). Cells were synchronised to prometaphase by Monastrol and released in fresh culture medium at t=0 of the acquisition. (A) Selected time-frames of Control and UCHL3 depleted cells. Frame t=0 shows DNA (red) and shRNA expression (green), following panels show DNA (grey). (B) Examples of segregation errors often observed upon UCHL3 downregulation. (C) Quantification of segregation errors shown as Mean percentage of cells with errors ± SEM of five different experiments. Control 26.1 % ± 3.2 % n= 125 cells, UCHL3 KD 50.7 % ± 5.4 % n= 118 cells. Statistical analysis by T-Test, P= 0.0069. (D) Quantification of the average time the cells needed to proceed from prometaphase to anaphase shown as Mean time ± SEM. Control 59.2 min ± 1.2 min, UCHL3 KD 68.7 min ± 4.5 min. Statistical analysis by T-Test, P= 0.1299. (E) qPCR analysis of cells transfected with shRNA to estimate the knockdown efficiency. Dld1 cells expressing sh2 UCHL3 were used for all live video experiments. (F-G) Summary of mitotic duration for individual cells from all experimental replicates. The percentage represents the number of cells that needed more than 75 minutes to reach anaphase. Comparison of two different cell lines, HeLa K (F) and Dld1 (G).

## 2.3.9 UCHL3 protein stabilizes KT-MT attachments by promoting the Astrin and CENP-E recruitment.

Next, I analyzed the kinetochore- microtubule (KT-MT) attachments, because both, prematurely stabilized kinetochore attachments to spindle microtubules, or weak attachments were reported to lead to segregation problems. To address the stability of KT-MT attachment, I used Astrin recruitment as a readout, because Astrin is only recruited to the kinetochores with stably attached microtubules. I transfected HeLa cells with control and UCHL3 siRNA and synchronized them in metaphase, using monastrol release protocol. (Figure 23A, B). I used Cell Profiler to quantify the intensity of the kinetochore (CREST) and Astrin signal in the control and in the UCHL3 depleted cells. As UCHL3 downregulation leads to increased number of misaligned chromosomes, I wanted to distinguish the recruitment of kinetochore proteins between aligned and misaligned chromosomes. Therefore, I selected two categories in UCHL3 knockdown cells: Aligned (chromosomes in the metaphase plate) versus misaligned (polar chromosomes) and I categorized them manually, assigning the alignment status (A, M) to each measured intensity (Methods and Appendix Figure 34). Interestingly, UCHL3 downregulation led to reduced recruitment of Astrin to the kinetochores of both, aligned and misaligned, chromosomes. In the absence of UCHL3, I observed 20% decrease in Astrin recruitment to the kinetochores of aligned chromosomes and even more dramatic decrease (up to 40%) of Astrin recruitment to the kinetochores of misaligned (polar) chromosomes (Figure 23C). I co-stained the cells with antibody against α-tubulin to be able to observe the kinetochore attachments. Overall the tubulin signal looked different in UCHL3 depleted cells compared to control cells. I observed that microtubules were more frequently spanning the equatorial zone in UCHL3 depleted cells (Figure 24A), suggesting that microtubules grow longer and form bipolar end-on attachments less often. As these attachments are necessary for proper positioning of chromosomes and formation of the metaphase plate, this could result in the observed alignment errors. To estimate the kinetochore attachment status in more detail, I processed tubulin and CREST images using Imaris software, which let me to reconstruct the images in 3D. I observed increased number of lateral attachments in UCHL3 depleted cells and polar chromosomes were often completely unattached (Figure 24B). Interestingly, downregulation of UCHL3 resulted in elongated spindle (Figure 24C). I measured the inter-polar distance in Image J and I observed that control spindle measured 6.5 μm on average and

the spindle of UCHL3 depleted cells was significantly longer and measured 8.3 µm on average (Figure 24D).

These results suggest that UCHL3 is important for proper KT-MT attachment. Absence of UCHL3 results in weaker KT attachment to the spindle microtubules and also leads to increased number of lateral attachments and altered spindle morphology, which could explain the segregation defects.
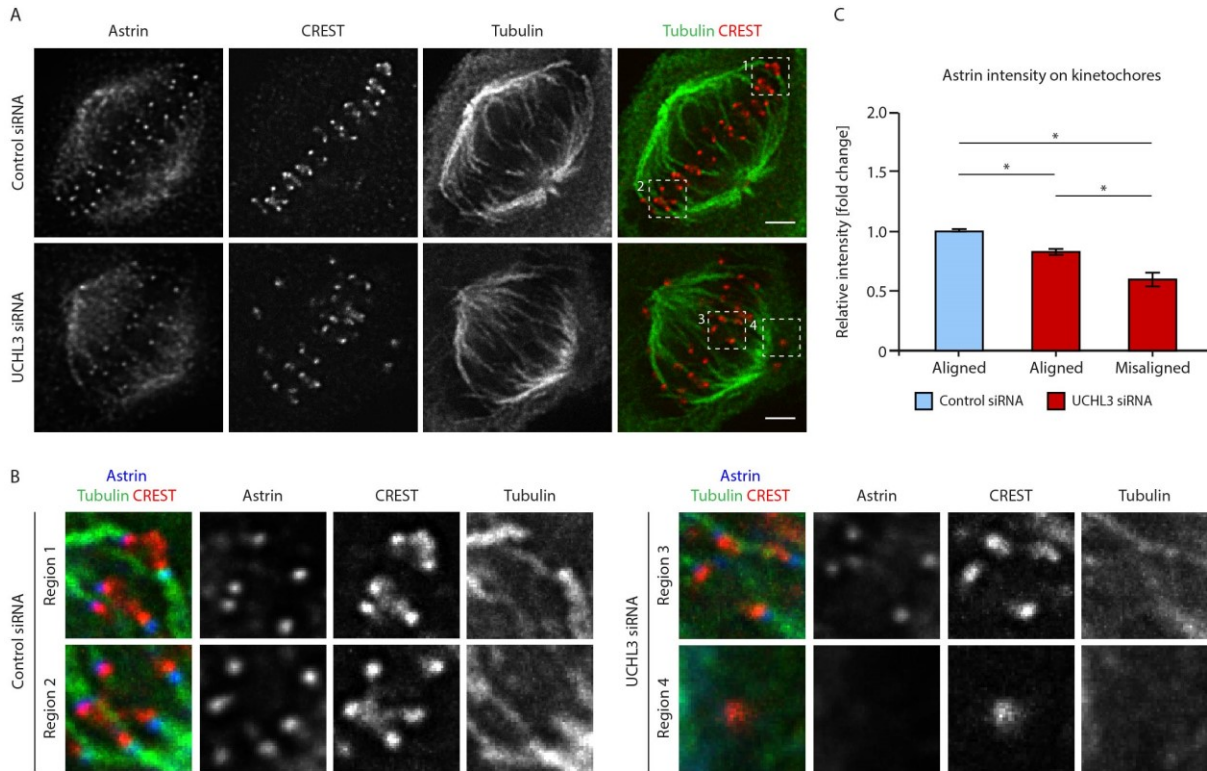
**Figure 23 UCHL3 promotes Astrin recruitment to the kinetochores.**

(A) Representative images of Tubulin, Astrin and CREST immunofluorescent staining. (B) Enlarged regions from A, showing Astrin (blue) localization to the kinetochores (red). (C) Quantification of A, relative Astrin intensity on kinetochores in four different experiments shown as Mean ± SD. Control = 1, n= 4017 kinetochores, UCHL3 siRNA Aligned = 0.82 ± 0.06, n= 3962 kinetochores, UCHL3 siRNA Misaligned = 0.59 ± 0.07, n = 470 kinetochores, p values: Control to KD Aligned p= 0.0114, control to KD misaligned p= 0.0107, KD Aligned to KD misaligned p= 0.0244.
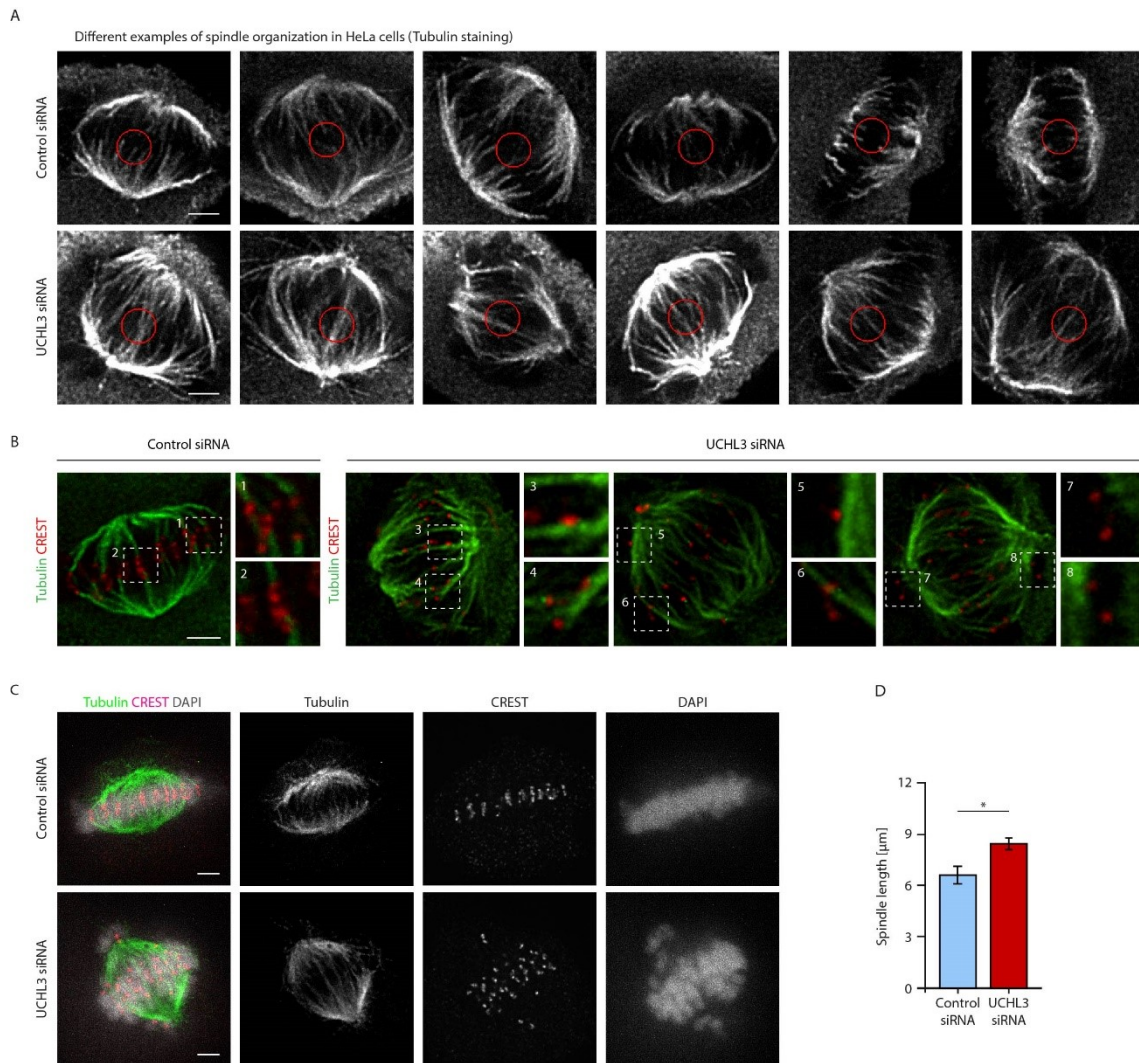
**Figure 24 UCHL3 promotes formation of bipolar stable kinetochore- microtubule attachments.**
Spindle microtubules in HeLa K cells transfected with control or UCHL3 3'UTR siRNA and synchronised by monastrol release protocol. Scale bar = 2 µm. (A) Examples of Tubulin staining showing the density of spindle microtubules in the central equatorial zone (red circle). (B) Examples of kinetochore- microtubule attachments in control and UCHL3 knockdown. 1-2 End-on attachments, 3-6 lateral attachments, 7-8 unattached kinetochores. (C) Representative images showing Tubulin (green), CREST (red) and DAPI (grey) staining. (D) Measurement of spindle length in C, represented by Mean ± SEM of six different experiments, control: spindle length= 6.56 µm ± 0.61 µm, UCHL3 siRNA: spindle length= 8.35 µm ± 0.25 µm. Statistical analysis by Student's t-test, p=0.0451.

It has been previously shown that Astrin is important for CENP-E recruitment to the kinetochores, which helps to maintain the chromosomes aligned at the metaphase plate[237]. Therefore, I decided to look at CENP-E recruitment to kinetochores in presence and absence of UCHL3 using HeLa K cells and monastrol release protocol combined with IF protocol for motor protein staining (Figure 25A, B). I measured the intensities of CREST and CENP-E signals and I plotted them as relative intensity (ratio of CENP-E to CREST signal) normalized to the control. Upon UCHL3 knockdown I observed about 40 % decrease of CENP-E recruitment to the kinetochores of aligned chromosomes. This is in line with the previous experiments where I observed reduced Astrin recruitment to kinetochores upon UCHL3 depletion which is necessary for the proper CENP-E recruitment to kinetochores. Surprisingly, I could observe more CENP-E present on the kinetochores of misaligned chromosomes and CENP-E signal was also enriched at the spindle. I quantified the relative kinetochore intensity of CENP-E on the polar chromosomes and I observed about 30% enrichment of CENP-E signal in the polar region compared to its intensity in control cells (difference not statistically significant, Figure 25C), which suggests that UCHL3 normally has an inhibitory action on CENP-E recruitment on the polar chromosomes. Next, I wanted to know whether CENP-E decrease on the aligned chromosomes correlates with reduced recruitment of Astrin to these structures. For this purpose, I co-stained HeLa cells with CENP-E and Astrin antibody together and measured signal intensities and I calculated their relative intensities to CREST. For each treatment condition I plotted the relative intensities on a dot plot. As expected, upon UCHL3 knockdown, I observed less Astrin recruitment to the kinetochores, which was proportional to the CENP-E recruitment (Figure 25D). Those results suggest that UCHL3 regulates kinetochore microtubule attachment stability by promoting Astrin and subsequently also CENP-E recruitment to the kinetochores, which increases the stability of microtubule attachment and maintains proper chromosome alignment in metaphase plate.
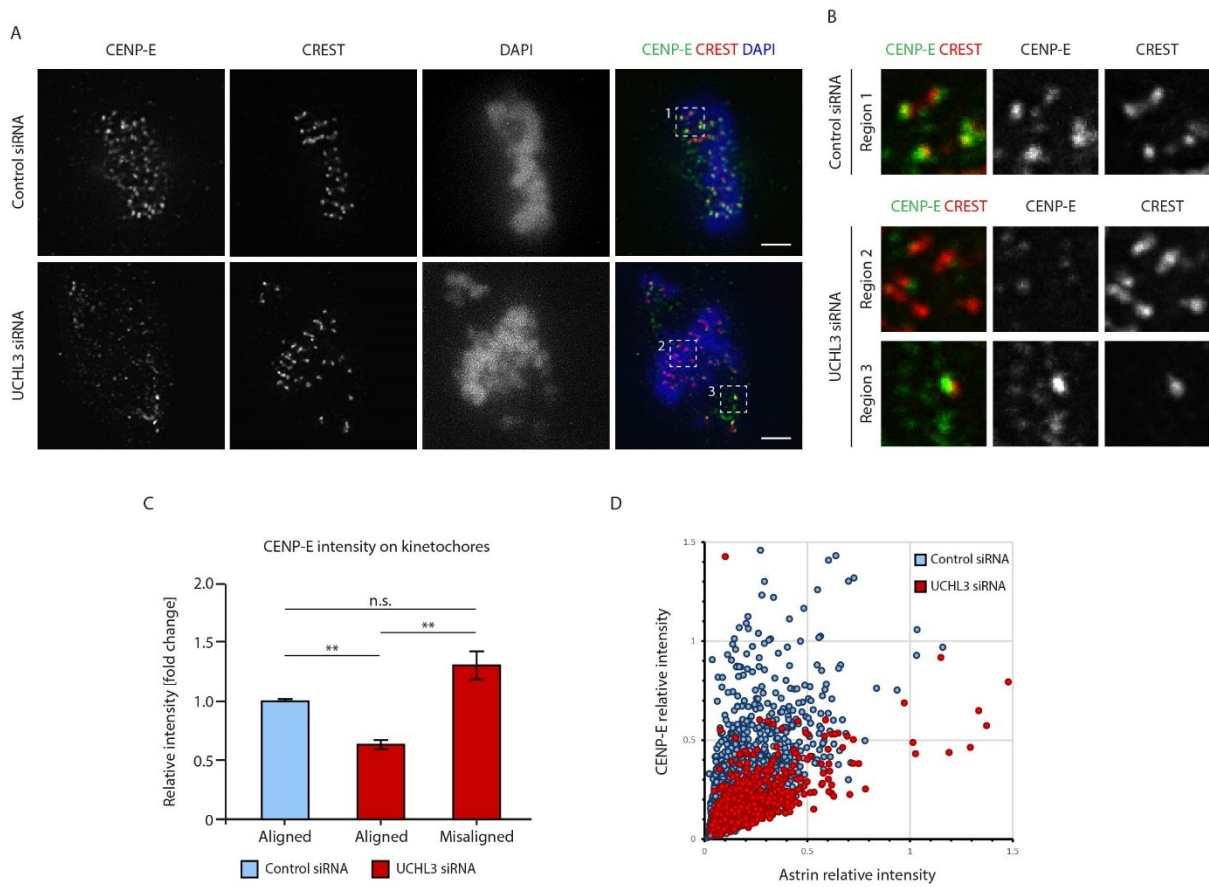
**Figure 25 UCHL3 is important for CENP-E recruitment to the metaphase kinetochores.**

(A) Representative images of CENP-E and CREST immunofluorescent staining. (B) Enlarged regions from A, showing CENP-E (green) localization to the kinetochores (red). (C) Quantification of A, relative CENP-E intensity on kinetochores in five different experiments shown as Mean ± SEM. Control = 1, n= 5846 kinetochores, UCHL3 siRNA Aligned = 0.61 ± 0.05, n= 5534 kinetochores, UCHL3 siRNA Misaligned = 1.29 ± 0.14, n = 855 kinetochores. P values: Control to KD Aligned p= 0.0019, control to KD misaligned p= 0.1025, KD Aligned to KD misaligned p= 0.0018. (D) Dot plot showing proportional decrease of CENP-E and Astrin intensities upon UCHL3 siRNA. Control n= 1770 kinetochores, UCHL3 siRNA n= 1669 kinetochores.

## 2.3.10  UCHL3 interacts with the mitotic kinase Aurora B and deubiquitinates it.

After establishing the UCHL3 function in mitosis, I aimed to understand what could be the potential substrate of UCHL3 that mediates its mitotic function. In order to answer this question, I followed two approaches, a candidate approach and an unbiased approach by Mass Spectrometric analysis.

UCHL3 is a DUB and therefore it is possible that it regulates protein levels of key mitotic elements. Based on the observed phenotypes, there are several candidates that could be regulated by UCHL3 activity, such as Aurora B kinase, PP1γ phosphatase or CENP-E motor protein, which all contribute to proper chromosome alignment at the metaphase plate. To see if levels of these proteins in mitosis are affected by the presence or absence of UCHL3, we used HeLa cells with or without CRISPR-Cas9 generated UCHL3 deletion. We synchronized these cells by monastrol washout protocol, collected total protein at different time points (0, 15, 30, 45 minutes) after the release and subjected them to western blot analysis (Figure 26A). We used Cyclin B as an internal control of the synchronization protocol, because it is degraded during anaphase by the proteasome. We did not observe any significant changes in protein levels of Aurora B, PP1γ and CENP-E, but we observed a strong degradation of Cyclin B at the last time-point, as expected. These results suggest that protein levels of neither of the candidates are regulated by UCHL3 mediated proteolytic degradation during the process of chromosome alignment and segregation. Interestingly, we observed a striking phenotype when we analyzed Aurora B signal on a full membrane. In time points 0 and 15 minutes after wash from monastrol, we observed a clear upshifted band at a size around 75 kDa and a smearing signal, characteristic for presence of ubiquitin conjugates, in cells deficient for UCHL3. Indeed, the size of Aurora B with four ubiquitin moieties is 74 kDa, which brought and interesting hypothesis that UCHL3 might specifically interact with Aurora B to deubiquitinate it.

In parallel, to perform an unbiased search for UCHL3 substrates, we performed immunoprecipitation experiment with GFP tagged wild-type and catalytically dead UCHL3 and Mass Spectrometry analysis. Interestingly, Aurora B was on the hit list among the identified candidate for UCHL3-interacting proteins, which encouraged us to further study the UCHL3-Aurora B relationship in greater detail. First, I wanted to validate the result from Mass Spectrometry and to confirm whether UCHL3 directly interacts with Aurora B. I performed immunoprecipitation experiments in the same setup as for the Mass Spectrometry analysis, but

instead of overexpressing protein by transient transfection, I used HeLa cell lines stably expressing either wild-type UCHL3 or catalytically dead mutant with GFP tags and synchronized them in prometaphase using STLC. Both proteins, UCHL3 WT and UCHL3 mutant bound Aurora B (Figure 26B). I repeated the experiment three times, using different clones of UCHL3 WT and UCHL3 C/S stable cell lines and in all cases I saw an interaction of Aurora B with both UCHL3 forms which indicates that Aurora B could be a potential substrate of UCHL3 during prometaphase.

Next, we aimed to understand if Aurora B is deubiquitinated by UCHL3, therefore we established IP under denaturing conditions to be able to observe only covalently bound ubiquitin conjugates. We used either control or UCHL3 knockout cell lines and we transfected them with GFP-Aurora B plasmid. After 24 hours we collected the proteins using GFP-trap beads and analyzed the samples by western blot (Figure 26C). To detect ubiquitinated Aurora B, we used FK2 ubiquitin antibody that specifically recognizes only conjugated ubiquitin and not the free ubiquitin. In line with previous WB experiments, we saw a stronger ubiquitin signal on Aurora B in the absence of UCHL3. Taken together, we hypothesize that UCHL3 interacts with Aurora B and deubiquitinates it during prometaphase to metaphase transition. Because the levels of Aurora B remained unchanged upon knockout of UCHL3, this ubiquitination appears to be a non-proteolytic type. In the next experiments, we would like to study, how this ubiquitination affects the Aurora B activity and localization.
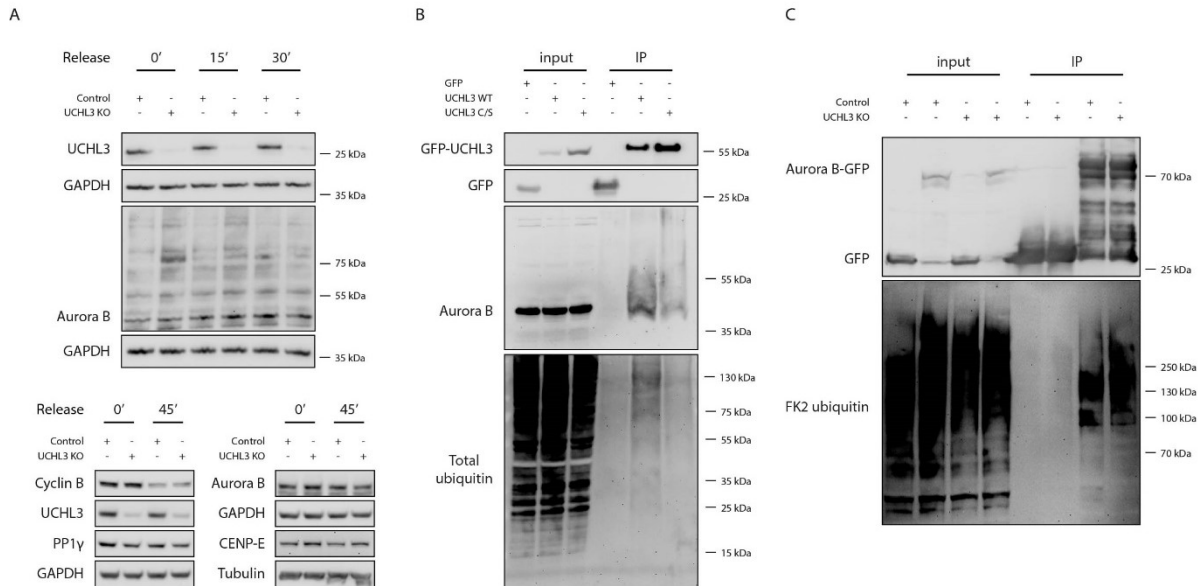
**Figure 26 UCHL3 interacts with Aurora B and deubiquitinates it.**

(A) Control and UCHL3 knockout (KO) HeLa K cells were synchronized by monastrol for 16 hours and after washout cells were released into fresh medium for 15, 30 or 45 minutes and analysed by western blot. (B) HeLa K cells stably expressing, GFP, GFP-UCHL3-WT or GFP-UCHL3-C/S were synchronized by STLC and after 16 hours collected for IP with GFP-Trap beads. (C) IP under denaturing conditions. Control and UCHL3 KO cells were transfected by Aurora B-GFP plasmid, synchronized by monastrol and collected for IP with GFP-Trap beads. Membranes were probed with GFP and FK2 antibody against conjugated ubiquitin.

# 2.4   DISCUSSION

During my PhD, I described a completely new role for the deubiquitinase UCHL3 protein during mitosis. Up to date only limited number of DUBs has been described to regulate mitosis including USP44, USP7 and USP39[176,238,239]. So far, UCHL3 has been mainly studied in the context of DNA repair signaling. Interestingly, other components of DNA repair pathway were implicated in mitosis, for example ATM is activated during mitosis, localizes to the centrosomes and controls integrity of the mitotic spindle[240], BRCA1 controls centrosome duplication and prevents centrosome amplification, which is crucial for proper chromosome segregation[241] and 53BP1 protein has been shown to localize to kinetochores[242], and it is important for resolving the merotelic attachments in an Aurora B dependent manner[243].

Our interest in UCHL3 was triggered by results we obtained in a high-throughput screen, in which we were looking for novel regulators of mitosis. UCHL3 was the best candidate from tested DUBs and as the screen revealed, downregulation of UCHL3 leads to irregular nuclei phenotype. Interestingly, control of nuclear shape was specific to UCHL3, but not UCHL1 another member from the UCH protein family (Figure 14). First, I confirmed that UCHL3 controls nuclear morphology (Figure 15). Since irregular nuclei are a frequent consequence of segregation errors during mitosis I therefore designed several experiments to test the hypothesis that UCHL3 might be involved in the regulation of mitotic progression. Using different molecular and cellular tools, I could show that UCHL3 controls chromosome alignment and chromosome segregation during mitosis. I observed that chromosome alignment is regulated by UCHL3 during prometaphase and the rescue experiments confirmed that it is dependent on the catalytic activity of UCHL3 (Figure 17). Experiments with UCHL3 inhibitor showed that only a short inhibition of UCHL3 during prometaphase results in severe alignment problems further confirming UCHL3 direct involvement in this process (Figure 19D, Figure 20D). In addition, I confirmed these results by live video imaging experiments where I observed increased number of lagging chromosomes in the absence of UCHL3 (Figure 21, Figure 22). These results collectively suggest that UCHL3 is an important factor controlling chromosome segregation and thereby maintenance of genome integrity. Importantly, I observed the same phenotype in human primary fibroblasts where inhibition of UCHL3 caused misalignment defects (Figure 20). This result suggests that UCHL3 also controls proper division of human somatic cells and its role is not restricted to cancer cells. This is further supported by data

available in GEO database[244] showing that human embryonic stem cells have higher levels of UCHL3 which drop upon cell differentiation. Furthermore, UCHL3 has been reported to regulate mammalian oocyte maturation during which UCHL3 colocalizes with the oocyte spindle and inhibition of UCHL3 leads to meiotic spindle defects[231]. Surprisingly, the UCHL3 knockout mice are fertile and they develop without any obvious abnormalities[245], suggesting an existence of a compensatory mechanism in the absence of UCHL3.

## 2.4.1 How does UCHL3 regulate the chromosome congression?

The most frequent phenotypes I observed include misaligned polar chromosomes in metaphase and lagging chromosomes during anaphase. The misalignment phenotype could result from the disruption of one or multiple mechanisms of chromosome positioning during mitosis for instance the transport of polar chromosomes to the equatorial zone. While the presence of lagging chromosomes could be a result of defects in the chromosomal attachment correction. Importantly, the UCHL3 catalytic activity is necessary for proper cell division suggesting that UCHL3 controls ubiquitination of one or more regulatory factors important for the chromosome alignment and/or segregation. In this chapter I would like to discuss the possible mechanisms by which UCHL3 could be involved in the regulation of chromosome congression and chromosome segregation.

One of the important mechanisms contributing to chromosome alignment includes dynein mediated poleward movement of polar chromosomes which are later transported to the equator by combined activity of CENP-E and MCAK. CENP-E is a motor protein which helps chromosome alignment by promoting congression of polar chromosomes[20,246,247] and it also actively helps to maintain alignment of already congressed chromosomes[19,127,248,249]. The MCAK protein does not move along MTs but it accumulates at the leading kinetochore and depolymerizes microtubules facilitating the chromosome congression[128]. MCAK, CENP-E and dynein downregulation lead to the congression defects observed as misaligned chromosomes[128,185]. In addition, MCAK downregulation causes accumulation of aberrant KT-MT attachments, syntelic and merotelic[128] which creates a potentially dangerous situation for the cell since merotelic attachments are not recognized by the SAC.

The alignment phenotype I observed in my experiments (Figure 16B) is very similar to CENP-E depletion phenotype[20,185]. Despite the high similarity of UCHL3 depletion to the depletion

of CENP-E, UCHL3 removal has no impact on total CENP-E protein levels (Figure 26A). When I quantified the localization of CENP-E by measuring its intensity on kinetochores during metaphase, I saw a significant decrease of CENP-E localized to the KTs of aligned chromosomes, but not of the misaligned ones (Figure 25 A-C). Based on these results, I can conclude that UCHL3 is important for CENP-E recruitment to kinetochores, rather than for regulation of CENP-E protein levels directly. CENP-E is recruited to the KTs indirectly by Aurora B which first promotes BubR1 recruitment[250] and this subsequently leads to CENP-E recruitment. In prometaphase, BubR1 is present at kinetochores in 1:1 ratio to CENP-E[251] under normal circumstances. After chromosome bi-orientation, BubR1 dissociates from kinetochores, but CENP-E stays attached to KNL1[19] and further maintains the KT-MT attachment[252]. In my experiments, I did not address the CENP-E recruitment to kinetochores in prometaphase, but I studied the recruitment of BubR1. My results demonstrate that upon UCHL3 knockdown, BubR1 recruitment to KTs is not affected during prometaphase (Figure 18C, D), yet I still observe decreased CENP-E levels in metaphase. There are three possible explanations for these observations. First, CENP-E is recruited to KTs normally during prometaphase, but upon MTs attachment it is not maintained at metaphase kinetochores and prematurely dissociates. Second possibility is that the CENP-E recruitment is also dependent on UCHL3 downstream of BubR1 loading onto the kinetochore. Third option could be a presence of an alternative mechanism for CENP-E KT recruitment, which is abolished by UCHL3 depletion. To prove or disprove one of the three possibilities, CENP-E localization during prometaphase needs to be addressed.

Additionally, it would be interesting to understand why CENP-E is depleted only from the KTs of aligned chromosomes, but not from the misaligned ones. Upon UCHL3 knockdown, CENP-E is more associated with the spindle, especially in the polar region (Figure 25A) and it is possible that this signal contributes to the increase in CENP-E kinetochore intensity. Nevertheless, CENP-E retention in the polar region could be an important indicator of impaired CENP-E movement. Interestingly, CENP-E movement towards equator is promoted by Aurora A and Aurora B phosphorylation[20].

In addition to CENP-E depletion at metaphase kinetochores, I also observed significant decrease in the levels of Astrin complex at kinetochores (Figure 23). Astrin is recruited in Plk1-Cdk1 dependent manner to kinetochores upon chromosome bi-orientation[253] and it is negatively regulated by Aurora B activity[254]. Interestingly, Astrin localization to kinetochores is important for recruitment of other kinetochore components such as CENP-E[237] which is in

line with my previous observations. Upon knockdown of UCHL3, I observed decreased recruitment of Astrin during metaphase which was proportional to the recruitment of CENP-E to the kinetochores (Figure 25D). From these observations I conclude that loss of CENP-E in the absence of UCHL3 is due to impaired Astrin recruitment. This phenotype could further contribute to the enrichment of misaligned chromosomes upon UCHL3 depletion since Astrin is necessary for chromosome congression and alignment maintenance[252,255] by forming a MT interacting platform together with Ndc80 complex[253].

## 2.4.2 UCHL3, spindle morphology and the KT- MT attachment status

UCHL3 depletion has also an effect on the spindle morphology. I observed more frequently the MTs that are spanning the equatorial region (Figure 24A) and that the metaphase spindle was elongated (Figure 24C). The appearance of microtubules spanning the equator could be due to aberrant bundling of spindle microtubules making the interpolar microtubules more visible or alternatively by increased bundling of the bridging fibers. This could be due to more PRC1 binding, making the fibers thicker and therefore more visible[256].

Spindle size is tightly controlled in cells and many experiments point to a precise scaling between the cell size and the spindle size suggesting that spindle size is evolutionary a well conserved feature[257]. Microtubule plus tips proteins are often connected with the regulation of spindle microtubules growth. For example, KIF4A has been implicated in the regulation of microtubule length in Aurora B-dependent manner during anaphase[258]. It is possible that KIF4A could regulate spindle microtubules in the same manner also during prometaphase and therefore it could contribute to the elongated spindle phenotype. As discussed earlier, PRC1 stabilizes microtubules[256] which could have an impact on the dynamics of microtubule polymerization and depolymerization, leading to the spindle elongation. It has also been shown that (+) end directed kinesin motor KLP61F bundles microtubules and determines the spindle length by promoting the sliding of the anti-parallel microtubules resulting in the spindle spacing[139]. Alternatively, the process of the microtubule nucleation and growth could be affected leading to the aberrant polymerization and elongation of spindle microtubules. MT nucleation from chromosomes occurs during mitosis and it is one of the determining factors for the spindle length, despite the fact that it is not essential in the presence of a functional spindle. MT nucleation is regulated by TPX2 which is a microtubule-associated protein

important for Aurora A activation. TPX2 mutants have short spindles, but they maintain their bipolar orientation[259]. It has been proposed by Young et al. that spindle size is important for proper chromosome segregation[260] and it is therefore probable that the aberrant spindle morphology contributes to the increased number of segregation errors in UCHL3 depleted cells.

In addition, I observed that UCHL3 depleted cells display lateral attachments more frequently (Figure 24B) which led me to the conclusion that UCHL3 regulates the end-on conversion process which is either delayed or inhibited in absence of UCHL3. Lateral to end-on conversion is a multistep process which requires CENP-E to tether microtubules to kinetochores and depolymerizing motor MCAK to release the laterally attached microtubules[261]. During early mitosis, also Aurora B has been reported to localize to the kinetochores, promoting end-on conversion process, which is counteracted by PP2A-B56 phosphatase[262]. It was shown that CENP-E, MCAK or Astrin deletion lead to increased number of laterally attached kinetochores resulting in congression defects and segregation errors[128,246,255] further underlying their importance for the conversion process. I have observed that UCHL3 knockdown led to depletion of both, Astrin and CENP-E from the kinetochores, which could lead to the impairment of the end-on conversion process and thus explain the higher abundancy of lateral attachments in UCHL3 depleted cells. I did not assess the MCAK protein levels and its localization during metaphase. These experiments would provide additional information about the mechanism by which UCHL3 regulates chromosome alignment. Taken my results together, UCHL3 is indispensable for proper Astrin and CENP-E recruitment to kinetochores as well as for proper lateral to end-on conversion process which is necessary for chromosome congression and error-free segregation of chromosomes during anaphase.

## 2.4.3 Regulation of the SAC response by UCHL3

As mentioned above, knockdown of UCHL3 results in polar chromosomes with only partially attached or completely unattached kinetochores. This state should generate a strong SAC response leading to the mitotic arrest. Intriguingly, my live video experiments did not confirm this hypothesis, because I did not observe a significant change in time the cells needed to proceed from prometaphase to anaphase (Figure 21D, Figure 22D), yet I have observed significant increase of lagging chromosomes in UCHL3 depleted cells (Figure 21C, Figure 22C). I performed the live video experiments in two different cell lines to gain more insight

and I also used different tools to achieve UCHL3 downregulation to avoid potential off-target effects. Nevertheless, I did not observe a mitotic arrest in any of my conditions. However, when I plotted values from all experimental replicates together, I could see a strong tendency for the UCHL3 depleted cells to take longer time before reaching anaphase (Figure 22F, G). It is puzzling why UCHL3 depleted cells do not manage to potentiate the SAC response enough to cause the mitotic arrest in presence of polar chromosomes and why they undergo a rather small delay and later enter anaphase regardless of the presence of the misaligned chromosomes.

The lagging chromosomes are often the result of the alignment and attachment problems in metaphase. In some cases, the erroneous attachments are not sensed by the SAC machinery, as it was demonstrated for the merotelic attachments[128,143,263,264], where all kinetochores are occupied by MT and under sufficient tension. Furthermore, the misalingment and attachment errors could be disregarded in the cases of the weakened SAC response[265,266] or in the case of impaired amplification or diffusion of the SAC signal[267–269]. Dysfunctional SAC response prevents the cell from resolving all the problems in time and therefore it leads to the appearance of lagging chromosomes in anaphase.

Weak SAC response means that the SAC components are not recruited to the kinetochores in the proper amount and therefore even in the presence of unattached chromosomes the SAC is satisfied and cells enter anaphase prematurely, resulting in the segregation errors. My data showed, that there is no difference in the recruitment of BubR1 to the kinetochores during prometaphase, meaning that the initial SAC response is triggered equally in the control and UCHL3-depleted cells. These experiments suggest that UCHL3 is not implicated in the generation of the checkpoint complex during prometaphase.

Aurora B kinase activity is necessary for the maintenance of the SAC response and it was shown that inactivation of Aurora B results in fast exit from mitosis and decrease in the mitotic index. In my experiments, UCHL3 depletion did not affect the mitotic index upon synchronization in mitosis (Figure 18A, B) therefore I conclude that Aurora B activity necessary for the SAC activation and maintenance during prometaphase is not controlled by UCHL3 confirming the initial hypothesis that the early steps of SAC response are not affected. Taken all experiments together, the SAC response is triggered normally during prometaphase, but it is not maintained long enough, or it is not propagated properly in the cell to prevent the anaphase onset. This finding is very surprising, because it is well established, that a single unattached kinetochore is enough to delay the anaphase onset[270,271]. The signal generated by a single kinetochore is amplified and stops the cell from dividing. Experiments in fused cells

where two spindles are present in one cell showed that the signal was propagated only to the spindle with unattached kinetochore, but it was not propagated to the second one. These experiments suggest that the diffusion of the signal has only a certain reach and it is limited to the vicinity of the spindle containing the unattached kinetochore. It was also observed that when mature spindle entered anaphase, the second spindle would enter anaphase shortly after, regardless of the attachment status, suggesting existence of 'wait' and 'start' signals that are diffused in the cell and that the start signal is able to override the stop signal generated by unattached kinetochores[272].

Chan et al. did a large study with use of computational modeling where they were investigating the relationship between the spindle size and the ability to silence SAC. They showed that the longer spindles had troubles to spread the SAC signal from chromosomes close to the poles, because the distance was too long and the signal was diluted before it reached the kinetochores at the equator[257]. I have observed elongated spindles upon UCHL3 knockdown and I did not observe a significant delay in mitotic onset upon UCHL3 depletion even in presence of misaligned, polar chromosomes. One possibility is that the elongated spindle could prevent sufficient diffusion of the SAC signal and therefore the polar chromosomes would not cause a significant mitotic delay.

Another possibility is that the pathway removing SAC components from the kinetochores is over-activated and SAC is prematurely silenced even in presence of unattached kinetochores. The SAC proteins are transported away from kinetochores by dynein motor [273] therefore an excessive dynein recruitment to kinetochores upon UCHL3 depletion could explain the phenotype. Another important antagonist of checkpoint response is p31Comet and its overexpression has been shown to result in the checkpoint override and mitotic exit[274,275]. To fully conclude whether it is a diffusion problem or premature disassembly of the checkpoint complex, localization studies of BubR1 and MAD2 to kinetochores of metaphase chromosomes should be performed.

## 2.4.4 Molecular mechanism for the mitotic role of the UCHL3 enzyme.

To shed some light on the molecular mechanism by which UCHL3 regulates chromosome congression, I aimed at identification of the substrates of UCHL3 DUB in mitosis. The mass Spectrometry analysis of UCHL3 interacting proteins identified several interesting candidate substrates including Aurora B, PP1α, PP1γ phosphatases and MCAK. In the following experiments, I confirmed the interaction of UCHL3 with Aurora B in whole cell lysates (Figure 26B) and therefore I focused on investigating whether Aurora B could be a substrate of UCHL3 in mitosis. Experiments with UCHL3 knockout cell lines showed that the absence of UCHL3 leads to the accumulation of upshifted bands recognized by Aurora B antibody, which are of an exact size of the ubiquitin tetramer (Figure 26A). This observation further confirmed a hypothesis that UCHL3 deubiquitinates Aurora B during mitosis. In addition, under denaturing conditions, we observed an increased ubiquitin signal on Aurora B in the absence of UCHL3 (Figure 26C).

Aurora B is a major mitotic kinase regulating many key events leading to proper mitotic progression and accurate chromosome segregation. In early mitosis, Aurora B localizes to the kinetochores with laterally attached microtubules and it promotes the end-on conversion process[262]. In metaphase, Aurora B is enriched at the merotelic attachment sites and is indispensable for correction of aberrant KT-MT attachments[159–161,276]. Interestingly, Aurora B negatively regulates MCAK activity[276] which provides another layer of merotelic attachment correction. After establishment of attachments to all kinetochores, Aurora B does not reach its substrates leading to MCAK activation. Afterwards, MCAK is relocalized to KTs where it promotes MT disassembly and thus correction of merotelic attachments[162]. Additionally, Aurora B also regulates CENP-E motor activity[20,277].

Taken my results together, I propose a model in which UCHL3 controls chromosome alignment by regulation of Aurora B kinase (Figure 27). My results demonstrate that Aurora B is polyubiquitinated in mitosis and this ubiquitinated form accumulates in the absence of UCHL3. Hwever, this ubiquitination does not target Aurora B for degradation by the 26S proteasome, because the total Aurora B protein levels are not changed upon UCHL3 depletion (Figure 26A). I have addressed the activity of Aurora B by monitoring the T232 phosporylation which is a marker of Aurora B activity, as well as phosphorylation status of Hec1, the Aurora B substrate. In none of these experiments I observed any changes in phosphorylation levels,

suggesting that the UCHL3-mediated deubiquitination does not affect Aurora B kinase activity directly (data not shown). I hypothesize that in the absence of UCHL3, Aurora B is polyubiquitinated and this aberrant modification blocks the interaction of Aurora B with its substrates and therefore results in a phenotype similar to its inhibition. This situation would affect only several Aurora B substrates and not all of them, because UCHL3 downregulation does not fully mimic Aurora B inhibition. For example, I did not observe fast mitotic exit upon UCHL3 depletion which is one of the consequences of Aurora B inhibition[159] (Figure 18A). Rather than inhibition of Aurora B kinase activity, I presume that this aberrant ubiquitination regulates Aurora B localization and interaction capacity with its substrates. This could be caused by a steric hindrance of the ubiquitin groups or by mislocalization. Indeed, further studies will be necessary to determine the interaction status of Aurora B during mitosis in the absence of UCHL3 and also to investigate its localization. Additionally, it would be interesting to identify the upstream E3 ligase and the type of ubiquitin-linkage that is present in this ubiquitin modification.

In summary, during my PhD I described the role of UCHL3 in mitosis and I discovered that UCHL3 is critical for proper chromosome segregation. Its absence leads to chromosome alignment problems and subsequently could lead to aneuploidy caused by increased number of segregation errors (lagging chromosomes). Therefore, UCHL3 controls the genome integrity of the cell. The role of aneuploidy in cancer has been studied and it is clear that most solid tumor cells are aneuploid[278] and various cancer cell lines show chromosomal instability. UCHL3 has been found to be overexpressed in several cancers including breast cancer, colorectal cancer and liver cancer[227,279,280]. It is probably the ability of UCHL3 to control genome integrity that makes it beneficial for cancer cells to survive their high rate of aneuploidy. It would be worth investigating whether targeting UCHL3 could improve cancer therapies. A few studies appeared already, supporting the idea to use UCHL3 inhibitors in combination with other commonly used chemotherapeutics[17,281]. Future studies will be necessary to investigate the significance of this approach in a greater detail.
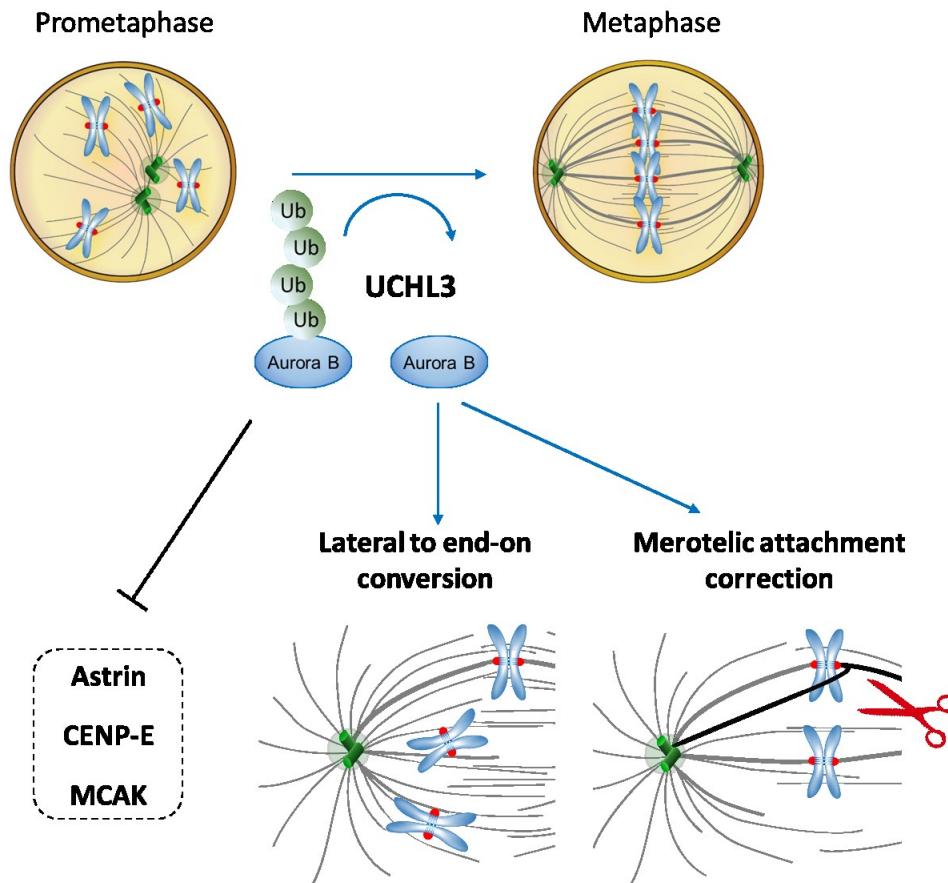
**Figure 27 Proposed model**

Suggested mechanism by which UCHL3 controls chromosome segregation. UCHL3 interacts with Aurora B in prometaphase and deubiquitinates it. This deubiquitination is necessary for proper Aurora B function in chromosome congression by promoting CENP-E movement, in lateral to end-on conversion process and in correction of merotelic attachments. Downregulation of UCHL3 results in chromosome congression and segregation defects.

# 3 TRIM15 IMPLICATION IN THE CELL CYCLE PROGRESSION AND MIGRATION

## 3.1 BACKGROUND

The tripartite motif (TRIM) proteins constitute a large subfamily of RING E3 ubiquitin ligases. More than 70 TRIM genes have been identified in human so far[282]. All TRIM proteins contain the tripartite motif usually comprised of a RING domain followed by one or two B-box motifs and a coiled-coil region at the N-terminus and a variable domain at the C-terminus[282]. Another common feature of TRIM proteins is their ability to form oligomers which is often essential for their biological activity[283,284]. They regulate many cellular activities, including the innate immune response and the antiviral response of a cell[285]. However, TRIM proteins also play important roles in cell proliferation[286,287], DNA repair[288], pluripotency[289] and apoptosis[290]. This broad involvement in diverse cellular processes is underscored by the association of many TRIM genes with various pathologies, such as viral infections[291,292], cardiovascular diseases[293], neuropsychiatric disorders[294], genetic diseases[295] and cancer either as oncogenes[296] or tumor supressors[297].

## 3.1.1 Evolution of the TRIM subfamily

The tripartite motif, which is the main characterizing module that defines the TRIM family of proteins, appeared for the first time in metazoans[298]. The other eukaryotes do possess the individual TRIM subdomains, but only in different arrangements. In metazoans, the order and even the spacing between the subdomains is highly conserved, which indicates that this structure is a functional module[299].

TRIM genes can be classified into two groups a) highly conserved TRIM genes often also present in invertebrates b) evolutionary younger group present only in vertebrates with poor sequence and functional conservation[298]. The first group contains a small set of C-terminal domains which have been maintained with little changes throughout the evolution. In vertebrates and particularly in mammals the variety of TRIM genes radically increased, indicating the evolutionary success of this domain arrangement[299]. A number of these "young" genes are species specific and they are often implicated in the response to viral and microbial

infections. Furthermore, these dynamic genes are poised to be involved in providing novel functions which will be required in the course of evolution[298].

## 3.1.2 Structural determinants of the TRIM proteins function

TRIM proteins are determined by their N-terminal tripartite motif and also possess highly variable C-terminal domain consisting of various subdomains[300]. In most TRIM proteins the tripartite motif begins with an N-terminal RING domain, which confers E3 ligase catalytic activity to this protein family. Following the RING domain, one or two B-box domains are positioned. Similarly to the RING domain, these domains coordinate two zinc ions to maintain their structure, however they do not possess the E3 ligase activity[301]. Despite some mutations in these domains are associated with disease phenotypes, not much is currently known about their exact role in the full length TRIM proteins[295]. The subsequent coiled-coil domain (CC) is necessary for the homodimerization of TRIM proteins and often also for their higher order oligomerization, which is in many cases strongly affecting their activity[302].

The C-terminal part of TRIM proteins contains a variety of domains and is considered to mediate the recognition and specificity towards their target. The family can be classified into 11 subgroups based on the C-terminal domain structure[303]. The most abundant subgroup contains the PRY-SPRY domain, which often mediates protein-protein interactions, particularly in the context of immune signaling[304]. TRIM15 also belongs to this subgroup. Other domains present in some TRIM proteins are PHD/Bromo domain, NHL domains, TRAF domain and others.

As mentioned previously, a crucial determinant of the activity of several TRIM proteins is their oligomerization. The most striking example is the interaction and organization of TRIM5$\alpha$ and related proteins. TRIM5$\alpha$ was shown to homodimerize through its CC domain and subsequently form higher order complexes via the RING and B-box2 domains. This greatly increases the avidity of the complex towards the capsid proteins of HIV-1 and allows it to act as a restriction factor[305]. It is interesting to consider, that TRIM protein transcripts are often extensively alternatively spliced producing proteins differing at their C-termini[306]. Such presence of different isoforms might constitute a regulatory activity. Adding further complexity, interactions between different TIRM proteins modulating the activity of the resulting complex were also reported[297].

### 3.1.3 TRIM proteins in the regulation of biological processes

As the TRIM proteins are one of the largest subfamilies of E3 ubiquitin ligases, it is maybe not surprising that they are regulating a wide variety of cellular processes[282].

Several specific substrates of TRIM E3 ligases were identified so far and many TRIM proteins preferentially bind to specific E2 enzymes[282,307]. E3 ligase activity of TRIM proteins is often associated with the regulation of immune responses. Besides the aforementioned role of TRIM5α in HIV-1 restriction, TRIM21 acts as a cytosolic receptor of IgG-bound pathogen, triggering cellular response upon binding[308]. Furthermore, more than a half of the TRIM proteins were shown to enhance innate immune response of cells and specific TRIM proteins were show to regulate the NFκB signaling[285,309].

However, the effects of TRIM proteins reach far beyond innate immunity. One of the first discovered TRIM proteins, TRIM19 also known as promyelocytic leukemia gene (PML) is necessary to transfer of small ubiquitin modifier (SUMO) onto its substrates[310]. This process is crucial for the formation of PML-nuclear bodies, important regulating centers of transcription. Another example is TRIM29 which can regulate the localization and activation of tumor protein 53 (p53) and prevent apoptosis of the cell[311]. DNA repair of double-stranded DNA breaks is another cellular process where a TRIM protein was shown to have a role. TRIM29, a histone binding protein, interacts with the chromatin around the break and acts as a scaffold, facilitating recruitment of the repair machinery[288].

Importantly, a number of TRIM proteins are involved in the control of cell cycle and in the regulation of mitosis[312]. TRIMs involved in interphase often facilitate progression through the cycle and their silencing in proliferating cells usually results in more cells dwelling in G1/G0 and less cells in S/G2 at any given time. Among the identified cell cycle pathways regulated by TRIMs, the most important are p53 and Janus kinase (JAK)/signal transducer and activator of transcription (STAT) pathways[313,314], but other like WNT/β-catenin and AKT pathways were also reported[315,316]. Furthermore, multiple TRIMs were shown to regulate the assembly and function of the mitotic spindle and thereby to affect cell division[312]. In particular, TRIMs can affect centrosome duplication and spindle pole assembly, kinetochore protein degradation, kinetochore-microtubule attachment and midbody formation.

# 3.1.4 Involvement of TRIM family proteins in human pathology

TRIM proteins have been shown and suggested to contribute to a wide variety of diseases in human. In response to viral infection TRIM25 leads to K-63 polyubiquitin chains formation on the viral RNA sensor protein Retinoic acid inducible gene I (RIG-I)[317]. This modification of RIG-I allows it to exert its downstream effects, namely activation of interferon (INF) production by the cell. Interestingly, Influenza A virus is capable to evade this INF mediated response thanks to the ability of its viral proteins to interact with TRIM25 and interfere with RIG-I polyubiquitylation[318]. Also, several TRIM proteins restrict HIV-1 at different stages of the infection cycle. As previously mentioned, TRIM5α interacts with the viral capsid affecting reverse transcription[292,319]. Additionally, TRIM22 inhibits long terminal repeat promoter driven transcription and TRIM28 inhibits viral integration into the genome[320,321].

Genome wide association studies uncovered connection of DNA polymorphisms of many TRIM proteins with neurological and psychiatric disorders, such as multiple sclerosis, Alzheimer's disease and attention deficit hyperactivity disorder[322]. Furthermore, multiple hereditary diseases such as Optiz syndrome, Limb-girdle muscular dystrophies and Bardet-Biedl syndrome are attributed to mutations in genes encoding TRIM proteins[295,323]. Many TRIMs regulating the cell cycle are involved in a wide variety of different cancer types, where they can strongly affect the progression of the disease in different ways[312].

TRIM proteins, such as TRIM28, TRIM14 and TRIM52 are upregulated in cancer cells and due to their positive effect on cell cycle progression, they act like oncogenes[316,324,325]. They do so by affecting the main cancer related signaling pathways, such as AKT and WNT and p53. In the opposite way, TRIM proteins also act as tumor suppressors often lost in cancer cells, whose restoration limits cancer progression and invasiveness. Specifically, TRIM8 has been shown to stabilize p53 and its absence in renal cell carcinoma leads to chemoresistance despite the presence of wild-type p53. Reactivation of TRIM8 in these cells re-establishes chemosensitivity mediated by p53[326].

TRIM proteins can also modulate cancer progression by regulating its metastatic potential. The ability of a particular cancer to metastasize is greatly influenced by the tendency of cancer cells to undergo epithelial to mesenchymal transition (EMT)[327]. TRIM14 associates with worse prognosis in patients with glioblastoma due to its ability to stabilize the transcription factor zinc finger E-box binding homeobox 2 (ZEB2) which facilitates the EMT of glioma cells[328].

Importantly, the regulation of cell adhesion and cell migration is an important determinant of the ability of a cancer to metastasize[329]. Accordingly, several TRIMs affecting cell adhesion were identified to play a role in cancer. In gastric cancer, TRIM25 expression acts as a marker of poor prognosis. Knockdown by RNA interference in patient cancer cells did not affect proliferation, but reduced cell migration and invasion characteristics[330]. Conversely, ectopic expression of TRIM25 promoted migration and invasion via activation of tumor growth factor β (TGF-β) signaling. Similarly, in colorectal cancer (CRC), TRIM14 knockdown reduced migration and adhesion of cancer cell lines, and its overexpression had the opposite effect[331]. In this context, the effect was shown to be mediated by sphingosine kinase 1 and STAT3 pathways. Only in a few cases has the effect of individual TRIM proteins on cancer progression been clearly linked to their E3 ubiquitin ligase activity. In prostate cancer, the TRIM25 polyubiquitylates ETS related gene (ERG) transcription factor, an oncogene driving many prostate cancers[332]. In a similar manner, TRIM31 promotes K48-linked polyubiquitylation and subsequent degradation of tuberous sclerosis complex (TSC) 1 and TSC2, the important suppressors of the mTORC pathway[333]. This in turn leads to overactivation of this oncogenic pathway. In gliomas, E3 ligase activity of TRIM45 mediates a tumor suppressor effect[334]. This is due to its ability to polyubiquitylate the p53 protein forming a K63-linked chain, and thereby inhibiting the availability of the residues for K48-linked polyubiquitylation which mediates p53 degradation.

## 3.1.5 TRIM15 background

TRIM15 is one of the less explored members of the TRIM family. An early GWA study uncovered a strong association of a single nucleotide polymorphism (SNP) in TRIM15 with the development of Alzheimer's disease[335]. Our interest in understanding the function of TRIM15 was inspired by the fact that it is a putative E3 ubiquitin ligase and by the reported ability of TRIM15 to activate mitogenic signaling[336]. Therefore, we set out to investigate whether there is a role of TRIM15 in cell cycle regulation and whether it acts via ubiquitin mediated signaling.

## 3.1.6　　Recent publications about TRIM15

Within a few months after I started to work on the TRIM15 project, the first of the three publications describing the function of TRIM15 was published, indicating the role of TRIM15 in focal adhesion maintenance[337]. This was later followed by two publications focusing on the role of TRIM15 in gastric and colon cancer[338,339]. This combined with a lack of evidence for the role of TRIM15 in regulation of the cell cycle led to our decision to discontinue the work on this project. The findings of these papers will be compared with my results in the discussion section.

# 3.2  METHODS

## 3.2.1    Plasmids

For my experiments I used Myc-FLAG, GFP and RFP expression vectors with human or mouse Trim15 cDNA. I purchased the full coding sequence of the human and mouse TRIM15 gene fused to a sequence of AA constituting the Myc-tag and DDK-tag (FLAG) at the C-terminus, TRIM15-Myc-FLAG (pCMV6 Entry Vector, Origine, human: RC207716, mouse: MR203968). I subcloned the coding sequence into different expression vectors: pCMV-AN-RFP (Origene PS100033) generating TRIM15 N-terminally fused with a red fluorescent protein (N-RFP-TRIM15) and pCMV-AC-GFP (Origene PS100010) generating Trim15 C-terminally fused with a green fluorescent protein (C-TRIM15-GFP).

## 3.2.2    TALEN mutagenesis

### 1. Design of TALEN pairs

I designed TALEN pairs for both human and mouse TRIM15 gene. To identify optimal DNA sequences targetable by TALENs, I used the TALEN Targeter tool designed by the Cornell University[340] (TAL Effector Nucleotide Targeter 2.0) which selected the best target site and designed the TALE subdomain arrangement according to DNA sequence. TALENs consist of repeat variable residue (RVD) domains, specific to different nucleotides (NN – G, NI – A, HD – C, NG – T).

### 2. Golden Gate cloning

To clone the individual TALEN plasmids, I used the Golden Gate cloning approach which allows to generate one plasmid from up to 10 source plasmids in a single step. TALENs are usually 15-20 RVDs long, therefore a two-step cloning is necessary. In the first step, I assembled arrays of 10 RVDs and 6-9 RVDs in two separate plasmids and in the second step I assembled them together to obtain a single TALEN targeting 16-20 AA long DNA sequence. TALENs are cloned into a backbone vector containing the C-terminal FokI domain necessary for DNA cleavage. The detailed mechanism of the Golden Gate cloning is visualized in Figure1D of the results section.

### 3. TALENs activity reporter system

Reporter plasmids were generated earlier in the laboratory of R. Sedlacek by P. Kasparek and R. Haneckova. This system consists of a plasmid containing the target DNA sequence which is cleaved by the TALEN pair. Neighboring on the 5' side is a fragment of a coding sequence of a selection marker (mRFP, blasticidine resistance gene) with a premature stop codon not allowing the production of the full protein. On the 3' side there is a full coding sequence of the same marker with the ATG translation start site removed. After cleavage the homologous recombination DNA repair machinery recombines the homologous sequences surrounding the cleavage site, leading to expression of the selection marker (graphical representation is shown in Figure 2A). I used three different reporter plasmids: pAR-RFP producing RFP signal, pAR-GFP-RFP producing RFP signal upon cleavage with basal GFP expression as a control of transfection efficiency and pAR-BSD reporter generating resistance to blasticidine antibiotic.

## 3.2.3    Genotyping by DNA-PAGE gels

To avoid large amount of sequencing I preselected my clones by DNA-PAGE genotyping which is sensitive enough to reveal a presence of point mutation in the genomic DNA. First, I isolated genomic DNA from my clones and then I amplified ~600bp regions around the sites of expected deletions using 83_hT15F, 84_hT15R and 85_mT15F, 86_T15R primer pairs. I also amplified the WT region and mixed the DNA from the clones with the WT PCR product. I heated the samples at 95ºC to fully denaturate the DNA and I let the DNA slowly reanneal. In the WT cells this generates only one product of double stranded DNA made of two fully complementary DNA sequences visible on the gel as one band. If mutations in the target sequence are present, both the WT and the mutated sequences are present and their annealing leads to all combinations of WT and mutated DNA strands with mismatched regions dependent on the specific mutations. Such regions are unable to properly reanneal and their presence slows the movement of the dsDNA through the gel, resulting in the appearance of multiple bands.

I run 10 µl of DNA sample in Tris-borate-EDTA (TBE) 5% Polyacrylamide gel (V= 7.5 ml: 750 µl 10x TBE buffer, 1.2 ml 30% Acrylamide, 5.6 ml water, 70 µl 10% APS, 4µl TEMED) at 100 V for 60 minutes and stained the gels for 30 min in TBE buffer containing a drop of Ethidium bromide (EtBr) before imaging. Courtesy of Björn Schuster.

## 3.2.4    TOPO cloning and sequencing

To sequence both alleles of mutant cell lines, I used TOPO cloning. First I amplified the target region by Phusion polymerase and I added A-tail to the PCR product by adding Taq polymerse (40 µl reaction= 8l PCR product, 1µl 10mM dATP, 5µl 10x PCR buffer (15mM $Mg^{2+}$), 0.2µl Taq polymerase) for 20 min at 72ºC. I transformed DH5α competent cells and performed blue-white selection using IPTG (0.1M) and X-gal (20 mg/ml) and I sent 5 clones per each mutant cell line for sequencing (SEQme, Sanger sequencing).

## 3.2.5    Cell culture

All cell lines were purchased from ATCC and cultured at 37 °C in 5% CO2 humidified incubator, if not stated otherwise. I used several different cell lines of human and mouse origin and cultured them according to the cell culture protocol given by ATCC webpage[341].

Human cell lines: BJ, CaCo2, HCT116, HEK293T, HepG2, Huh7, Jurkat, MCF7, Mo57J, Mo57K, THP-1, U2OS and mouse cell lines: Neuro2A, NIH3T3, NMuMG, Raw267.3.

For all immunofluorescence experiments I was seeding cells on 12 mm glass coverslips (Menzel-Glaser) in 24-well plates at a density 15 000 cells per well.

## 3.2.6    Generation of Trim15 knockout cell lines

To generate TRIM15 knockout cell lines, I used human U2OS cells and mouse NMuMG cells which I transfected with the plasmids for TALEN pair expression together with the activity reporter plasmid producing GFP selection marker. I cultured the cells in 6 cm dish and transfected them with 2 µg of TAL1, 2 µg of TAL2 and 1 µg of reporter plasmid using Lipofectamine2000 reagent according to manufacturer's protocol. After 24 hours, I sorted them using FACS and I collected RFP negative cells (control) and RFP positive cells (Trim15 KO) into 96 well plates, 1 cell per well. I cultured them until they grew in 10 cm dish, I froze 1 half of the dish and I isolated genomic DNA from the other half (Quiagen, DNA isolation Kit), I genotyped the clones using DNA page gels, TOPO cloning and sequencing as described above. I selected the clones having biallelic mutations.

## 3.2.7    Mice

### 1. Trim15 knockout mice

To generate a mouse model of TRIM15 loss we used an EUCOMM generated embryo harboring the "knockout first" allele of TRIM15 using selection driven recombination of the target site in mouse embryonic stem (ES) cells. A lacZ trapping cassette and a floxed promoter-driven neomycin selection cassette was inserted into the intron of TRIM15. Recombination of tm1a with Flp recombinase generates a conditional allele (tm1c), which posesses gene activity. Recombination of the tm1a allele with Cre recombinase deletes the neomycin selection cassette and a floxed exon of the tm1a allele to generate a lacZ– tagged, Trim15 knockout allele (tm1b). Cre recombination of the tm1c allele deletes the floxed exon and generates a frameshift mutation (tm1d) (Figure 2F). The tm1a embryos were obtained from the EMMA repository and implanted in pseudo-pregnant female mice. The tm1a line was established and mouse embryonic fibroblasts were isolated from WT and homozygous embryos at E8.5. The presence of a WT allele was verified using a PCR with primers surrounding the construct insertion site and the tm1a allele was detected with a primer set recognizing region flanking the LacZ sequence. All mice were crossed into Bl/6J background.

### 2. Colorectal carcinoma model

We used the $Apc^{cKO/cKO}$ mice that harbor two loxP sites surrounding APC, the commonly mutated gene in human colorectal carcinoma. We crossed the mice with Villin gene promoter driven expression of Cre recombinase coupled to estrogen receptor (Villin-CreER) which allowed the recombination to be activated selectively in the colon epithelium by administration of tamoxifen (Sigma Aldrich, 100 µl of 100 mg/ml stock). We sacrificed the mice four days after tamoxifen-induced recombination.

## 3.2.8    Isolation of MEFs

I isolated the mouse embryonic fibroblasts (MEF) from E8.5 embryos. I washed them in PBS and removed the organs, mainly liver to prevent contamination of the culture. I homogenized the tissue using small scissors. I plated the cells on gelatine coated 10 cm dishes. After 24 hours I changed medium to eliminate the debris.

### 3.2.9 RNA isolation and cDNA preparation

To isolate RNA from mouse tissue samples I used Trizol reagent and for isolation of RNA from cultured cells I used RNA Isolation Kit (RNeasy Mini Kit – QIAGEN) according to manufacturer's instructions. All RNA samples were DNAse I treated. For reverse transcription I always used 2 µg of RNA and M-MLV Reverse Transcriptase from Sigma Aldrich.

### 3.2.10 Quantitative PCR analysis

I used 20 ng of cDNA as a template, SybrGreen master mix from Sigma Aldrich (S4438) and 1 µM primers in final volume of 10µl per reaction as listed in primer sequences (Appendix Table 7). I normalized the TRIM15 expression to a combination of three housekeeping genes (β-actin, Hprt, Gapdh for mouse and GAPDH, HPRT and Glucose-6-phosphate isomerase (GPI) for human) and I run them at 62ºC annealing temperature. I used the software from Roche (LightCycler® 480 SW 1.5.1) to analyze my data.

### 3.2.11 Proliferation assays

**ATP**: I used the ATP Cell Viability Luciferase Assay Kit from Millipore containing D-Luciferin, (CS224519), Firefly Luciferase (CS224520, ATP Assay Buffer (CS224521) and ATP 2 µM (CS224522). To detect my signal I used chemiluminiscence method in 384 well plate and measured cell density in different time points.

**Alamar Blue**: As a second method, I did Alamar blue assay using a reagent from Thermo Fisher (DAL1025). First I estimated the optimal cell seeding density and after I measured Absorbance at 600 nm from which I calculated the cell number in different conditions during the course of 24 or 40 hours.

**FACS**: As a third method to estimate the cell growth I used FACS to measure DNA content in the cells. I used Propidium Iodide (PI) stain from Thermo Fisher (P1304MP), I fixed the cells 5 minutes in ice cold ethanol, resuspended them in 100 µl of PBS and stained with 3 µM PI in a staining buffer (100 mM Tris, pH 7.4, 150 mM NaCl) for 30 minutes in the dark. I analysed the results using FlowJo program.

## 3.2.12　Migration assays

I seeded the cells in 12-well plates 24 hours prior the experiment. I performed a scratch using 200 μl pipette tip and I washed the well once with warm medium to remove floating cells. I placed my plate to a heated chamber 37ºC with 5% $CO_2$ and I started acquisition for 12 - 24 hours using TIRF microscope. I analysed the data and measured all parameters in ImageJ software.

## 3.2.13　Immunofluorescence

I fixed the cells in 4% PFA for 20 minutes at room temperature, washed them 3x in PBS and permeabilized in 0.5% NP-40 for 5 min followed by wash, 3x in PBS-T and blocking in 3% BSA in PBS-T for 1 hour at room temperature (RT). I diluted primary antibodies in blocking buffer and incubated them overnight at 4ºC, I washed the cells 3x, 5 min in PBS-T and incubated them with secondary antibodies at 1:500 dilution for one hour at RT in dark followed by 3x 10 min wash in PBS-T and staining with 1 μg/ml DAPI in PBS for 10 min at RT and wash 2x in PBS-T. I mounted them on glass slides using Mowiol and dried them overnight at RT in dark. I used rabbit polyclonal Trim15 antibody (Proteintech, 13623-1-AP) at 1: 500 dilution.

## 3.2.14　Statistics

To statistically evaluate my data I used parametric Student's t-test for all experiments. I considered the values significantly different when P value was smaller than 0.05 and I assigned stars according to P values as follows: P<0.05 *, P<0.01 **, P<0.001 *** P< 0.0001 ****. In all graphs I show my results as Mean ± SD of minimum three independent experiments. I used GraphPad software for all statistics and graphs.

# 3.3 RESULTS

## 3.3.1 Design and generation of molecular-biology tools to study TRIM15 function

To characterize the function of TRIM15 I decided to prepare several tools to study the effects of TRIM15 in cells and in the whole organism.

First, to be able to determine the localization of TRIM15 in the living cell, I generated mammalian DNA constructs expressing TRIM15 fused with fluorescent proteins. To get a vast image of TRIM15 localization, I cloned the human as well as mouse TRIM15 coding sequence into different vectors with C- or N- terminal GFP and RFP tags as it is described in methods section and illustrated in the plasmid maps of TRIM15-Myc-FLAG, N-RFP-Trim15 and C-TRIM15-GFP vectors (Figure 28A).

To study the effect of TRIM15 loss on the function of the cell I decided to knock out the TRIM15 gene in mouse and human cell lines. To achieve TRIM15 deletion, I decided to perform gene editing of the chosen cell lines using transcription activator-like effector (TALE) nucleases. TALE nucleases (TALENs) are a highly specific genome editing tool, whose precision is achieved by generating of a pair of DNA-binding proteins interacting with a specific DNA sequence. To cleave DNA at a specific site, two TALE proteins need to bind DNA sequences surrounding the cleavage site allowing the C-terminal FokI endonuclease domains to dimerize. The resulting double stranded DNA break is then repaired by the cellular DNA-repair machinery. Most frequently the cell uses non-homologous end joining (NHEJ) DNA repair which is an error- prone repair generating deletions, insertions or mutations around the cleavage site often leading to a frameshift of the open reading frame.

To knock out the TRIM15 gene in the target cells, I designed two pairs of TALENs, one set targeting the human and the other set targeting the mouse Trim15 gene. In both cases, the cleavage site was positioned downstream but in close proximity of the translation start site codon (ATG) (Figure 28B). I used a software designed by Cornell University to identify the best regions for TALEN mutagenesis (Figure 28C) and I used the Golden Gate cloning approach to create TALEN pairs in two step process (Methods and Figure 28D). To verify the success of the cloning, the final constructs were digested with KpnI restriction enzyme. This cloning approach leads to the presence of a KpnI target sequence in the HD domains which are not on the 1$^{st}$ or 10$^{th}$ position in the first assembly step as well as in the backbone sequence

(Figure 28C). The resulting pattern of bands allows the assessment of the correct order of the subdomain assembly (Figure 28E). I managed to clone all the necessary plasmids for targeting of human Trim15 by a single TALEN pair as well as for targeting the mouse Trim15 by a second TALEN pair.

## 3.3.2 Generation of cell and animal models to study the TRIM15 function

**Mutant cell lines**

In order to address the function of TRIM15 in cells I decided to knock out the TRIM15 gene by TALENs that I generated previously. For my experiments I chose two cell lines in which I deleted the TRIM15 gene: U2OS (human) and NMuMG (mouse) cell line. To improve the efficiency of generating TRIM15 knockout cells, I used the TALENs activity reporter system. It is a unique tool that allows to test the activity of TALEN pairs. If the TALEN pair is active, it cleaves the reporter vector and by homologous recombination the cell gains new selection markers (GFP, RFP signal or resistance to antibiotics) (Figure 29A). This allows enrichment of cells where TALEN mediated cleavage occurred, either by flow cytometry (Fluorescence-activated cell sorting (FACS)) or antibiotics selection.

I used the TALENs activity reporter system with RFP expression marker and I sorted the RFP positive cells by FACS, to isolate individual clones of U2OS and NMuMG cells where the DNA was successfully cleaved by TALENs (Figure 29B). I tested the individual clones for presence of mutations in the genomic sequence of TRIM15 by the DNA PAGE genotyping. (Figure 29C). Based on these results, I selected clones for further validation by sequencing with use of the TOPO cloning which allowed me to distinguish mutations in individual alleles of the gene. For my future experiments, I selected the clones where both alleles were successfully mutated.

In NMuMG clone no. 2, each allele had a different mutation, either a deletion of 2 base pairs (bp) at the cleavage site or a larger deletion of 14bp centered on the cleavage site. Both of these deletions lead to a frameshift of the open reading frame and a predicted appearance of an early stop codon, which should lead to the loss of the protein (Figure 29D). I validated Trim15 deletion on the mRNA level using RT-PCR (Figure 29E) as well as on the protein level using western blot (Figure 29F). In U2OS clone no. 1, each allele also had a different mutation. In the first case deletion of 83bp and in the second a deletion of 52bp occurred. As the cleavage

site was targeted to the ATG start site, the deletions led to loss of a part of 5'UTR, translation initiation site and several AA codons, potentially ablating the protein production (Figure 29D).

**Mouse model**

To generate a mouse model of TRIM15 loss we used a EUCOMM generated embryo harboring the "knockout first" allele of TRIM15 (tm1a). These embryos were generated using selection driven recombination of the target site in mouse embryonic stem (ES) cells. The tm1a embryos were obtained from the EMMA repository and implanted in pseudo-pregnant female mice. The tm1a line was established in the transgenic unit (IMG, Prague). The tm1a line can be crossed with Flippase or Cre mouse lines driven by different promoter producing various genotypes. The tm1c is a conditional allele possessing WT Trim15 function, which can further serve to generate tissue specific Trim15 deletions, tm1b is a knockout allele harboring LacZ gene which can be used to monitor Trim15 expression during development or in adult mice (Figure 29G). For my experiments I was using the tm1b Trim15 knockout animals. I always confirmed that the mice which I have selected had the desired genotype. I used site specific primers to distinguish between the WT and the tm1b (knockout) allele (Figure 29H).

## 3.3.3   Expression pattern and subcellular localization of TRIM15 protein

Due to the unknown function of TRIM15 at that time, I decided to assess the distribution of the protein within the cell to help identify cellular processes it could be involved in. To this purpose I first decided to use the fluorescently labelled protein expression vectors. I co-transfected U2OS cells using polyethyleneimine (PEI) transfection reagent, with two plasmids containing the human TRIM15 coding sequence (N-RFP-TRIM15 and C-TRIM15-GPF). After fixation and mounting I visualized the fluorescent signal using confocal microscopy. Surprisingly, the distribution patterns of the two different fusion proteins were not overlapping (Figure 30A). N-RFP-TRIM15 seemed to have mainly cytoplasmic localization, while the C-TRIM15-GFP localized to distinct foci within the cell. To help to resolve this conflicting result, I took advantage of a newly appeared commercial antibody recognizing the endogenous human TRIM15 protein. The immunostaining revealed accumulation of endogenous TRIM15 in multiple foci within the cell, a pattern that was similar to the localization of C-TRIM15-GFP (Figure 30B).

To further characterize TRIM15, I analyzed its expression in 21 different mouse tissues as well as in multiple mouse and human cell lines using qPCR. Interestingly, the intestinal tissues had high levels of TRIM15 expression, in comparison to other organs (Figure 30C). Notable expression could be observed also in kidney, stomach and mammary gland tissues. However, screening human and mouse cell lines did not reveal similar pattern based on their tissue of origin. In human cell lines, the highest expression was detected in hepatocellular carcinoma cell line HepG2. Higher expression was also present in colorectal adenocarcinoma cell line CaCO2, but also in cell lines derived from osteosarcoma (U2OS), T lymphoma (Jurkat) and another hepatocellular carcinoma cell line (Huh7). Another hepatocellular carcinoma derived cell line Hct116 did not show high expression of TRIM15. In mouse cell lines, the highest expression was observed in a cell line derived from neuroblastoma (Neuro2A) (Figure 30D). Despite this variability, both human and mouse cell lines show higher expression of TRIM15 when compared to the primary (BJ) or non-transformed (NIH3T3) cells. This indicates, that increased levels of TRIM15 could be advantageous for growth of some cancer cells and therefore actively upregulated in the malignant cells.

To test this hypothesis, we chose to measure the expression level of TRIM15 in a mouse model of inducible colorectal carcinoma (CRC). For this experiment, I used mouse model for CRC expressing a tamoxifen inducible transgene for APC deletion selectively in the colon epithelium driven by Villin Cre promoter[342]. Additionally, I assessed the TRIM15 expression in another colorectal carcinoma model, the azoxymethane (AOM) induced colon carcinogenesis in C57BL6J wild-type mice[343]. In both models, induction of the carcinogenic process led to increased expression of TRIM15 (Figure 30E). This was more pronounced in the conditionally ablated APC mice, in comparison to the random mutagenesis/ inflammation driven CRC model. Furthermore, analysis of RNA expression data from The Cancer Genome Atlas (TCGA) revealed that TRIM15 is often increasingly expressed in CRC samples (Figure 30F). This indicates, that TRIM15 upregulation may be particularly involved in colorectal carcinomas driven by mutations of APC.

### 3.3.4    Effects of TRIM15 on cell proliferation

To investigate our original assumption, that TRIM15 is likely involved in cell cycle regulation, I decided to assess its effect on cell proliferation. For this purpose, I used mouse embryonic fibroblasts isolated from the Trim15$^{-/-}$ animals (tm1b allele). To reliably measure cell growth, I took advantage of a high-throughput assay measuring the cellular ATP level by ATP dependent, luciferase mediated bioluminescence. As ATP levels in cells are tightly regulated, increase in cell number is directly proportional to the increase of total ATP-luciferase signal. Similar increase in ATP signal after three days of culture could be seen in both, WT and Trim15$^{-/-}$ MEFs indicating, that loss of Trim15 does not affect cellular proliferation (Figure 31A). This was further confirmed by a time-course measurement of cell viability using the Alamar blue assay. Following the cells over 40 hours revealed no difference between the WT and Trim15$^{-/-}$ (Figure 31B).

Another approach to assess the effect of TRIM15 on cell cycle regulation I used, was flow-cytometric cell cycle phase analysis by measurement of the DNA content. Similarly, as in the previous assay, the distribution of cells in different phases of cell cycle was not different between WT and Trim15$^{-/-}$ MEFs (Figure 31C). Also, in NMuMG, the ablation of Trim15 did not lead to noticeable changes in cell cycle phase distribution (Figure 31D).

Lastly, I measured the effect of TRIM15 overexpression on cell proliferation in U2OS cells using Alamar blue assay. For this purpose, I transiently transfected the cells with available human TRIM15 expression constructs and measured the amount of cells after 24 hours. In line with previous results, overexpression of TRIM15 did not lead to changes in proliferation (Figure 31E).

### 3.3.5    TRIM15 regulates cell migration

As the next step, we decided to investigate the effect of TRIM15 on cell motility. This was triggered by the publication of a study by Uchil et.al. which shows that TRIM15 is often localized to focal adhesions and it affects the focal adhesion turnover[344]. To measure the capacity of cells to migrate in presence or absence of TRIM15, I performed a scratch assay. First, I used MEFs from WT and Trim15$^{-/-}$ mice and I observed reduced invasion of the Trim15$^{-/-}$ cells (Figure 32A). After 12 hours the WT cells were able to cover the wound area almost completely, whereas the KO cells were covering only around 80%. Similar result could be observed in the NMuMG Trim15$^{-/-}$ cells, although the difference seemed more pronounced

(Figure 32B). After 12 hours, the WT cells covered the area completely, but the KO cells reached only about 60%. Surprisingly, no difference of cell movement was observed in the U2OS cells (Figure 32C).

We hypothesized, that the observed migratory effect could be due to an effect of TRIM15 on epithelial to mesenchymal transition. Despite the lack of effect on cell cycle, such a role could have an important effect on cancer progression or metastasis and based on the animal and human expression data, we decided to investigate the role of TRIM15 in colorectal cancer. Unfortunately, shortly after that, Ok-Hee et al. published their work which describes the role of TRIM15 in human colorectal cancer[339]. This led to us abandon the project completely.
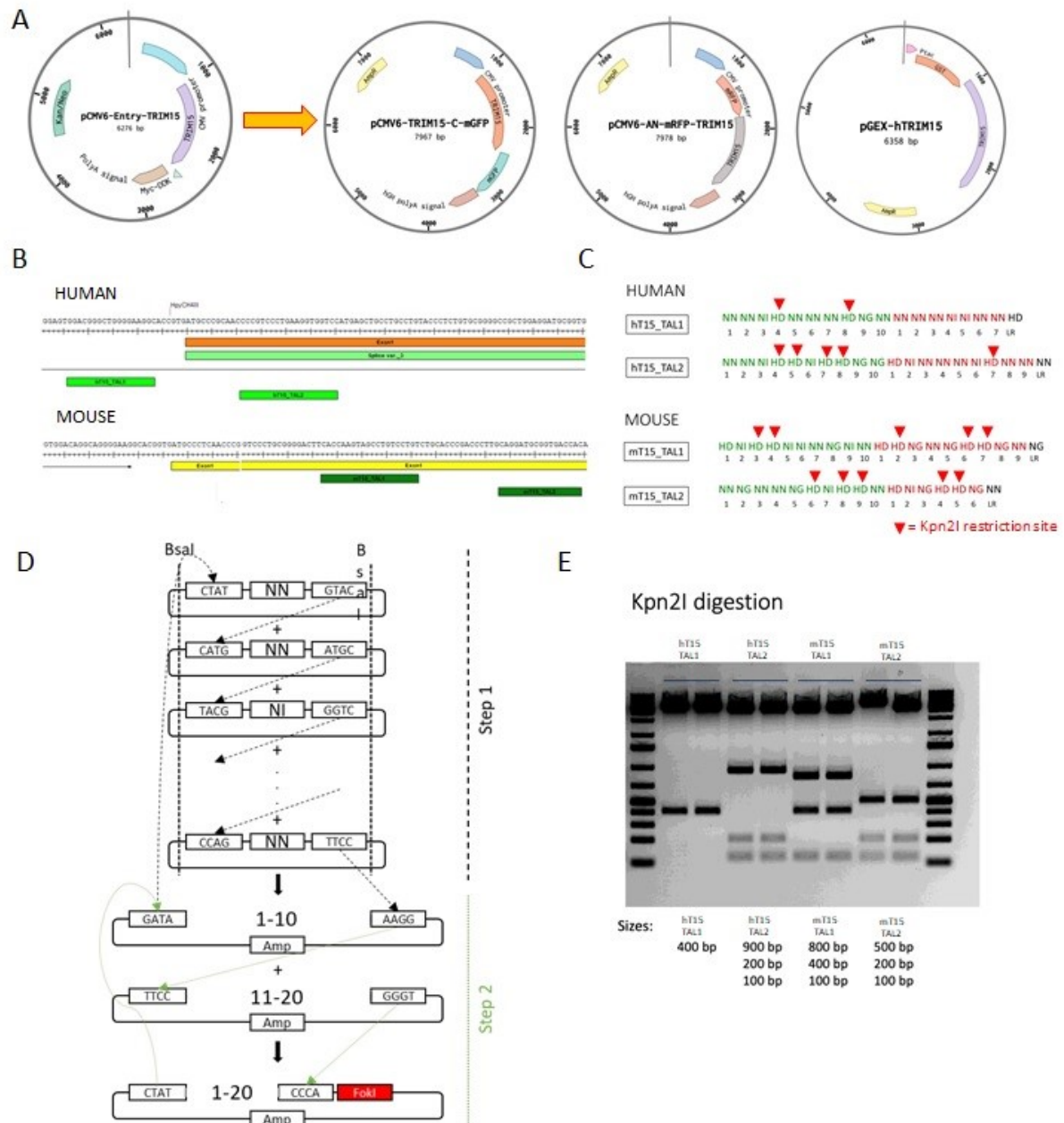
**Figure 28 Generating molecular tools for TRIM15 functional analysis.**

(A) Using restriction endonucleases, the coding sequences of human and mouse Trim15 were subcloned into vectors, creating TRIM15 fused with fluorescent protein at the C- or N- terminus. (B) TALEN pairs targeting human and mouse TRIM15 genomic sequences close to the transcription start site were designed using TALEN Targeter tool. (C) TALE subdomains arrangement of the designed TALENs was prepared for cloning. Red arrowheads indicate Kpn2I restriction site presence, used for cloning validation. (D) Golden Gate cloning of TALENs consisting of two assembly steps of TALE subdomains. In the first step two plasmids are assembled, one containing the first 10 subdomains and the second one with the remaining subdomains. In the next step the two parts are cloned into the full TALEN plasmid. (E) Restriction analysis of the final TALEN constructs. The position of Kpn2I sites predicts the expected band sizes after digestion.
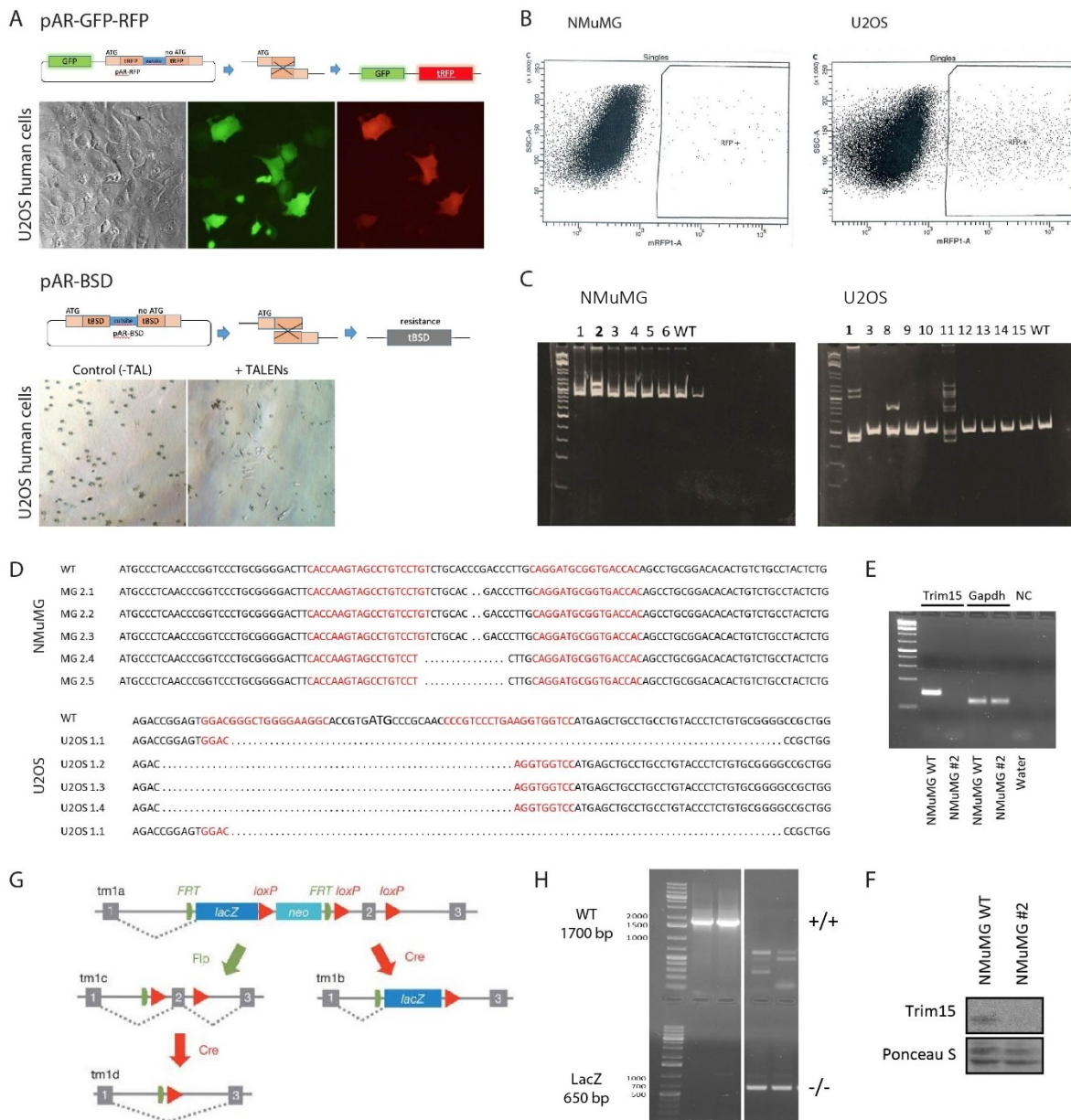
**Figure 29 TRIM15 knockout in cells and in the mouse**

(A-D) TRIM15 knockout was generated using TALENs in different cell lines. (A) To increase the likelihood of isolating cellular clones with mutations of interest, TALEN activity reporter plasmid containing the target sequence were used. Successful plasmid cleavage and subsequent recombination leads to expression of either mRFP or blasticidine resistance. (B) FACS sorting of individual cells positive for the TALEN activity reporter. (C) PCR and DNA PAGE analysis of the isolated clones. Reannealing of the PCR amplified genomic target sequence with WT sequence leads to multiple bands in clones with mutation. (D) Results of sequencing of the TOPO cloned PCR amplified genomic target region. Red letters indicate binding of individual TALENs, dashes indicate deletion of a base. (E) RT-PCR with Trim15 and Gapdh primers confirming absence ofTrim15 mRNA. (F) Western blot showing absence of Trim15 protein in NMuMG cells upon TALEN mutagenesis. (G) Design of the allele of TRIM15-/- mice obtained from EMMA repository. In the tm1a allele the expression of TRIM15 is stopped and LacZ expression can be detected instead. (H) PCR genotyping of the WT and the TRIM15-/- mice.
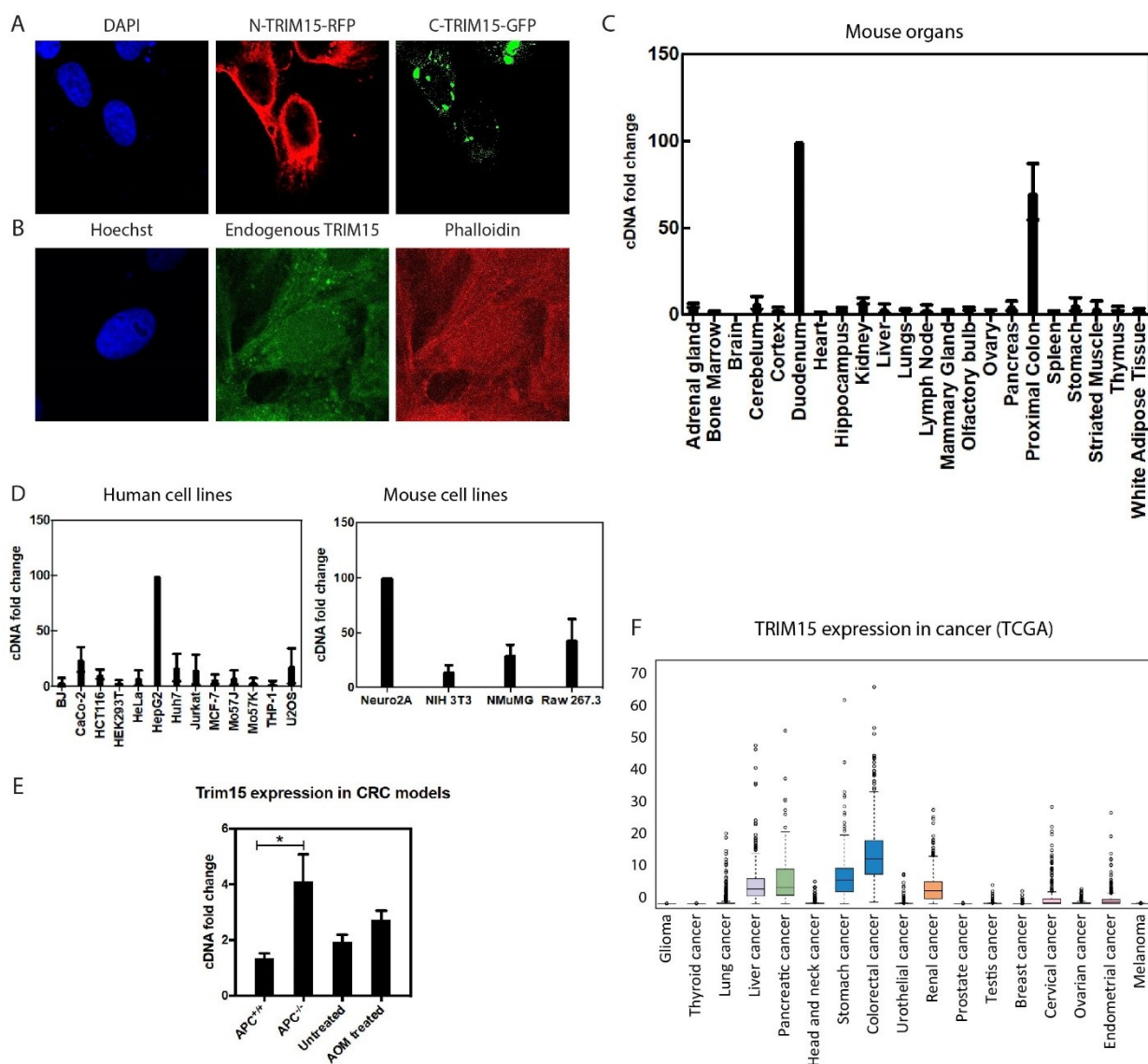
**Figure 30 Localization and expression of Trim15 in human and mouse samples**

(A-B) Localization of TRIM15 in human U2OS cell line. (A) Overexpression of differently labelled TRIM15 plasmids, N- RFP-TRIM15 and C-TRIM15-GFP. (B) Immunofluorescence staining of the endogenous TRIM15 (green) co-stained with actin marker Phalloidin (red). (C) Trim15 expression in different mouse organs isolated from adult Bl/6J mice. Normalized to β-actin, Hprt and Gapdh. (D) Trim15 expression in selected human (left) and mouse (right) cell lines and normalized to the mean of three housekeeping genes. (E) Trim15 expression in two different models of colorectal cancer. From the left: Rows 1, 2 represent data from APCcKO/cKO mice, without tamoxifen and four days after tamoxifen administration. Rows 3, 4 represent data from azoxymethane (AOM) induced cancer in Bl/6 adult mice. Bars show Trim15 expression in vehicle and AOM treated mice. (F) TRIM15 expression profile in human samples of cancer tissue from different origins. Data are available in the protein atlas online database.
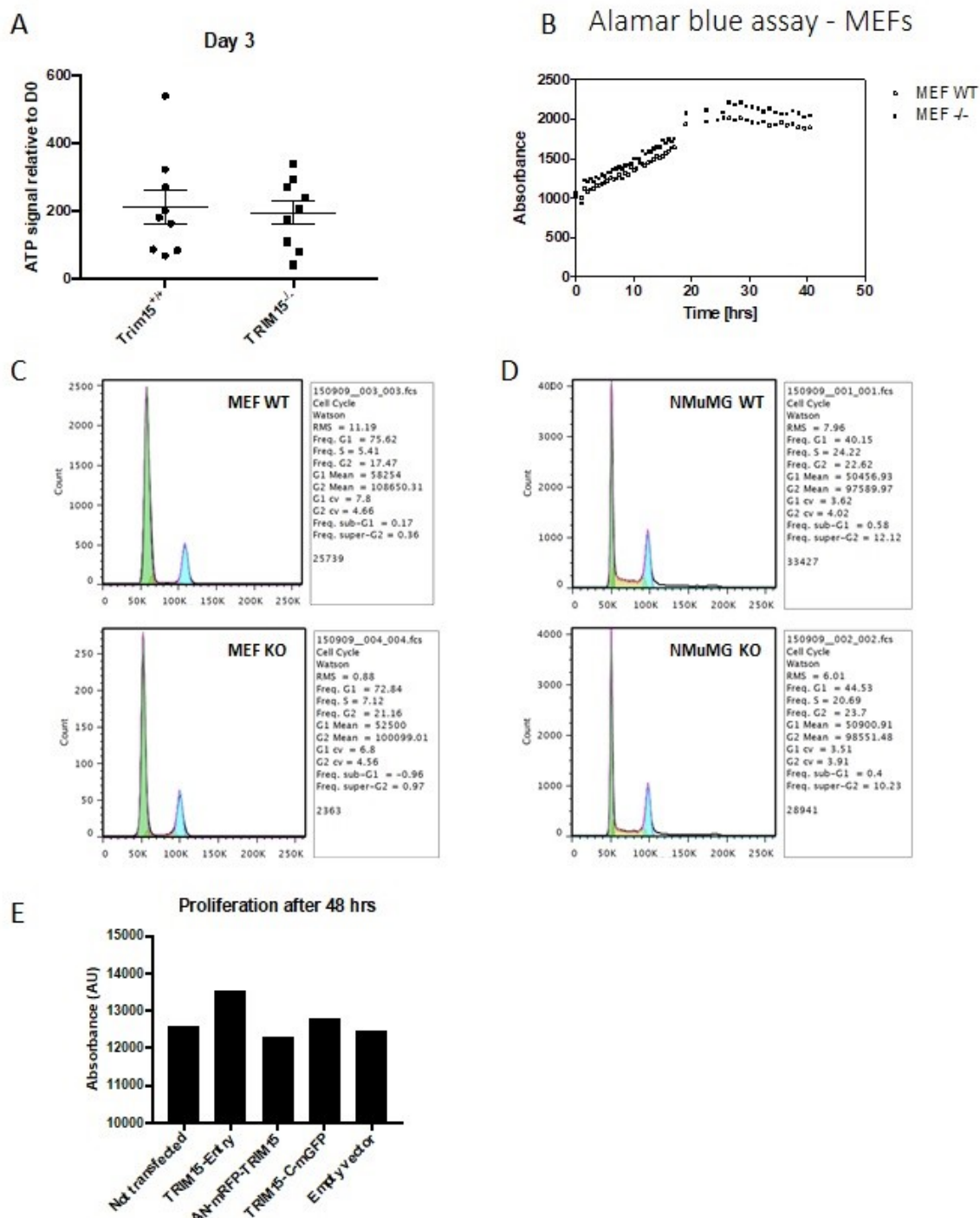
**Figure 31 The role of Trim15 in proliferation**

(A) Trim15$^{+/+}$ and Trim15$^{-/-}$ MEFs were used to measure the ATP content in two time points. First, 16 hours after seeding (D0) and second after 3 days in culture (D3). Graph represents data from D3 normalized to D0. (B) Trim15$^{+/+}$ and Trim15$^{-/-}$ MEFs were seeded in 96 well plate and their proliferation rate was measure by Alamar Blue dye in the time course of 40 hours. (C) Analysis of cell cycle distribution by FACS in Trim15$^{+/+}$ and Trim15$^{-/-}$ MEFs by PI staining. (D) FACS analysis of cell cycle distribution in TALEN generated WT and Trim15 KO NMuMG cell lines. (E) Study of the effect of TRIM15 overexpression in human U2OS cells by Alamar Blue Assay. From left to right: control cells, Trim15-Myc-FLAG, RFP-TRIM15, TRIM15-GFP, empty vector transfection.
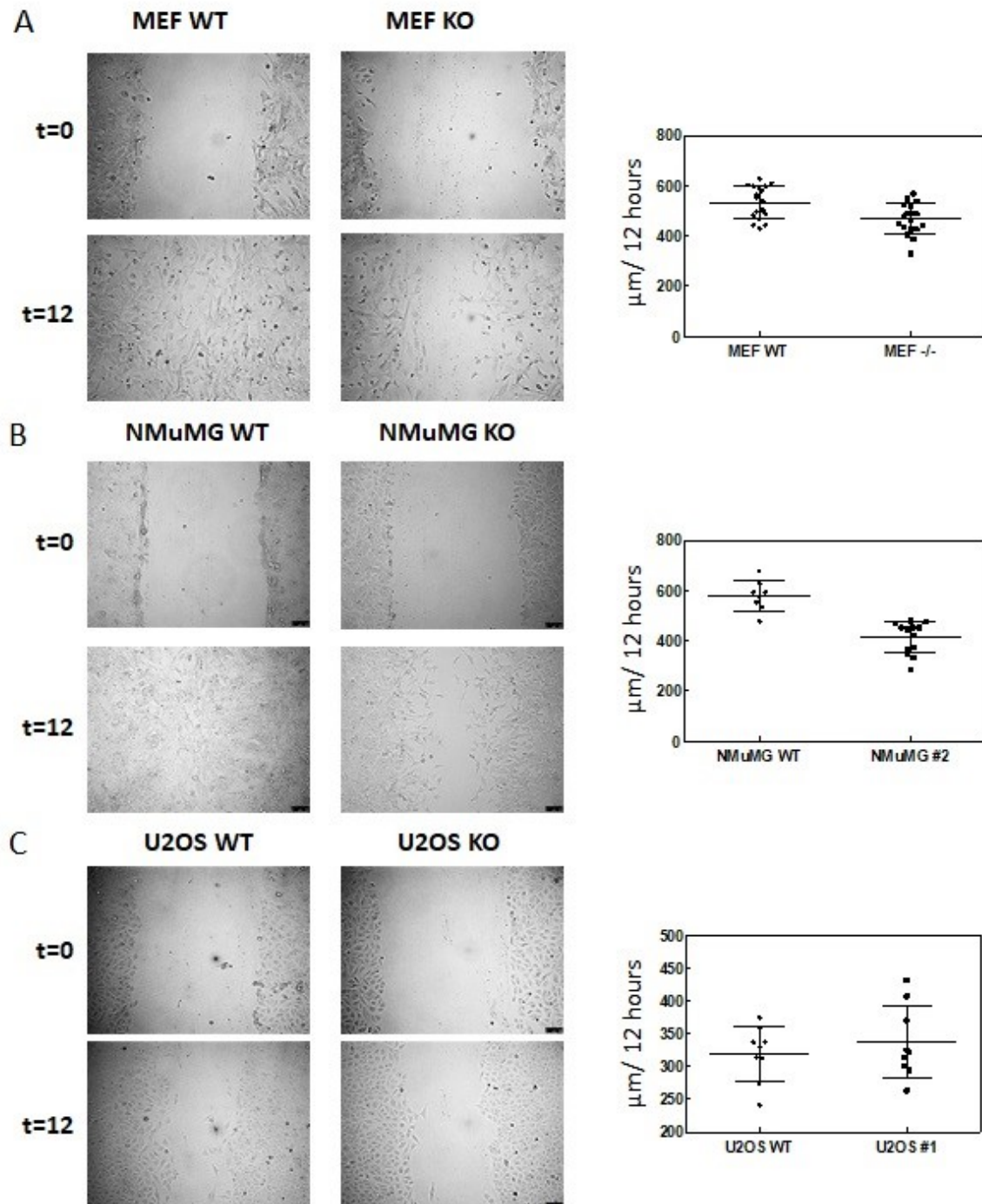
**Figure 32 Implication of Trim15 in cell migration**

Migration experiments with different cell lines. All experiments were done in the same setup. Migration ability of different cell types was analysed by the scratch assay. Cells were filmed and the distance migrated was measured in ImageJ. The graph represents the total distance migrated during 12 hours by individual cells. (A) Migration of Trim15$^{+/+}$ and Trim15$^{-/-}$ MEFs. (B) Migration of TALEN generated Trim15 WT and Trim15 KO NMuMG cells. (C) Migration of TALEN generated Trim15 WT and Trim15 KO U2OS cells.

# 3.4 DISCUSSION

In this project I was focusing on the characterization of TRIM15 and its roles in cells and animals, with a special emphasis on the cell cycle. To this purpose I generated multiple cellular models and acquired a mouse model of a TRIM15 knockout. Unfortunately, in publishing of the results on TRIM15 function I was preceded by two other research groups. The findings they reported greatly overlapped with our findings and this led to a decision to stop this project. As the first aspect of TRIM15 function I investigated its localization within the cell. Using protein expression constructs of TRIM15 fused with fluorescent proteins I was able to assess the localization of TRIM15 using confocal imaging. This led to a discrepant result, between the N-terminally and the C-terminally labelled TRIM15 proteins (Figure 30A). This contradiction was resolved by the appearance of a commercial antibody against endogenous human TRIM15. Stainings with this antibody revealed a similar pattern of localization as shown by the C-terminal labelled TRIM15, in multiple foci within the cells (Figure 30B). The mislocalization of the N-terminally labelled TRIM15 is likely due to the conserved structure of the TRIM domain which resides in the N-terminal part of the protein. Several subdomains of TRIM are important for mediating oligomerization or interaction with other proteins. Furthermore, their spatial arrangement in the protein forms a relatively rigid structure and therefore an addition of a bulky fluorescent protein could either block access to or destabilize the organization of these domains. In contrast, the C-terminal domain is much less conserved in the TRIM family of proteins and is often of modular character indicating that it could be capable of tolerating the addition of GFP more easily. This localization of TRIM15 was also reported in the other two publications. Both identified TRIM15 as a component of focal adhesions displaying similar speckled localization. Furthermore, they both report that deletion of the B-box domain leads to loss of this pattern and shows TRIM15 diffused in cytoplasm[345,346].

I also assessed the expression of TRIM15 in different human and mouse cell lines and in several mouse organs. From all the different tissues, TRIM15 showed a clear high expression in the intestines (Figure 30C). This is supported by the data from The Human Protein Atlas, where RNA sequencing shows strong expression only in the intestines (data not shown). Ok-Hee et al. performed TRIM15 mRNA expression analysis by qPCR in human tissues. In contrast to the Human Protein Atlas and to our data obtained from mice, the highest expression was

detected in the kidney. This was then followed by medium expression in the colon and a modest expression was detected in the small intestine[346]. Such difference could be potentially explained by the different normalization method used, as 18S ribosomal RNA expression has been reported to be variable in different tissues[347] The tissue specific pattern was not maintained in human and mouse cell lines in respect to their tissue of origin.

The abundant expression of TRIM15 in colon led me to investigate whether its expression levels are affected by malignant transformation. In a genetic model of CRC by a knock-out of APC in colon epithelia I observed an increased expression of TRIM15 in the malignant tissue. Similar trend could be observed in another CRC model induced by treatment with azoxymethane, however to a lesser extent and not reaching statistical significance (Figure 30E). Interestingly, Ok-Hee et al. reported reduced TRIM15 mRNA expression in matched human normal and CRC samples and suggested that TRIM15 could be acting as a tumor suppressor. In line with this conclusion, they showed, that overexpression reduces the anchorage independent growth of cancer cells and also slightly reduces tumor growth in a xenograft model of human CRC[346]. This difference could potentially be explained by our experimental setup. We isolated RNA from the whole small intestine of mice 4 days after induction of the APC knockout. At this time point, there is substantial hyperplasia of intestinal crypts, but no recognizable adenomas can yet be detected[348]. It could be that further transcriptional changes such as reduction in TRIM15 levels are required before a proper adenoma can be formed.

Supporting data were reported by Chen et al. who showed an association of lower TRIM15 expression in the tumors with reduced survival in gastric carcinoma patients[349]. This suggests that TRIM15 indeed may act as a tumor suppressor and that reduction of its expression allows the malignant cells to propagate more rapidly.

One way by which TRIM15 could affect cancer patient outcome and tumor growth is via an action on the cell cycle regulation. This was also suggested by the results reported by Uchil et al. where TRIM15 overexpression lead to the activation of the AP-1 pathway. Out of these reasons I performed proliferation assays and cell cycle phases distribution analysis in various cells missing or overexpressing TRIM15. Neither the absence nor the overexpression affected the proliferation in a noticeable way and cells lacking TRIM15 had their cell cycle phase duration unaffected (Figure 31). Recently, Chen et al. reported the same finding[349]. The MTT proliferation assay on gastric carcinoma cells with a siRNA mediated TRIM15 knockdown, or with transient TRIM15 overexpression revealed no effects on the proliferation.

Other important cellular processes which can affect the outcomes of cancer are cell migration and invasion. Both cell behaviors depend on reorganization of the cytoskeleton and on the cell-to-cell and cell-to- extracellular matrix (ECM) adhesion. Increase in adhesion and the subsequent reduction in cell migration reduces cancer metastasis[350], but many cell adhesion molecules have independent tumor suppressing characteristics[351]. This is likely due to their ability to affect the cellular signaling pathways and impair tumor growth for example by strengthening the contact inhibition. I investigated the role of TRIM15 deletion in cell migration by using a scratch (wound closure) assay. Interestingly, TALEN mediated deletion of Trim15 in NMuMG cells as well as absence of Trim15 in MEF cells isolated from Trim15 KO animals led to reduced speed of the wound closure in these cells (Figure 32 A-C). Surprisingly, no such effect could be observed in U2OS cells where TRIM15 was knocked out. This leads to a question whether TRIM15 was completely deleted in the genome. Sequencing of the TRIM15$^{-/-}$ U2OS cells clearly shows that the cells contain one allele with an 83bp and one with 52bp deletion, both removing the ATG translation start site and a bit of the surrounding sequence (Figure 29D). However, this deletion is about 120bp downstream from the transcription start site, which means that TRIM15 mRNA could still be produced. Also, recent improvements in the annotation of the human transcriptome indicate, that there could be another transcript variant of TRIM15, which is lacking the RING domain, but this is not supported by strong experimental evidence. Another possibility is that a different ATG site which lies in frame with the original ORF and its surrounding bases resemble a transcriptional start site and could originate the transcription of a truncated form of TRIM15. Using a transcription start site prediction tool I identified another ATG with favorable consensus 150bp downstream of the original ATG. Similarly, as in the previous case, this protein does not contain its RING domain, but it could potentially still replace the full length TRIM15 in its function in cell migration, since the RING domain has been shown not to be essential to regulate migration[345]. Another important factor to take into account is the karyotype of selected cell lines. Unlike NMuMG which are mostly diploid[352], the U2OS cells have large chromosomal rearrangements with altered chromosome counts[353] and therefore it is possible that the U2OS clone no. 1 had more than two copies of Trim15 gene which was not detected among the five sequenced colonies.

The first publication exploring the role of TRIM15 in adhesion and migration was the report of Uchil et.al. He shows that TRIM15 localizes to the focal adhesions and this is mediated by its direct interaction with scaffold protein paxillin. When TRIM15 was knocked down using

RNA interference in HeLa cells the cell migration in a scratch assay was reduced, which is in full accordance with my results. Additionally, he reports that TRIM15 is involved in focal adhesion turnover where it mediates the disassembly of the FA complex. The knockdown of TRIM15 therefore leads to FA which are stable for extended periods of time and this prevents the cells from invading the empty surface.

On the other hand, the publications of Ok-Hee et al.[346] and Chen et al.[349] report seemingly opposite observations. In both cases they measured cell migration in a trans-well invasion assay, where a knockdown of TRIM15 led to an increased migration of colon and gastric cancer cells, respectively. Furthermore, overexpression of TRIM15 in this setup caused migration impairment. However, the readouts from the scratch assay and the trans-well invasion assay are not completely equivalent. The first one models wound closure and it is strongly dependent on cellular migratory behavior and proliferation, while the second one is a model for extracellular matrix invasion and therefore it also reflects the ability of the cell to interact with the ECM. Also, the fact that different cells were used in these reports could also influence the outcome of the change in the levels of TRIM15.

In summary, my data indicate that TRIM15 is a protein involved in cell-to-ECM adhesion. Its localization pattern resembling focal adhesion distribution and the reduced speed of wound closure in a scratch assay suggests that it has an important influence on cell migration. In contrast, I was not able to confirm our expected role of TRIM15 in cell cycle regulation. My and publicly available data indicate, that TRIM15 could play a role in the cells of the intestine and even that its regulation could be important in colorectal cancer. In particular, the association of low TRIM15 expression in tumor tissue with reduced survival rates makes it potentially a useful prognostic marker in CRC. However, the observed tumor suppressive effects and its role in cell invasion make it an interesting gene for research as a potential therapeutic target.

# 4 CONCLUSIONS

During my PhD study I was interested in studying the role of ubiquitin signaling in cell cycle regulation. I started my PhD while studying a ubiquitin ligase, Trim15 which at that time was a relatively unknown protein. Expression profiling showed higher expression of Trim15 in the intestine and further studies using different cancer models revealed increased expression of Trim15 especially in the colorectal carcinoma model. Based on those results, I focused on determining the role of Trim15 in the control of cell proliferation. Trim15 deletion or overexpression did not have any effect on cell number or the distribution of cell cycle phases, therefore I concluded that Trim15 does not regulate cell proliferation. Next to cell proliferation, cell invasiveness is a very important parameter of cancer cells therefore I decided to address the role of Trim15 in cell migration. From my experiments with various knockout cells I concluded that Trim15 promotes cell migration and therefore it could promote cancer invasiveness and metastasis formation. Unfortunately, during the course of my PhD several studies were published associating Trim15 with colorectal cancer and cell migration. This led me to the decision to stop working on the project and shift my attention to the second project which was focused on the deubiquitinating enzyme UCHL3. We identified UCHL3 in a high-throughput siRNA screen which aimed at finding new regulators of mitosis from the ubiquitin-proteasome network. During my PhD I investigated the function of UCHL3 and how it is implicated in cell division. Based on my results I conclude that UCHL3 controls chromosome alignment and chromosome segregation in human cells by controlling the proper kinetochore-microtubule attachments. My results show that UCHL3 is necessary for recruitment of key kinetochore components (CENP-E, Astrin) that are necessary for formation of stable microtubule attachments. UCHL3 downregulation results in congression defects which I observed in human cancer cells as well as in human primary cells. Based on proteomics data, I identified Aurora B kinase as a potential substrate of UCHL3 during mitosis and I confirmed the interaction between Aurora B and UCHL3 in human cells. The role of Aurora B in mitosis has been well described and misregulation of Aurora B function leads to mitotic defects. From my experiments I conclude that UCHL3 interacts with Aurora B and deubiquitinates it. The ubiquitination is not targeting Aurora B for proteasomal degradation, since deletion of UCHL3 does not affect Aurora B levels and the ubiquitination has merely a signaling role. My findings

are exciting because UCHL3 has not been associated with mitosis up to date and therefore they provide novel insights into the control of mitosis. The implication of ubiquitin ligases in mitosis has been studied extensively, but not many deubiquitinating enzymes have been described to regulate mitosis so far. My study brings important findings about regulation of chromosome segregation by ubiquitin signaling and its role in the maintenance of genome integrity. Indeed, UCHL3 is an interesting protein because understanding its mechanism of action could also be relevant for the study of cancer development and cancer progression. As my results collectively point to, UCHL3 is crucial for preventing segregation errors therefore it protects the cell from aneuploidy, the hallmark of many cancer cells.

# AUTHOR'S CONTRIBUTION

If it is not stated otherwise, Katerina Jerabkova designed and performed all the experiments listed in her thesis. Yongrong Liao performed experiments shown in Figure 26A and Figure 26C. Matej Ďurík designed and cloned shRNAs for UCHL3 knockdown and by use of retroviral infection he generated the HeLa K and Dld1 cell lines which I used for experiments shown in Figure 18A-B and Figure 22. Jolana Turečková was taking care of the $APC^{cKO/cKO}$ mice and she was administrating the treatment for both CRC models. The results are shown in the Figure 30E.

Thesis supervisor signature:

# LIST OF PUBLICATIONS AND COMMUNICATIONS

1. Jerabkova K, Sumara I: Cullin 3, a cellular scripter of the non-proteolytic ubiquitin code. Semin Cell Dev Biol. 2018 Dec 28. pii: S1084-9521(18)30033-8. DOI: 10.1016/j.semcdb.2018.12.007

2. Katerina Jerabkova, Yongrong Liao, Sadek Fournane, Charlotte Kleiss, Matej Durik, Laurent Brino, Radislav Sedlacek and Izabela Sumara: Deubiquitinating enzyme UCHL3 controls genome segregation in human cells. (Manuscript in preparation)

3. Marina Peralta, Katerina Jerabkova*, Tommaso Lucchesi*, Laia Ortiz Lopez, Benjamin Vitre, Dong Han, Chaitanya Dingare, Izabela Sumara, Nadia Mercader, Virginie Lecaudey, Benedicte Delaval, Sigolène M. Meilhac and Julien Vermot: Intraflagellar transport complex B proteins regulate the Hippo effector Yap1 during cardiogenesis. (Manuscript is ready to resubmission after revision in Plos Biology)

4. Jakub Ziak, Romana Weissova*, Kateřina Jeřábková*, Martina Janikova, Roy Maimon, Tomas Petrasek, Barbora Pukajova, Mengzhe Wang, Monika S. Brill, Marie Kleisnerova, Petr Kasparek, Xunlei Zhou, Gonzalo Alvarez-Bolado, Radislav Sedlacek, Thomas Misgeld, Ales Stuchlik, Eran Perlson and Martin Balastik. (Manuscript in revision, EMBO Reports)

Poster presentation: Chromosome segregation and structure: Cold Spring Harbor, 2017, USA

Poster presentation: LMB-IGBMC Symposium, Cambridge, 2018, UK

Internal seminar: IGBMC, Strasbourg, 2018, France

Poster presentation: Cell Signaling and Cancer Therapy, EMBO, 2018, Croatia

# APPENDIX

**Table 1 Sequences of shRNAs used for generation of stable cell lines by retroviral infection**

| Name | | Sequence 5' → 3' |
|---|---|---|
| Control (Firefly Luciferase) | shLuc | TAATCAGAGACTTCAGGCGG |
| UCHL3 silencing | sh1 | TCAGGGACAAGATGTTACATCA |
| | sh2 | ATAGAAGTTTGCAAGAAGTTTA |
| | sh3 | CACCAACCAGTTTCTTAAACAA |
| | sh4 | GACCCTGATGAACTAAGATTTA |

**Table 2 sequences of siRNAs used for UCHL3 knockdown**

| Name | Sequence |
|---|---|
| UCHL3 siRNA-05 | CAG CAU AGC UUG UCA AUA A |
| UCHL3 siRNA-06 | GCA AUU CGU UGA UGU AUA U |
| UCHL3 siRNA-07 | GAA CAA UUG GAC UGA UUC A |
| UCHL3 siRNA-08 | GGG CAU CUC UAU GAA UUA G |
| UCHL3 3'UTR siRNA | CUG CCA UAC ACU AAC UCA A |

siRNA 05-08 belongs to UCHL3 On-TARGET smartpool, Dharmacon (L-006059-00-0005), UCHL3 3'UTR was ordered from Microsynth.

**Table 3 Optimized protocol for siRNA transfection using Oligofectamine in different dish sizes.**

| | 10 cm dish | 6 cm dish | 12 well | 24 well | Incubation [min] |
|---|---|---|---|---|---|
| Oligofectamine [µl] | 30 | 10 | 2.4 | 1.2 | 5' |
| Opti MEM [µl] | 70 | 40 | 48 | 24 | |
| | | | | | 20' |
| siRNA 40uM [µl] | 9 | 3 | 0.75 | 0.4 | 5' |
| Opti MEM [µl] | 400 | 200 | 100 | 50 | |
| Add Opti MEM | 500 | 250 | | | |
| Medium/ plate [ml] | 4 | 2 | 0.6 | 0.3 | |
| ul / plate [µl] | 1000 | 500 | 150 | 75 | |

**Table 4 List of all primers used for qPCR determining UCHL3 expression**

| Name | Sequence |
|------|----------|
| Oligo_dT | AATGCCAGCTCCGCGGCCGCGTTTTTTTTTTTT |
| h_UCHL3_F | GCCTGTGGAACAATTGGACT |
| h_UCHL3_R | TCTGACCTTCATGGGCACT |
| h_GAPDH_F | GAAGGTGAAGGTCGGAGTCA |
| h_GAPDH_R | GACAAGCTTCCCGTTCTCAG |
| h_PO_F | GTGATGTGCAGCTGATCAAGACT |
| h_PO_R | GATGACCAGCCCAAAGGAGA |
| h_HPRT_F | TCCTCCTCCTGAGCAGTCA |
| h_HPRT_R | ACCCTTTCCAAATCCTCAGC |
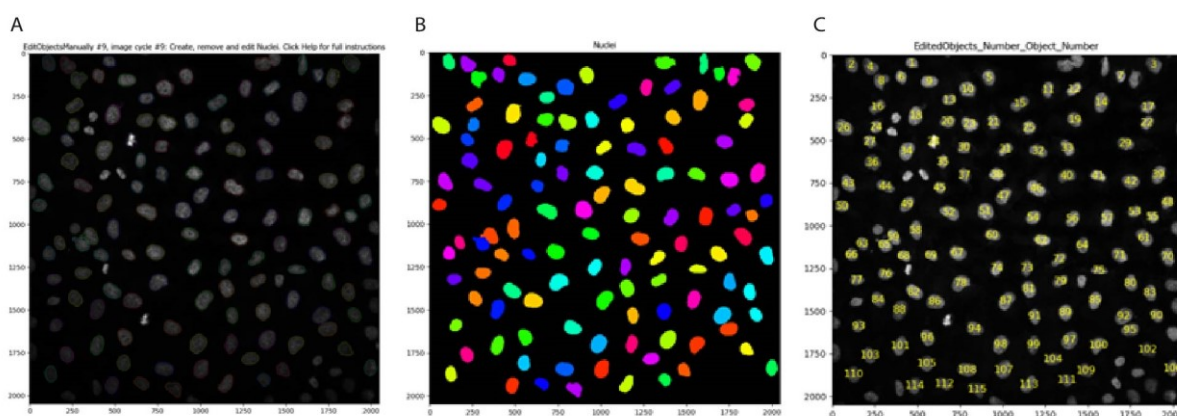


**Figure 33 Cell Profiler analysis of nuclear shape.**

(A) Original image in DAPI channel. (B) Mask for individual nuclei automatically recognised by the software.

(C) Numbered nuclei, these numbers correspond to numbered form factor values in the exported file.
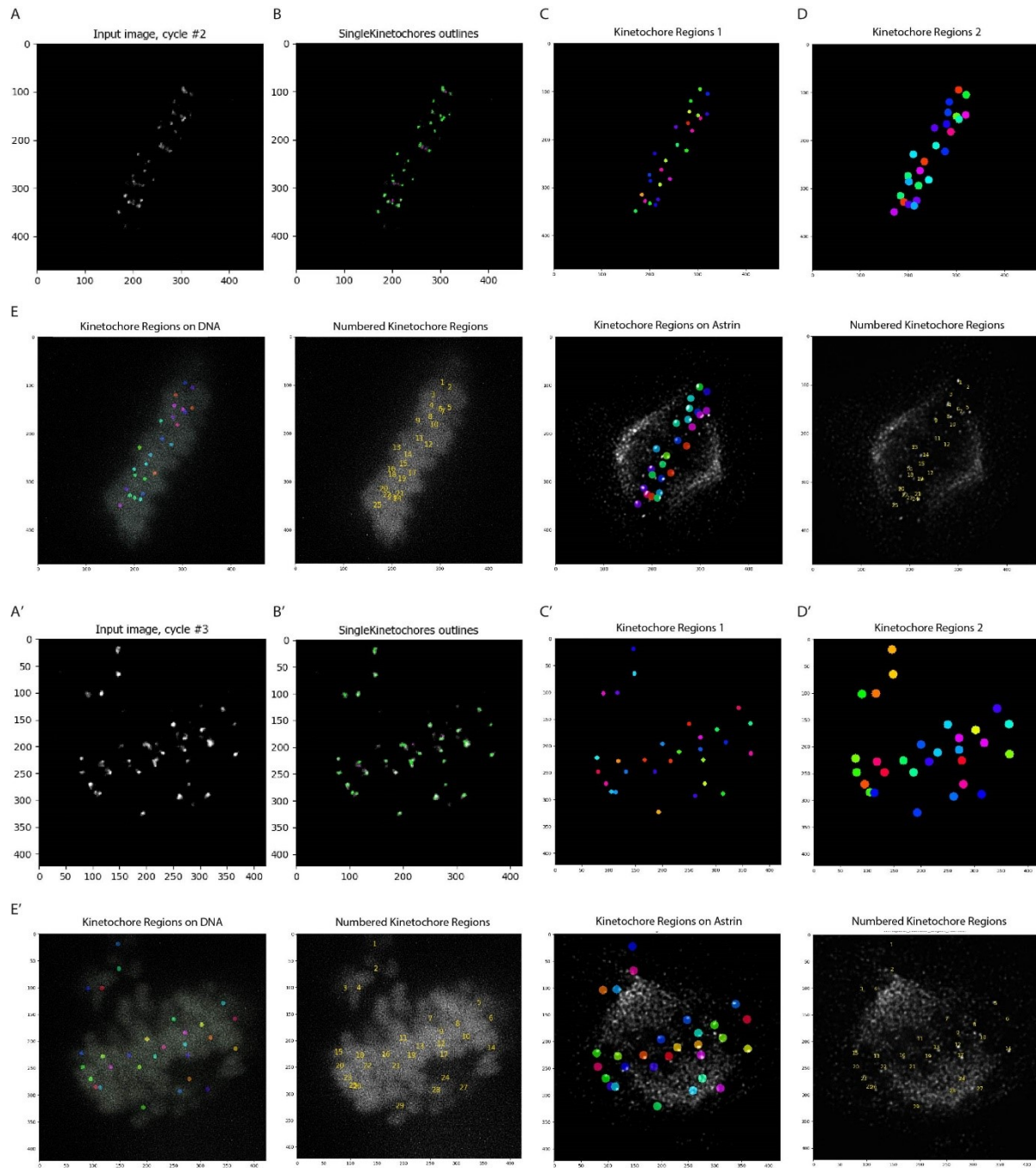
**Figure 34 Example of a Cell Profiler pipeline for quantification of Astrin intensity on kinetochores.**
(A-E) Control, (A'-E') UCHL3 downregulation. (A) Example of CREST intensity image used for B kinetochore recognition in (B). (C) Primary objects identified by the software. (D) Enlarged circular area of the kinetochores used for Astrin measurement. (E) Examples of exported images showing kinetochore position and their numbering which were used to distinguish aligned and misaligned chromosomes.

**Table 5 Detailed summary of rescue experiments presenting percentage of cells having misaligned chromosomes for all categories in four different experiments.**

| Sample | NT GFP | 3' GFP | NT WT | 3' WT | NT C/S | 3' C/S |
|---|---|---|---|---|---|---|
| Mean % of cells -Average of 4 experiments | | | | | | |
| Average | **37.3** | **46.2** | **37.5** | **40.9** | **39.0** | **46.7** |
| SD | 4.9 | 3.3 | 5.3 | 5.9 | 5.4 | 1.8 |
| SEM | 2.5 | 1.7 | 2.6 | 3.0 | 2.7 | 0.9 |
| % of cells - individual experiments | | | | | | |
| Exp I | 34.2 | 44.4 | 33.1 | 38.2 | 34.1 | 45.8 |
| Exp II | 33.6 | 44.7 | 33.5 | 35.7 | 35.3 | 45.1 |
| Exp III | 37.2 | 44.6 | 39.2 | 40.2 | 40.8 | 46.6 |
| Exp IV | 44.3 | 51.2 | 44.2 | 49.3 | 45.9 | 49.3 |
| Number of cells counted per condition per experiment | | | | | | |
| Exp I | 38 | 304 | 323 | 319 | 299 | 301 |
| Exp II | 156 | 269 | 97 | 107 | 196 | 163 |
| Exp III | 645 | 850 | 545 | 614 | 686 | 601 |
| Exp IV | 831 | 1209 | 978 | 1048 | 1085 | 1084 |
| Total # | 1670 | 2632 | 1943 | 2088 | 2266 | 2149 |

**Table 6 Genotyping primers for Trim15 mutant cell lines and for Trim15 KO mice**

| Name | Sequence 5' -> 3' |
|---|---|
| Mutant cell lines | |
| 83_hT15F | CCTGGAATTTGGACCCACT |
| 84_hT15R | CGTGCTCCTCGCAGTAAGTT |
| 85_mT15F | ACCTCGCTGAGCTGACATTC |
| 86_mT15R | TAACCGACTCCTGAGACGAT |
| Mice Trim15tm1b (EUCOMM) Hmgu for PCR genotyping | |
| LacZ-F | ACGGTTTCCATATGGGGATT |
| Trim15-R | GCTTTGAGGGTCAAAAGCAC |
| wtTrim15F | GTCCGTGGTCCTAACAATCTAAG |

**Table 7 Primer sequences for qPCR analysis of Trim15 expression**

| Name | Sequence 5' -> 3' |
|------|-------------------|
| Primers for human genes | |
| 1_h TRIM15 F | GGAGTCGACTGGAAGCTCTG |
| 2_h TRIM15 R | TGCTTCTTGCTTTCGATCTG |
| h_Gapdh_F | CCCCGGTTTCTATAAATTGAGC |
| h_Gapdh_R | CACCTTCCCCATGGTGTCT |
| h_HPRT_F | TGACCTTGATTTATTTTGCATACC |
| h_HPRT_R | CGAGCAAGACGTTCAGTCCT |
| h_GPI_F | GGTTTTGACAACTTCGAGCAG |
| h-GPI_R | CCAAAGCAGTTGATGTACCAGA |
| Primers for mouse genes | |
| mTrim15 F | GATGAAGCCATCCAACCCTA |
| mTrim15 F | TCCTGGAGCTTCTGGTCTTC |
| mActb_F | CTAAGGCCAACCGTGAAAAG |
| mActb_R | ACCAGAGGCATACAGGGACA |
| mHprt_F | TCCTCCTCAGACCGCTTTT |
| mHprt_R | CCTGGTTCATCATCGCTAATC |
| mGapdh_F | CGTCCCGTAGACAAAATGGT |
| mGapdh_R | TTGATGGCAACAATCTCCAC |

**Table 8 UCHL3 sequence used for cloning of WT and catalytically dead (C > S) mutant**

| UCHL3 sequence, TGT is coding for cysteine 95 residue, the catalytic site |
|---|
| atggagggtcaacgctggctgccgctggaggccaatcccgaggtcaccaaccagtttcttaaacaattaggtctacatcct aactggcaattcgttgatgtatatggaatggatcctgaactccttagcatggtaccaagaccagtctgtgcagtcttacttctctttccta ttacagaaaagtatgaagtattcagaacagaagaggaagaaaaaataaaatctcagggacaagatgttacatcatcagtatatttcat gaagcaaacaatcagcaatgcc**TGT**ggaacaattggactgattcatgctattgcaaacaataaagacaagatgcactttgaatct ggatcaaccttgaaaaaattcctggaggaatctgtgtcaatgagccctgaagaacgagccagatacctggagaactatgatgccat ccgagttactcatgagaccagtgcccatgaaggtcagactgaggcaccaagtatagatgagaaagtagatcttcattttattgcatta gttcatgtagatgggcatctctatgaattagatgggcggaagccatttccaattaaccatggtgaaactagtgatgaaactttattaga ggatgccatagaagtttgcaagaagtttatggagcgcgaccctgatgaactaagatttaatgcgattgctctttctgcagcaag |

**Table 9 List of candidate genes in the High-throughput siRNA screen with gene ID and Dharmacon reference number for siRNA SMARTpool.**

| Catalog # | Gene Symbol | GENE ID | Catalog # | Gene Symbol | GENE ID | Catalog # | Gene Symbol | GENE ID | Catalog # | Gene Symbol | GENE ID |
|---|---|---|---|---|---|---|---|---|---|---|---|
| **Control genes** | | | M-028950-01 | ANKIB1 | 54467 | M-025327-01 | KIAA0363 | 23148 | M-006079-02 | USP48 | 84196 |
| M-006823-01 | INCENP | 3619 | M-003603-00 | PARK2 | 5071 | M-008541-01 | RABGEF1 | 27342 | M-006099-02 | USP9X | 8239 |
| M-003326-08 | AURKB | 9212 | M-010993-01 | AIRE | 326 | M-013680-01 | NXF1 | 10482 | M-006100-02 | USP9Y | 8287 |
| M-003290-01 | PLK1 | 5347 | M-018070-00 | FLJ32440 | 286053 | M-010445-01 | NXF2 | 56001 | M-006085-01 | USP37 | 57695 |
| M-004101-02 | BUB1B | 701 | M-003279-04 | MDM2 | 4193 | M-013801-01 | SMARCAD1 | 56916 | M-031837-01 | USP50 | 373509 |
| M-010224-02 | CUL3 | 8452 | M-006536-03 | MDM4 | 4194 | M-016930-01 | TOLLIP | 54472 | M-021192-00 | USP52 | 9924 |
| **Targeted genes** | | | M-006597-01 | BRAP | 8315 | M-017578-00 | TTRAP | 51567 | M-006087-01 | USP39 | 10713 |
| M-015375-01 | ATG3 | 64422 | M-038171-01 | LOC648245 | 648245 | M-017222-00 | NSFL1C | 55968 | M-006489-00 | ASPSCR1 | 79058 |
| M-020623-01 | UFC1 | 51506 | M-022683-00 | WDR59 | 79726 | M-023533-01 | KIAA0794 | 26043 | M-025945-01 | LOC137886 | 137886 |
| M-003215-02 | CCNF | 899 | M-003004-02 | CBLB | 868 | M-006401-02 | APPBP1 | 8883 | M-018376-01 | MGC46534 | 127002 |
| M-014930-01 | FBXL10 | 84678 | M-006522-01 | AMFR | 267 | M-020112-01 | ATG7 | 10533 | M-023237-01 | DKFZP761G21 | 56970 |
| M-012881-00 | GGA3 | 23163 | M-006977-01 | UHRF1 | 29128 | M-006406-00 | MOCS3 | 27304 | M-015442-02 | DKFZP547N04 | 83932 |
| M-012066-00 | TOM1 | 10043 | M-007117-01 | UHRF2 | 115426 | M-013382-01 | UBB | 7314 | M-018651-02 | FLJ31031 | 199990 |
| M-003911-01 | TOM1L1 | 10040 | M-021044-01 | C1orf164 | 55182 | M-019408-01 | UBC | 7316 | M-024738-01 | LOC153918 | 153918 |
| M-018810-01 | TOM1L2 | 146691 | M-004591-00 | RAD18 | 56852 | M-010212-02 | ATG12 | 9140 | M-021000-00 | CGI-62 | 51101 |
| M-005314-02 | EIF2AK4 | 440275 | M-007098-00 | ZNRF1 | 84937 | M-013149-01 | FAU | 2197 | M-007038-01 | KIAA1536 | 57658 |
| M-020439-01 | IMPACT | 55364 | M-007165-01 | ZNRF2 | 223082 | M-019650-01 | POLI | 11201 | M-010637-01 | NDP52 | 10241 |
| M-020946-01 | RWDD1 | 51389 | M-006949-01 | UBOX5 | 22888 | M-008234-01 | REV1L | 51455 | M-004012-02 | EEA1 | 8411 |
| M-015117-01 | RWDD2 | 112611 | M-020569-01 | C20ORF43 | 51507 | M-004668-02 | PRPF19 | 27339 | M-003767-02 | IKBKG | 8517 |
| M-013856-00 | C21ORF6 | 10069 | M-021181-01 | FLJ20323 | 54468 | M-007201-02 | STUB1 | 10273 | M-020327-01 | KIAA1018 | 22909 |
| M-016719-01 | RWDD3 | 25950 | M-015603-01 | DHX57 | 90957 | M-007200-00 | UBE4A | 9354 | M-016269-02 | OPTN | 10133 |
| M-016803-01 | MGC10198 | 201965 | M-004779-03 | KIAA0999 | 23387 | M-007202-01 | UBE4B | 10277 | M-015381-01 | PCF11 | 51585 |
| M-016816-00 | FLJ32642 | 137492 | M-004632-00 | LATS1 | 9113 | M-007203-01 | WDSUB1 | 151525 | M-006454-01 | POLH | 5429 |
| M-007193-01 | HACE1 | 57531 | M-003865-02 | LATS2 | 26524 | M-004609-01 | CYLD | 1540 | M-021038-00 | POLK | 51426 |
| M-007185-01 | HUWE1 | 10075 | M-004259-03 | MARK1 | 4139 | M-027332-03 | DUB3 | 377630 | M-005255-02 | TANK | 10010 |
| M-017674-01 | JOSD1 | 9929 | M-003517-03 | MARK3 | 4140 | M-008570-00 | TEX27 | 60685 | M-016892-01 | TAX1BP1 | 8887 |
| M-015500-01 | SBBI54 | 126119 | M-005345-02 | MARK4 | 57787 | M-009701-01 | ZNF216 | 7763 | M-020406-01 | PROSAPIP2 | 9755 |
| M-012013-01 | MJD | 4287 | M-019752-00 | RHBDD3 | 25807 | M-006061-02 | USP1 | 7398 | M-014328-00 | TNIP2 | 79155 |
| M-024927-01 | ATXN3L | 92552 | M-003959-05 | SNF1LK | 150094 | M-006062-02 | USP10 | 9100 | M-010072-02 | WRNIP1 | 56897 |
| M-005798-02 | CXORF53 | 79184 | M-003517-03 | MARK3 | 4140 | M-006063-01 | USP11 | 8237 | M-005067-01 | XPA | 7507 |
| M-018630-01 | FLJ14981 | 84954 | M-005345-02 | MARK4 | 57787 | M-027148-00 | USP12 | 219333 | M-014036-01 | ZFYVE20 | 64145 |
| M-005905-02 | MYSM1 | 114803 | M-019752-00 | RHBDD3 | 25807 | M-006066-01 | USP15 | 9958 | M-005791-00 | BAP1 | 8314 |
| M-012252-02 | PRPF8 | 10594 | M-003959-05 | SNF1LK | 150094 | M-004236-03 | USP18 | 11274 | M-004309-00 | UCHL1 | 7345 |
| M-012202-01 | STAMBP | 10617 | M-004778-03 | SIK2 | 23235 | M-006068-02 | USP19 | 10869 | M-006059-02 | UCHL3 | 7347 |
| M-005783-02 | STAMBPL1 | 57559 | M-004322-05 | SNRK | 54861 | M-006069-03 | USP2 | 9099 | M-006060-03 | UCHL5 | 51377 |
| M-005814-01 | COPS5 | 10987 | M-008533-01 | KIAA1959 | 84959 | M-006071-00 | USP21 | 27005 | M-008768-03 | AKTIP | 64400 |
| M-006024-00 | PSMD14 | 10213 | M-014655-00 | TDRD3 | 81550 | M-006073-02 | USP24 | 23358 | M-003549-01 | TSG101 | 7251 |
| M-019535-02 | EIF3S5 | 8665 | M-003102-04 | TNK2 | 10188 | M-006075-01 | USP26 | 83844 | M-010064-03 | UBE2V1 | 7335 |
| M-003883-01 | EIF3S3 | 8667 | M-019399-00 | KIAA1582 | 57690 | M-031532-01 | USP27X | 389856 | M-008823-00 | UBE2V2 | 7336 |
| M-017017-00 | COPS6 | 10980 | M-017914-00 | PHGDHL1 | 337867 | M-006077-01 | USP29 | 57663 | M-008494-02 | UEVLD | 55293 |
| M-009621-01 | PSMD7 | 5713 | M-017474-00 | UBAP1 | 51271 | M-021294-03 | USP30 | 84749 | M-027120-00 | ANKRD13 | 88455 |
| M-004771-01 | MAP3K7IP2 | 23118 | M-013168-00 | UBAP2 | 55833 | M-022513-02 | USP31 | 57478 | M-018787-01 | FLJ25555 | 124930 |
| M-015572-01 | TAB3 | 257397 | M-021220-01 | NICE-4 | 9898 | M-006082-01 | USP34 | 9736 | M-026603-01 | LOC338692 | 338692 |
| M-020939-02 | NEIL3 | 55247 | M-008616-00 | UBASH3A | 53347 | M-006083-01 | USP35 | 57558 | M-017685-01 | DNAJB2 | 3300 |
| M-005283-00 | NUP153 | 9972 | M-021567-01 | VPS13D | 55187 | M-006084-01 | USP36 | 57602 | M-004724-00 | EPN1 | 29924 |
| M-004746-02 | RANBP2 | 5903 | M-006095-02 | USP5 | 8078 | M-006086-01 | USP38 | 84640 | M-004725-01 | EPN2 | 22905 |
| M-009065-00 | RBM10 | 8241 | M-010522-01 | M17S2 | 4077 | M-004974-01 | USP4 | 7375 | M-021006-01 | EPN3 | 55040 |
| M-020032-01 | RBM6 | 10180 | M-010230-00 | SQSTM1 | 8878 | M-006088-01 | USP40 | 55230 | M-004005-01 | EPS15 | 2060 |
| M-015936-01 | RYBP | 23429 | M-019158-01 | NYREN18 | 51667 | M-031434-01 | USP41 | 373856 | M-004006-00 | EPS15L1 | 58513 |
| M-018575-02 | SHARPIN | 81858 | M-005231-00 | RAD23A | 5886 | M-006089-01 | USP42 | 84132 | M-016835-00 | HGS | 9146 |
| M-006037-00 | SOLH | 6650 | M-011759-01 | RAD23B | 5887 | M-023019-03 | USP43 | 124739 | M-011423-00 | STAM | 8027 |
| M-009265-01 | YAF2 | 10138 | M-020776-01 | UBADC1 | 10422 | M-006092-03 | USP46 | 64854 | M-017361-01 | STAM2 | 10254 |
| M-010158-00 | ZNF265 | 9406 | M-015044-00 | BMSC-UBP | 84993 | M-006093-01 | USP47 | 55031 | M-016586-01 | LOC130617 | 130617 |
| M-010025-01 | ZRANB3 | 84083 | M-012942-01 | UBQLN1 | 29979 | M-027186-01 | USP53 | 54532 | M-011365-01 | PSMD4 | 5710 |
| M-020796-01 | NPL4 | 55666 | M-013566-00 | UBQLN2 | 29978 | M-016853-01 | USP54 | 159195 | M-006995-03 | RAP80 | 51720 |
| M-021061-01 | OTUB1 | 55611 | M-013398-00 | UBQLN3 | 50613 | M-006096-03 | USP6 | 9098 | M-006357-00 | SENP1 | 29843 |
| M-010983-01 | OTUB2 | 78990 | M-021178-00 | C1ORF6 | 56893 | M-006097-01 | USP7 | 7874 | M-006033-01 | SENP2 | 59343 |
| M-026487-01 | OTUD1 | 220213 | M-009106-01 | FAF1 | 11124 | M-005203-01 | USP8 | 9101 | M-006034-01 | SENP3 | 26168 |
| M-009927-00 | OTUD4 | 54726 | M-008652-00 | LOC51035 | 51035 | M-017741-00 | C13ORF22 | 10208 | M-005946-01 | SENP5 | 205564 |
| M-013823-00 | OTUD5 | 55593 | M-010649-01 | ETEA | 23197 | M-006067-01 | USP16 | 10600 | M-006044-01 | SENP6 | 26054 |
| M-032033-00 | HSHIN6 | 139562 | M-016458-00 | ASC1P100 | 84164 | M-006070-01 | USP20 | 10868 | M-006035-01 | SENP7 | 57337 |
| M-008553-01 | OTUD6B | 51633 | M-012410-01 | AUP1 | 550 | M-006072-01 | USP22 | 23326 | M-004071-00 | SENP8 | 123228 |
| M-016115-01 | PARP11 | 57097 | M-031847-00 | CUEDC1 | 404093 | M-006078-02 | USP3 | 9960 | M-029321-01 | LOC392188 | 392188 |
| M-009270-01 | ZRANB1 | 54764 | M-019139-01 | DCUN1D1 | 54165 | M-006081-00 | USP33 | 23032 | M-009477-01 | ZFAND6 | 54469 |
| M-019137-01 | VCPIP1 | 80124 | M-020261-01 | DCUN1D2 | 55208 | M-006091-01 | USP44 | 84101 | M-036937-00 | LOC645402 | 645402 |
| M-027369-00 | YOD1 | 55432 | M-031988-00 | DMRT3 | 58524 | M-010054-01 | USP45 | 85015 | M-183279-00 | LOC645836 | 645836 |
| M-003499-00 | HDAC6 | 10013 | M-026122-00 | DMRTA1 | 63951 | M-005945-01 | USP49 | 25862 | M-028352-02 | DUB1A | 402164 |
| M-003966-05 | MAP2K5 | 5607 | M-021793-01 | DMRTA2 | 63950 | M-032247-01 | USP51 | 158880 | M-014021-01 | RBAF600 | 23352 |
| M-003582-04 | MAP3K2 | 10746 | M-015987-01 | LOC124402 | 124402 | M-006064-00 | USP13 | 8975 | M-017918-01 | UFD1L | 7353 |
| M-006932-02 | C20ORF18 | 10616 | M-018939-00 | MGC29814 | 283991 | M-006074-02 | USP25 | 29761 | M-008727-01 | VCP | 7415 |
| M-021419-01 | RNF31 | 55072 | M-016841-00 | HYPK | 25764 | M-006076-01 | USP28 | 57646 | M-004701-02 | C13ORF9 | 51028 |
| M-019984-00 | ARIH1 | 25820 | M-019063-01 | N4BP2 | 55728 | M-006065-02 | USP14 | 9097 | | | |
| M-020104-01 | ARIH2 | 10425 | M-027161-02 | NACA | 4666 | M-006080-03 | USP32 | 84669 | | | |

# 5 REFERENCES

1. Swatek, K. N. & Komander, D. Ubiquitin modifications. *Cell Res.* **26**, 399–422 (2016).

2. Meroni, G. & Diez-Roux, G. TRIM/RBCC, a novel class of 'single protein RING finger' E3 ubiquitin ligases. *BioEssays News Rev. Mol. Cell. Dev. Biol.* **27**, 1147–1157 (2005).

3. Kano, S., Miyajima, N., Fukuda, S. & Hatakeyama, S. Tripartite motif protein 32 facilitates cell growth and migration via degradation of Abl-interactor 2. *Cancer Res.* **68**, 5572–5580 (2008).

4. Watanabe, M., Tsukiyama, T. & Hatakeyama, S. TRIM31 interacts with p52(Shc) and inhibits Src-induced anchorage-independent growth. *Biochem. Biophys. Res. Commun.* **388**, 422–427 (2009).

5. Masuda, Y. *et al.* TRIM29 regulates the assembly of DNA repair proteins into damaged chromatin. *Nat. Commun.* **6**, 7299 (2015).

6. Sato, T., Okumura, F., Ariga, T. & Hatakeyama, S. TRIM6 interacts with Myc and maintains the pluripotency of mouse embryonic stem cells. *J. Cell Sci.* **125**, 1544–1555 (2012).

7. Jensen, K., Shiels, C. & Freemont, P. S. PML protein isoforms and the RBCC/TRIM motif. *Oncogene* **20**, 7223–7233 (2001).

8. Uchil, P. D., Quinlan, B. D., Chan, W.-T., Luna, J. M. & Mothes, W. TRIM E3 ligases interfere with early and late stages of the retroviral life cycle. *PLoS Pathog.* **4**, e16 (2008).

9. Stremlau, M. *et al.* The cytoplasmic body component TRIM5alpha restricts HIV-1 infection in Old World monkeys. *Nature* **427**, 848–853 (2004).

10. Chen, S. N. *et al.* Human molecular genetic and functional studies identify TRIM63, encoding Muscle RING Finger Protein 1, as a novel gene for human hypertrophic cardiomyopathy. *Circ. Res.* **111**, 907–919 (2012).

11. Arra, M. *et al.* The M694V variant of the familial Mediterranean fever gene is associated with sporadic early-onset Alzheimer's disease in an Italian population sample. *Dement. Geriatr. Cogn. Disord.* **23**, 55–59 (2007).

12. Trockenbacher, A. *et al.* MID1, mutated in Opitz syndrome, encodes an ubiquitin ligase that targets phosphatase 2A for degradation. *Nat. Genet.* **29**, 287–294 (2001).

13. Tsai, W.-W. *et al.* TRIM24 links a non-canonical histone signature to breast cancer. *Nature* **468**, 927–932 (2010).

14. Herquel, B. *et al.* Transcription cofactors TRIM24, TRIM28, and TRIM33 associate to form regulatory complexes that suppress murine hepatocellular carcinoma. *Proc. Natl. Acad. Sci. U. S. A.* **108**, 8212–8217 (2011).

15. Nigg, E. A. Mitotic kinases as regulators of cell division and its checkpoints. *Nat. Rev. Mol. Cell Biol.* **2**, 21 (2001).

16. Komander, D., Clague, M. J. & Urbé, S. Breaking the chains: structure and function of the deubiquitinases. *Nat. Rev. Mol. Cell Biol.* **10**, 550–563 (2009).

17. Luo, K. *et al.* A phosphorylation–deubiquitination cascade regulates the BRCA2–RAD51 axis in homologous recombination. *Genes Dev.* **30**, 2581–2595 (2016).

18. Liao, C. *et al.* UCHL3 Regulates Topoisomerase-Induced Chromosomal Break Repair by Controlling TDP1 Proteostasis. *Cell Rep.* **23**, 3352–3365 (2018).

19. Wu, M. *et al.* LUBAC controls chromosome alignment by targeting CENP-E to attached kinetochores. *Nat. Commun.* **10**, (2019).

20. Kim, Y., Holland, A. J., Lan, W. & Cleveland, D. W. Aurora kinases and protein phosphatase 1 mediate chromosome congression through regulation of CENP-E. *Cell* **142**, 444–455 (2010).

21. Goldstein, G. *et al.* Isolation of a polypeptide that has lymphocyte-differentiating properties and is probably represented universally in living cells. *Proc. Natl. Acad. Sci. U. S. A.* **72**, 11–15 (1975).

22. Kulak, N. A., Pichler, G., Paron, I., Nagaraj, N. & Mann, M. Minimal, encapsulated proteomic-sample processing applied to copy-number estimation in eukaryotic cells. *Nat. Methods* **11**, 319–324 (2014).

23. Kimura, Y. & Tanaka, K. Regulatory mechanisms involved in the control of ubiquitin homeostasis. *J. Biochem. (Tokyo)* **147**, 793–798 (2010).

24. Grou, C. P., Pinto, M. P., Mendes, A. V., Domingues, P. & Azevedo, J. E. The *de novo* synthesis of ubiquitin: identification of deubiquitinases acting on ubiquitin precursors. *Sci. Rep.* **5**, 12836 (2015).

25. Handley, P. M., Mueckler, M., Siegel, N. R., Ciechanover, A. & Schwartz, A. L. Molecular cloning, sequence, and tissue distribution of the human ubiquitin-activating enzyme E1. *Proc. Natl. Acad. Sci. U. S. A.* **88**, 258–262 (1991).

26. Chiu, Y.-H., Sun, Q. & Chen, Z. J. E1-L2 Activates Both Ubiquitin and FAT10. *Mol. Cell* **27**, 1014–1023 (2007).

27. Jin, J., Li, X., Gygi, S. P. & Harper, J. W. Dual E1 activation systems for ubiquitin differentially regulate E2 enzyme charging. *Nature* **447**, 1135–1138 (2007).

28. Stewart, M. D., Ritterhoff, T., Klevit, R. E. & Brzovic, P. S. E2 enzymes: more than just middle men. *Cell Res.* **26**, 423–440 (2016).

29. Li, W. *et al.* Genome-Wide and Functional Annotation of Human E3 Ubiquitin Ligases Identifies MULAN, a Mitochondrial E3 that Regulates the Organelle's Dynamics and Signaling. *PLoS ONE* **3**, (2008).

30. Berndsen, C. E. & Wolberger, C. New insights into ubiquitin E3 ligase mechanism. *Nat. Struct. Mol. Biol.* **21**, 301–307 (2014).

31. Williams, C., Berg, M. van den, Sprenger, R. R. & Distel, B. A Conserved Cysteine Is Essential for Pex4p-dependent Ubiquitination of the Peroxisomal Import Receptor Pex5p. *J. Biol. Chem.* **282**, 22534–22543 (2007).

32. Skieterska, K., Rondou, P., Lintermans, B. & Van Craenenbroeck, K. KLHL12 Promotes Non-Lysine Ubiquitination of the Dopamine Receptors D4.2 and D4.4, but Not of the ADHD-Associated D4.7 Variant. *PLOS ONE* **10**, e0145654 (2015).

33. McDowell, G. S., Kucerova, R. & Philpott, A. Non-canonical ubiquitylation of the proneural protein Ngn2 occurs in both Xenopus embryos and mammalian cells. *Biochem. Biophys. Res. Commun.* **400**, 655–660 (2010).

34. Tatham, M. H., Plechanovová, A., Jaffray, E. G., Salmen, H. & Hay, R. T. Ube2W conjugates ubiquitin to α-amino groups of protein N-termini. *Biochem. J.* **453**, 137–145 (2013).

35. Nakasone, M. A., Livnat-Levanon, N., Glickman, M. H., Cohen, R. E. & Fushman, D. Mixed-linkage ubiquitin chains send mixed messages. *Struct. Lond. Engl. 1993* **21**, 727–740 (2013).

36. Meyer, H.-J. & Rape, M. Enhanced protein degradation by branched ubiquitin chains. *Cell* **157**, 910–921 (2014).

37. Swaney, D. L., Rodríguez-Mias, R. A. & Villén, J. Phosphorylation of ubiquitin at Ser65 affects its polymerization, targets, and proteome-wide turnover. *EMBO Rep.* **16**, 1131–1144 (2015).

38. Koyano, F. *et al.* Ubiquitin is phosphorylated by PINK1 to activate parkin. *Nature* **510**, 162–166 (2014).

39. Ohtake, F. *et al.* Ubiquitin acetylation inhibits polyubiquitin chain elongation. *EMBO Rep.* **16**, 192–201 (2015).

40. Qiu, J. *et al.* Ubiquitination independent of E1 and E2 enzymes by bacterial effectors. *Nature* **533**, 120 (2016).

41. Tatham, M. H., Matic, I., Mann, M. & Hay, R. T. Comparative Proteomic Analysis Identifies a Role for SUMO in Protein Quality Control. *Sci. Signal.* **4**, rs4–rs4 (2011).

42. Kirkin, V. & Dikic, I. Role of ubiquitin- and Ubl-binding proteins in cell signaling. *Curr. Opin. Cell Biol.* **19**, 199–205 (2007).

43. Husnjak, K. & Dikic, I. Ubiquitin-Binding Proteins: Decoders of Ubiquitin-Mediated Cellular Functions. *Annu. Rev. Biochem.* **81**, 291–322 (2012).

44. Spence, J., Sadis, S., Haas, A. L. & Finley, D. A ubiquitin mutant with specific defects in DNA repair and multiubiquitination. *Mol. Cell. Biol.* **15**, 1265–1273 (1995).

45. Chau, V. *et al.* A multiubiquitin chain is confined to specific lysine in a targeted short-lived protein. *Science* **243**, 1576–1583 (1989).

46. Lu, Z. & Hunter, T. Ubiquitylation and proteasomal degradation of the p21(Cip1), p27(Kip1) and p57(Kip2) CDK inhibitors. *Cell Cycle Georget. Tex* **9**, 2342–2352 (2010).

47. Klotz, K. *et al.* SCF(Fbxw7/hCdc4) targets cyclin E2 for ubiquitin-dependent proteolysis. *Exp. Cell Res.* **315**, 1832–1839 (2009).

48. Lindon, C. & Pines, J. Ordered proteolysis in anaphase inactivates Plk1 to contribute to proper mitotic exit in human cells. *J. Cell Biol.* **164**, 233–241 (2004).

49. Pinto, M. J., Pedro, J. R., Costa, R. O. & Almeida, R. D. Visualizing K48 Ubiquitination during Presynaptic Formation By Ubiquitination-Induced Fluorescence Complementation (UiFC). *Front. Mol. Neurosci.* **9**, 43 (2016).

50. Cui, C.-P. *et al.* Dynamic ubiquitylation of Sox2 regulates proteostasis and governs neural progenitor cell differentiation. *Nat. Commun.* **9**, 4648 (2018).

51. Mallette, F. A. & Richard, S. K48-linked ubiquitination and protein degradation regulate 53BP1 recruitment at DNA damage sites. *Cell Res.* **22**, 1221–1223 (2012).

52. Jin, L., Williamson, A., Banerjee, S., Philipp, I. & Rape, M. Mechanism of Ubiquitin-Chain Formation by the Human Anaphase-Promoting Complex. *Cell* **133**, 653–665 (2008).

53. Matsumoto, M. L. *et al.* K11-Linked Polyubiquitination in Cell Cycle Control Revealed by a K11 Linkage-Specific Antibody. *Mol. Cell* **39**, 477–484 (2010).

54. Dammer, E. B. *et al.* Polyubiquitin linkage profiles in three models of proteolytic stress suggest the etiology of Alzheimer disease. *J. Biol. Chem.* **286**, 10457–10465 (2011).

55. Boutet, S. C., Disatnik, M.-H., Chan, L. S., Iori, K. & Rando, T. A. Regulation of Pax3 by proteasomal degradation of monoubiquitinated protein in skeletal muscle progenitors. *Cell* **130**, 349–362 (2007).

56. Kravtsova-Ivantsiv, Y., Cohen, S. & Ciechanover, A. Modification by Single Ubiquitin Moieties Rather Than Polyubiquitination Is Sufficient for Proteasomal Processing of the p105 NF-κB Precursor. *Mol. Cell* **33**, 496–504 (2009).

57. Dimova, N. V. *et al.* APC/C-mediated multiple monoubiquitination provides an alternative degradation signal for cyclin B1. *Nat. Cell Biol.* **14**, 168–176 (2012).

58. Duncan, L. M. *et al.* Lysine-63-linked ubiquitination is required for endolysosomal degradation of class I molecules. *EMBO J.* **25**, 1635–1645 (2006).

59. Zhang, L., Xu, M., Scotti, E., Chen, Z. J. & Tontonoz, P. Both K63 and K48 ubiquitin linkages signal lysosomal degradation of the LDL receptor. *J. Lipid Res.* **54**, 1410–1420 (2013).

60. Ordureau, A. *et al.* Defining roles of PARKIN and ubiquitin phosphorylation by PINK1 in mitochondrial quality control using a ubiquitin replacement strategy. *Proc. Natl. Acad. Sci.* **112**, 6637–6642 (2015).

61. Bellare, P. *et al.* A role for ubiquitin in the spliceosome assembly pathway. *Nat. Struct. Mol. Biol.* **15**, 444–451 (2008).

62. Spence, J. *et al.* Cell cycle-regulated modification of the ribosome by a variant multiubiquitin chain. *Cell* **102**, 67–76 (2000).

63. Lauwers, E., Jacob, C. & André, B. K63-linked ubiquitin chains as a specific signal for protein sorting into the multivesicular body pathway. *J. Cell Biol.* **185**, 493–502 (2009).

64. Tanno, H., Yamaguchi, T., Goto, E., Ishido, S. & Komada, M. The Ankrd 13 family of UIM-bearing proteins regulates EGF receptor endocytosis from the plasma membrane. *Mol. Biol. Cell* **23**, 1343–1353 (2012).

65. Deng, L. *et al.* Activation of the IkappaB kinase complex by TRAF6 requires a dimeric ubiquitin-conjugating enzyme complex and a unique polyubiquitin chain. *Cell* **103**, 351–361 (2000).

66. Adhikary, S. *et al.* The Ubiquitin Ligase HectH9 Regulates Transcriptional Activation by Myc and Is Essential for Tumor Cell Proliferation. *Cell* **123**, 409–421 (2005).

67. Hofmann, R. M. & Pickart, C. M. Noncanonical MMS2-encoded ubiquitin-conjugating enzyme functions in assembly of novel polyubiquitin chains for DNA repair. *Cell* **96**, 645–653 (1999).

68. Liu, P. *et al.* K63-linked polyubiquitin chains bind to DNA to facilitate DNA damage repair. *Sci. Signal.* **11**, (2018).

69. Sobhian, B. *et al.* RAP80 Targets BRCA1 to Specific Ubiquitin Structures at DNA Damage Sites. *Science* **316**, 1198–1202 (2007).

70. Clague, M. J., Heride, C. & Urbé, S. The demographics of the ubiquitin system. *Trends Cell Biol.* **25**, 417–426 (2015).

71. Maerki, S. *et al.* The Cul3–KLHL21 E3 ubiquitin ligase targets Aurora B to midzone microtubules in anaphase and is required for cytokinesis. *J. Cell Biol.* **187**, 791–800 (2009).

72. Su, Y.-T. *et al.* Monoubiquitination of Filamin B Regulates Vascular Endothelial Growth Factor-Mediated Trafficking of Histone Deacetylase 7. *Mol. Cell. Biol.* **33**, 1546–1560 (2013).

73. Sasaki, A. T. *et al.* Ubiquitination of K-Ras enhances activation and facilitates binding to select downstream effectors. *Sci. Signal.* **4**, ra13 (2011).

74. Pavri, R. *et al.* Histone H2B monoubiquitination functions cooperatively with FACT to regulate elongation by RNA polymerase II. *Cell* **125**, 703–717 (2006).

75. Pan, M.-R., Peng, G., Hung, W.-C. & Lin, S.-Y. Monoubiquitination of H2AX protein regulates DNA damage response signaling. *J. Biol. Chem.* **286**, 28599–28607 (2011).

76. Chen, S. *et al.* Histone H2B monoubiquitination is a critical epigenetic switch for the regulation of autophagy. *Nucleic Acids Res.* **45**, 1144–1158 (2017).

77. Rittinger, K. & Ikeda, F. Linear ubiquitin chains: enzymes, mechanisms and biology. *Open Biol.* **7**, (2017).

78. Rahighi, S. *et al.* Specific recognition of linear ubiquitin chains by NEMO is important for NF-kappaB activation. *Cell* **136**, 1098–1109 (2009).

79. Tokunaga, F. *et al.* Involvement of linear polyubiquitylation of NEMO in NF-κB activation. *Nat. Cell Biol.* **11**, 123–132 (2009).

80. Tang, Y. *et al.* Linear ubiquitination of cFLIP induced by LUBAC contributes to TNFa-induced apoptosis. *J. Biol. Chem.* jbc.RA118.005449 (2018). doi:10.1074/jbc.RA118.005449

81. Taraborrelli, L. *et al.* LUBAC prevents lethal dermatitis by inhibiting cell death induced by TNF, TRAIL and CD95L. *Nat. Commun.* **9**, 3910 (2018).

82. Nijman, S. M. B. *et al.* A Genomic and Functional Inventory of Deubiquitinating Enzymes. *Cell* **123**, 773–786 (2005).

83. Mevissen, T. E. T. & Komander, D. Mechanisms of Deubiquitinase Specificity and Regulation. *Annu. Rev. Biochem.* **86**, 159–192 (2017).

84. Abdul Rehman, S. A. *et al.* MINDY-1 Is a Member of an Evolutionarily Conserved and Structurally Distinct New Family of Deubiquitinating Enzymes. *Mol. Cell* **63**, 146–155 (2016).

85. Gong, L., Kamitani, T., Millas, S. & Yeh, E. T. Identification of a novel isopeptidase with dual specificity for ubiquitin- and NEDD8-conjugated proteins. *J. Biol. Chem.* **275**, 14212–14216 (2000).

86. Wada, H., Kito, K., Caskey, L. S., Yeh, E. T. H. & Kamitani, T. Cleavage of the C-Terminus of NEDD8 by UCH-L3. *Biochem. Biophys. Res. Commun.* **251**, 688–692 (1998).

87. Cope, G. A. *et al.* Role of predicted metalloprotease motif of Jab1/Csn5 in cleavage of Nedd8 from Cul1. *Science* **298**, 608–611 (2002).

88. Faesen, A. C. *et al.* The Differential Modulation of USP Activity by Internal Regulatory Domains, Interactors and Eight Ubiquitin Chain Types. *Chem. Biol.* **18**, 1550–1561 (2011).

89. Mevissen, T. E. T. *et al.* OTU Deubiquitinases Reveal Mechanisms of Linkage Specificity and Enable Ubiquitin Chain Restriction Analysis. *Cell* **154**, 169–184 (2013).

90. Bremm, A., Freund, S. M. V. & Komander, D. Lys11-linked ubiquitin chains adopt compact conformations and are preferentially hydrolyzed by the deubiquitinase Cezanne. *Nat. Struct. Mol. Biol.* **17**, 939–947 (2010).

91. Virdee, S., Ye, Y., Nguyen, D. P., Komander, D. & Chin, J. W. Engineered diubiquitin synthesis reveals Lys29-isopeptide specificity of an OTU deubiquitinase. *Nat. Chem. Biol.* **6**, 750–757 (2010).

92. Sato, Y. *et al.* Structural basis for specific cleavage of Lys 63-linked polyubiquitin chains. *Nature* **455**, 358–362 (2008).

93. McCullough, J., Clague, M. J. & Urbé, S. AMSH is an endosome-associated ubiquitin isopeptidase. *J. Cell Biol.* **166**, 487–492 (2004).

94. Kristariyanto, Y. A., Abdul Rehman, S. A., Weidlich, S., Knebel, A. & Kulathu, Y. A single MIU motif of MINDY-1 recognizes K48-linked polyubiquitin chains. *EMBO Rep.* **18**, 392–402 (2017).

95. Liao, C. *et al.* UCHL3 Regulates Topoisomerase-Induced Chromosomal Break Repair by Controlling TDP1 Proteostasis. *Cell Rep.* **23**, 3352–3365 (2018).

96. Ye, Y. *et al.* Polyubiquitin binding and cross-reactivity in the USP domain deubiquitinase USP21. *EMBO Rep.* **12**, 350–357 (2011).

97. Hospenthal, M. K., Freund, S. M. V. & Komander, D. Assembly, analysis and architecture of atypical ubiquitin chains. *Nat. Struct. Mol. Biol.* **20**, 555–565 (2013).

98. Wauer, T. *et al.* Ubiquitin Ser65 phosphorylation affects ubiquitin structure, chain assembly and hydrolysis. *EMBO J.* **34**, 307–325 (2015).

99. Lee, B.-H. *et al.* USP14 deubiquitinates proteasome-bound substrates that are ubiquitinated at multiple sites. *Nature* **532**, 398–401 (2016).

100. Verma, R. *et al.* Role of Rpn11 Metalloprotease in Deubiquitination and Degradation by the 26S Proteasome. *Science* **298**, 611–615 (2002).

101. Huang, T.-H., Shen, Z.-J., Sleckman, B. P. & Tyler, J. K. The histone chaperone ASF1 regulates the activation of ATM and DNA-PKcs in response to DNA double-strand breaks. *Cell Cycle* **17**, 1413–1424 (2018).

102. Nam, E. A. & Cortez, D. ATR signalling: more than meeting at the fork. *Biochem. J.* **436**, 527–536 (2011).

103. Yuan, J., Luo, K., Zhang, L., Cheville, J. C. & Lou, Z. USP10 regulates p53 localization and stability by deubiquitinating p53. *Cell* **140**, 384–396 (2010).

104. Ke, J. *et al.* USP11 regulates p53 stability by deubiquitinating p53. *J. Zhejiang Univ. Sci. B* **15**, 1032–1038 (2014).

105. Luo, J. *et al.* OTUD5 regulates p53 stability by deubiquitinating p53. *PloS One* **8**, e77682 (2013).

106. Flemming, W. *Zellsubstanz, Kern und Zelltheilung.* (F.C.W. Vogel, 1882).

107. Harrison, C. J., Allen', T. D., Britch, M. & Harris, R. HIGH-RESOLUTION SCANNING ELECTRON MICROSCOPY OF HUMAN METAPHASE CHROMOSOMES. 14 (1982).

108. Hirano, T. & Mitchison, T. J. A heterodimeric coiled-coil protein required for mitotic chromosome condensation in vitro. *Cell* **79**, 449–458 (1994).

109. Batty, P. & Gerlich, D. W. Mitotic Chromosome Mechanics: How Cells Segregate Their Genome. *Trends Cell Biol.* (2019). doi:10.1016/j.tcb.2019.05.007

110. Kimura, K., Hirano, M., Kobayashi, R. & Hirano, T. Phosphorylation and activation of 13S condensin by Cdc2 in vitro. *Science* **282**, 487–490 (1998).

111. Terakawa, T. *et al.* The condensin complex is a mechanochemical motor that translocates along DNA. *Science* **358**, 672–676 (2017).

112. Gibcus, J. H. *et al.* A pathway for mitotic chromosome formation. *Science* **359**, eaao6135 (2018).

113. Strukov, Y. G. & Belmont, A. S. Mitotic Chromosome Structure: Reproducibility of Folding and Symmetry between Sister Chromatids. *Biophys. J.* **96**, 1617–1628 (2009).

114. Hudson, D. F., Vagnarelli, P., Gassmann, R. & Earnshaw, W. C. Condensin Is Required for Nonhistone Protein Assembly and Structural Integrity of Vertebrate Mitotic Chromosomes. *Dev. Cell* **5**, 323–336 (2003).

115. Clarke, D. J., Johnson, R. T. & Downes, C. S. Topoisomerase II inhibition prevents anaphase chromatid segregation in mammalian cells independently of the generation of DNA strand breaks. *J. Cell Sci.* **105**, 563–569 (1993).

116. Losada, A., Hirano, M. & Hirano, T. Cohesin release is required for sister chromatid resolution, but not for condensin-mediated compaction, at the onset of mitosis. *Genes Dev.* **16**, 3004–3016 (2002).

117. Sumara, I. *et al.* The dissociation of cohesin from chromosomes in prophase is regulated by Polo-like kinase. *Mol. Cell* **9**, 515–525 (2002).

118. Silva, R. D. *et al.* Absence of the Spindle Assembly Checkpoint Restores Mitotic Fidelity upon Loss of Sister Chromatid Cohesion. *Curr. Biol.* **28**, 2837-2844.e3 (2018).

119. Steiner, F. A. & Henikoff, S. Holocentromeres are dispersed point centromeres localized at transcription factor hotspots. *eLife* **3**, e02025 (2014).

120. Melters, D. P. *et al.* Elastic and Rigidified CENP-A Nucleosomes govern Centromeric Chromatin Plasticity. *bioRxiv* 392787 (2018). doi:10.1101/392787

121. Rieder, C. L. The structure of the cold-stable kinetochore fiber in metaphase PtK1 cells. *Chromosoma* **84**, 145–158 (1981).

122. Howman, E. V. *et al.* Early disruption of centromeric chromatin organization in centromere protein A (Cenpa) null mice. *Proc. Natl. Acad. Sci. U. S. A.* **97**, 1148–1153 (2000).

123. Carroll, C. W., Milks, K. J. & Straight, A. F. Dual recognition of CENP-A nucleosomes is required for centromere assembly. *J. Cell Biol.* **189**, 1143–1155 (2010).

124. Hori, T. *et al.* CCAN Makes Multiple Contacts with Centromeric DNA to Provide Distinct Pathways to the Outer Kinetochore. *Cell* **135**, 1039–1052 (2008).

125. Cheeseman, I. M., Chappie, J. S., Wilson-Kubalek, E. M. & Desai, A. The conserved KMN network constitutes the core microtubule-binding site of the kinetochore. *Cell* **127**, 983–997 (2006).

126. Wei, R. R., Al-Bassam, J. & Harrison, S. C. The Ndc80/HEC1 complex is a contact point for kinetochore-microtubule attachment. *Nat. Struct. Mol. Biol.* **14**, 54–59 (2007).

127. Putkey, F. R. *et al.* Unstable Kinetochore-Microtubule Capture and Chromosomal Instability Following Deletion of CENP-E. *Dev. Cell* **3**, 351–365 (2002).

128. Kline-Smith, S. L., Khodjakov, A., Hergert, P. & Walczak, C. E. Depletion of Centromeric MCAK Leads to Chromosome Congression and Segregation Defects Due to Improper Kinetochore Attachments. *Mol. Biol. Cell* **15**, 1146–1159 (2004).

129. Lawo, S., Hasegan, M., Gupta, G. D. & Pelletier, L. Subdiffraction imaging of centrosomes reveals higher-order organizational features of pericentriolar material. *Nat. Cell Biol.* **14**, 1148–1158 (2012).

130. Moritz, M., Braunfeld, M. B., Sedat, J. W., Alberts, B. & Agard, D. A. Microtubule nucleation by γ-tubulin-containing rings in the centrosome. *Nature* **378**, 638–640 (1995).

131. Kwok, B. H., Yang, J. G. & Kapoor, T. M. The rate of bipolar spindle assembly depends on the microtubule-gliding velocity of the mitotic kinesin Eg5. *Curr. Biol. CB* **14**, 1783–1788 (2004).

132. Booth, D. G., Hood, F. E., Prior, I. A. & Royle, S. J. A TACC3/ch-TOG/clathrin complex stabilises kinetochore fibres by inter-microtubule bridging. *EMBO J.* **30**, 906–919 (2011).

133. Royle, S. J., Bright, N. A. & Lagnado, L. Clathrin is required for the function of the mitotic spindle. *Nature* **434**, 1152–1157 (2005).

134. Nixon, F. M. *et al.* The mesh is a network of microtubule connectors that stabilizes individual kinetochore fibers of the mitotic spindle. *eLife* **4**,

135. Rieder, C. L. Kinetochore fiber formation in animal somatic cells: dueling mechanisms come to a draw. *Chromosoma* **114**, 310–318 (2005).

136. Khodjakov, A., Copenagle, L., Gordon, M. B., Compton, D. A. & Kapoor, T. M. Minus-end capture of preformed kinetochore fibers contributes to spindle morphogenesis. *J. Cell Biol.* **160**, 671–683 (2003).

137. Maiato, H., Rieder, C. L. & Khodjakov, A. Kinetochore-driven formation of kinetochore fibers contributes to spindle assembly during animal mitosis. *J. Cell Biol.* **167**, 831–840 (2004).

138. Deutsch, J. M. & Lewis, I. P. Motor function in interpolar microtubules during metaphase. *J. Theor. Biol.* **370**, 1–10 (2015).

139. Tao, L. *et al.* A Homotetrameric Kinesin-5, KLP61F, Bundles Microtubules and Antagonizes Ncd in Motility Assays. *Curr. Biol.* **16**, 2293–2302 (2006).

140. Sharp, D. J., Yu, K. R., Sisson, J. C., Sullivan, W. & Scholey, J. M. Antagonistic microtubule-sliding motors position mitotic centrosomes in Drosophila early embryos. *Nat. Cell Biol.* **1**, 51–54 (1999).

141. Tolić, I. M. & Pavin, N. Bridging the gap between sister kinetochores. *Cell Cycle* **15**, 1169–1170 (2016).

142. Kajtez, J. *et al.* Overlap microtubules link sister k-fibres and balance the forces on bi-oriented kinetochores. *Nat. Commun.* **7**, 10298 (2016).

143. Cimini, D. *et al.* Merotelic kinetochore orientation is a major mechanism of aneuploidy in mitotic mammalian tissue cells. *J. Cell Biol.* **153**, 517–527 (2001).

144. Thompson, S. L. & Compton, D. A. Examining the link between chromosomal instability and aneuploidy in human cells. *J. Cell Biol.* **180**, 665–672 (2008).

145. Petrone, A., Adamo, M. E., Cheng, C. & Kettenbach, A. N. Identification of Candidate Cyclin-dependent kinase 1 (Cdk1) Substrates in Mitosis by Quantitative Phosphoproteomics. *Mol. Cell. Proteomics MCP* **15**, 2448–2461 (2016).

146. Tsukahara, T., Tanno, Y. & Watanabe, Y. Phosphorylation of the CPC by Cdk1 promotes chromosome bi-orientation. *Nature* **467**, 719–723 (2010).

147. Kimmins, S. *et al.* Differential functions of the Aurora-B and Aurora-C kinases in mammalian spermatogenesis. *Mol. Endocrinol. Baltim. Md* **21**, 726–739 (2007).

148. Ounis, L. *et al.* Mutations of the aurora kinase C gene causing macrozoospermia are the most frequent genetic cause of male infertility in Algerian men. *Asian J. Androl.* **17**, 68–73 (2015).

149. Cazales, M. *et al.* CDC25B phosphorylation by Aurora-A occurs at the G2/M transition and is inhibited by DNA damage. *Cell Cycle Georget. Tex* **4**, 1233–1238 (2005).

150. Eot-Houllier, G. *et al.* Aurora A-dependent CENP-A phosphorylation at inner centromeres protects bioriented chromosomes against cohesion fatigue. *Nat. Commun.* **9**, 1888 (2018).

151. Courthéoux, T. *et al.* Microtubule nucleation during central spindle assembly requires NEDD1 phosphorylation on serine 405 by Aurora A. *J. Cell Sci.* **132**, (2019).

152. Tanenbaum, M. E. *et al.* A Complex of Kif18b and MCAK Promotes Microtubule Depolymerization and Is Negatively Regulated by Aurora Kinases. *Curr. Biol.* **21**, 1356–1365 (2011).

153. Jang, C.-Y., Coppinger, J. A., Seki, A., Yates, J. R. & Fang, G. Plk1 and Aurora A regulate the depolymerase activity and the cellular localization of Kif2a. *J. Cell Sci.* **122**, 1334–1341 (2009).

154. Jeyaprakash, A. A. *et al.* Structure of a Survivin–Borealin–INCENP Core Complex Reveals How Chromosomal Passengers Travel Together. *Cell* **131**, 271–285 (2007).

155. Vagnarelli, P. & Earnshaw, W. C. Chromosomal passengers: the four-dimensional regulation of mitotic events. *Chromosoma* **113**, 211–222 (2004).

156. Kawashima, S. A., Yamagishi, Y., Honda, T., Ishiguro, K. & Watanabe, Y. Phosphorylation of H2A by Bub1 prevents chromosomal instability through localizing shugoshin. *Science* **327**, 172–177 (2010).

157. Wang, F. *et al.* A Positive Feedback Loop Involving Haspin and Aurora B Promotes CPC Accumulation at Centromeres in Mitosis. *Curr. Biol. CB* **21**, 1061–1069 (2011).

158. Lipp, J. J., Hirota, T., Poser, I. & Peters, J.-M. Aurora B controls the association of condensin I but not condensin II with mitotic chromosomes. *J. Cell Sci.* **120**, 1245–1255 (2007).

159. Hauf, S. *et al.* The small molecule Hesperadin reveals a role for Aurora B in correcting kinetochore–microtubule attachment and in maintaining the spindle assembly checkpoint. *J. Cell Biol.* **161**, 281–294 (2003).

160. Lampson, M. A., Renduchitala, K., Khodjakov, A. & Kapoor, T. M. Correcting improper chromosome-spindle attachments during cell division. *Nat. Cell Biol.* **6**, 232–237 (2004).

161. Cimini, D., Wan, X., Hirel, C. B. & Salmon, E. D. Aurora kinase promotes turnover of kinetochore microtubules to reduce chromosome segregation errors. *Curr. Biol. CB* **16**, 1711–1718 (2006).

162. Andrews, P. D. *et al.* Aurora B Regulates MCAK at the Mitotic Centromere. *Dev. Cell* **6**, 253–268 (2004).

163. Krupina, K. *et al.* Ubiquitin Receptor Protein UBASH3B Drives Aurora B Recruitment to Mitotic Microtubules. *Dev. Cell* **36**, 63–78 (2016).

164. Norden, C. *et al.* The NoCut pathway links completion of cytokinesis to spindle midzone function to prevent chromosome breakage. *Cell* **125**, 85–98 (2006).

165. Lee, K. & Rhee, K. PLK1 phosphorylation of pericentrin initiates centrosome maturation at the onset of mitosis. *J. Cell Biol.* **195**, 1093–1101 (2011).

166. Mardin, B. R., Agircan, F. G., Lange, C. & Schiebel, E. Plk1 Controls the Nek2A-PP1γ Antagonism in Centrosome Disjunction. *Curr. Biol.* **21**, 1145–1151 (2011).

167. Smith, E. *et al.* Differential control of Eg5-dependent centrosome separation by Plk1 and Cdk1. *EMBO J.* **30**, 2233–2245 (2011).

168. Foley, E. A., Maldonado, M. & Kapoor, T. M. Formation of stable attachments between kinetochores and microtubules depends on the B56-PP2A phosphatase. *Nat. Cell Biol.* **13**, 1265–1271 (2011).

169. Elowe, S., Hümmer, S., Uldschmid, A., Li, X. & Nigg, E. A. Tension-sensitive Plk1 phosphorylation on BubR1 regulates the stability of kinetochore microtubule interactions. *Genes Dev.* **21**, 2205–2219 (2007).

170. Beck, J. *et al.* Ubiquitylation-dependent localization of PLK1 in mitosis. *Nat. Cell Biol.* **15**, 430–439 (2013).

171. Bastos, R. N. & Barr, F. A. Plk1 negatively regulates Cep55 recruitment to the midbody to ensure orderly abscission. *J. Cell Biol.* **191**, 751–760 (2010).

172. Aressy, B. *et al.* A screen for deubiquitinating enzymes involved in the G2/M checkpoint identifies USP50 as a regulator of HSP90-dependent Wee1 stability. *Cell Cycle* **9**, 3839–3846 (2010).

173. Giovinazzi, S., Morozov, V. M., Summers, M. K., Reinhold, W. C. & Ishov, A. M. USP7 and Daxx regulate mitosis progression and taxane sensitivity by affecting stability of Aurora-A kinase. *Cell Death Differ.* **20**, 721–731 (2013).

174. Stegmeier, F. *et al.* Anaphase initiation is regulated by antagonistic ubiquitination and deubiquitination activities. *Nature* **446**, 876–881 (2007).

175. Zhuo, X. *et al.* Usp16 regulates kinetochore localization of Plk1 to promote proper chromosome alignment in mitosis. *J. Cell Biol.* **210**, 727–735 (2015).

176. van Leuken, R. J., Luna-Vargas, M. P., Sixma, T. K., Wolthuis, R. M. F. & Medema, R. H. Usp39 is essential for mitotic spindle checkpoint integrity and controls mRNA-levels of aurora B. *Cell Cycle Georget. Tex* **7**, 2710–2719 (2008).

177. Vong, Q. P., Cao, K., Li, H. Y., Iglesias, P. A. & Zheng, Y. Chromosome Alignment and Segregation Regulated by Ubiquitination of Survivin. *Science* **310**, 1499–1504 (2005).

178. Song, E. J. *et al.* The Prp19 complex and the Usp4Sart3 deubiquitinating enzyme control reversible ubiquitination at the spliceosome. *Genes Dev.* **24**, 1434–1447 (2010).

179. Fang, G., Yu, H. & Kirschner, M. W. Direct binding of CDC20 protein family members activates the anaphase-promoting complex in mitosis and G1. *Mol. Cell* **2**, 163–171 (1998).

180. Wickström, S. A., Masoumi, K. C., Khochbin, S., Fässler, R. & Massoumi, R. CYLD negatively regulates cell-cycle progression by inactivating HDAC6 and increasing the levels of acetylated tubulin. *EMBO J.* **29**, 131–144 (2010).

181. Mukai, A. *et al.* Dynamic regulation of ubiquitylation and deubiquitylation at the central spindle during cytokinesis. *J. Cell Sci.* **121**, 1325–1333 (2008).

182. Lindon, C., Grant, R. & Min, M. Ubiquitin-Mediated Degradation of Aurora Kinases. *Front. Oncol.* **5**, (2016).

183. Park, J., Kwon, M.-S., Kim, E. E., Lee, H. & Song, E. J. USP35 regulates mitotic progression by modulating the stability of Aurora B. *Nat. Commun.* **9**, 688 (2018).

184. Winters, L. *et al.* Pivoting of microtubules driven by minus-end-directed motors leads to spindle assembly. *BMC Biol.* **17**, 42 (2019).

185. Itoh, G. *et al.* Lateral attachment of kinetochores to microtubules is enriched in prometaphase rosette and facilitates chromosome alignment and bi-orientation establishment. *Sci. Rep.* **8**, 3888 (2018).

186. Rieder, C. L. & Alexander, S. P. Kinetochores are transported poleward along a single astral microtubule during chromosome attachment to the spindle in newt lung cells. *J. Cell Biol.* **110**, 81–95 (1990).

187. Hays, T. S., Wise, D. & Salmon, E. D. Traction force on a kinetochore at metaphase acts as a linear function of kinetochore fiber length. *J. Cell Biol.* **93**, 374–389 (1982).

188. Hyman, A. A. & Mitchison, T. J. Two different microtubule-based motor activities with opposite polarities in kinetochores. *Nature* **351**, 206–211 (1991).

189. Khodjakov, A. & Rieder, C. L. Kinetochores moving away from their associated pole do not exert a significant pushing force on the chromosome. *J. Cell Biol.* **135**, 315–327 (1996).

190. Mitchison, T. J. Polewards microtubule flux in the mitotic spindle: evidence from photoactivation of fluorescence. *J. Cell Biol.* **109**, 637–652 (1989).

191. Dhonukshe, P., Vischer, N. & Gadella, T. W. J. Contribution of microtubule growth polarity and flux to spindle assembly and functioning in plant cells. *J. Cell Sci.* **119**, 3193–3205 (2006).

192. Maddox, P., Desai, A., Oegema, K., Mitchison, T. J. & Salmon, E. D. Poleward microtubule flux is a major component of spindle dynamics and anaphase a in mitotic Drosophila embryos. *Curr. Biol. CB* **12**, 1670–1674 (2002).

193. Buster, D. W., Zhang, D. & Sharp, D. J. Poleward Tubulin Flux in Spindles: Regulation and Function in Mitotic Cells. *Mol. Biol. Cell* **18**, 3094–3104 (2007).

194. Sudakin, V., Chan, G. K. & Yen, T. J. Checkpoint inhibition of the APC/C in HeLa cells is mediated by a complex of BUBR1, BUB3, CDC20, and MAD2. *J. Cell Biol.* **154**, 925–936 (2001).

195. Ditchfield, C. *et al.* Aurora B couples chromosome alignment with anaphase by targeting BubR1, Mad2, and Cenp-E to kinetochores. *J. Cell Biol.* **161**, 267–280 (2003).

196. Saurin, A. T., van der Waal, M. S., Medema, R. H., Lens, S. M. A. & Kops, G. J. P. L. Aurora B potentiates Mps1 activation to ensure rapid checkpoint establishment at the onset of mitosis. *Nat. Commun.* **2**, 316 (2011).

197. Tsuda, Y. *et al.* Mitotic slippage and the subsequent cell fates after inhibition of Aurora B during tubulin-binding agent–induced mitotic arrest. *Sci. Rep.* **7**, 16762 (2017).

198. Yang, M. *et al.* Insights into mad2 regulation in the spindle checkpoint revealed by the crystal structure of the symmetric mad2 dimer. *PLoS Biol.* **6**, e50 (2008).

199. Howell, B. J. *et al.* Cytoplasmic dynein/dynactin drives kinetochore protein transport to the spindle poles and has a role in mitotic spindle checkpoint inactivation. *J. Cell Biol.* **155**, 1159–1172 (2001).

200. Rosenberg, J. S., Cross, F. R. & Funabiki, H. KNL1/Spc105 recruits PP1 to silence the spindle assembly checkpoint. *Curr. Biol. CB* **21**, 942–947 (2011).

201. Shah, J. V. *et al.* Dynamics of centromere and kinetochore proteins; implications for checkpoint signaling and silencing. *Curr. Biol. CB* **14**, 942–952 (2004).

202. Yang, M. *et al.* p31comet blocks Mad2 activation through structural mimicry. *Cell* **131**, 744–755 (2007).

203. Xia, G. *et al.* Conformation-specific binding of p31(comet) antagonizes the function of Mad2 in the spindle checkpoint. *EMBO J.* **23**, 3133–3143 (2004).

204. Knouse, K. A., Wu, J., Whittaker, C. A. & Amon, A. Single cell sequencing reveals low levels of aneuploidy across mammalian tissues. *Proc. Natl. Acad. Sci. U. S. A.* **111**, 13409–13414 (2014).

205. Santaguida, S. *et al.* Chromosome Mis-segregation Generates Cell-Cycle-Arrested Cells with Complex Karyotypes that Are Eliminated by the Immune System. *Dev. Cell* **41**, 638-651.e5 (2017).

206. Thompson, S. L. & Compton, D. A. Proliferation of aneuploid human cells is limited by a p53-dependent mechanism. *J. Cell Biol.* **188**, 369–381 (2010).

207. Hinchcliffe, E. H. *et al.* Chromosome missegregation during anaphase triggers p53 cell cycle arrest through histone H3.3 Ser31 phosphorylation. *Nat. Cell Biol.* **18**, 668–675 (2016).

208. Stingele, S. *et al.* Global analysis of genome, transcriptome and proteome reveals the response to aneuploidy in human cells. *Mol. Syst. Biol.* **8**, 608 (2012).

209. Potapova, T. A., Zhu, J. & Li, R. Aneuploidy and chromosomal instability: a vicious cycle driving cellular evolution and cancer genome chaos. *Cancer Metastasis Rev.* **32**, 377–389 (2013).

210. Kim, J. Y., Lee, J.-M. & Cho, J.-Y. Ubiquitin C-terminal hydrolase-L3 regulates Smad1 ubiquitination and osteoblast differentiation. *FEBS Lett.* **585**, 1121–1126 (2011).

211. Frickel, E.-M. *et al.* Apicomplexan UCHL3 retains dual specificity for ubiquitin and Nedd8 throughout evolution. *Cell. Microbiol.* **9**, 1601–1610 (2007).

212. Transcript: UCHL3-201 (ENST00000377595.7) - Exons - Homo sapiens - Ensembl genome browser 97. Available at: https://www.ensembl.org/Homo_sapiens/Transcript/Exons?db=core;g=ENSG00000118939;r=13:75549480-75606020;t=ENST00000377595. (Accessed: 22nd July 2019)

213. Pan, M. *et al.* Chemical Protein Synthesis Enabled Mechanistic Studies on the Molecular Recognition of K27-linked Ubiquitin Chains. *Angew. Chem. Int. Ed.* **58**, 2627–2631 (2019).

214. Johnston, S. C., Larsen, C. N., Cook, W. J., Wilkinson, K. D. & Hill, C. P. Crystal structure of a deubiquitinating enzyme (human UCH-L3) at 1.8 A resolution. *EMBO J.* **16**, 3787–3796 (1997).

215. Setsuie, R., Suzuki, M., Tsuchiya, Y. & Wada, K. Skeletal muscles of Uchl3 knockout mice show polyubiquitinated protein accumulation and stress responses. *Neurochem. Int.* **56**, 911–918 (2010).

216. Deshaies, R. J., Emberley, E. D. & Saha, A. Control of cullin-ring ubiquitin ligase activity by nedd8. *Subcell. Biochem.* **54**, 41–56 (2010).

217. Larsen, C. N., Krantz, B. A. & Wilkinson, K. D. Substrate specificity of deubiquitinating enzymes: ubiquitin C-terminal hydrolases. *Biochemistry* **37**, 3358–3368 (1998).

218. Misaghi, S. *et al.* Structure of the ubiquitin hydrolase UCH-L3 complexed with a suicide substrate. *J. Biol. Chem.* **280**, 1512–1520 (2005).

219. Larsen, C. N., Price, J. S. & Wilkinson, K. D. Substrate Binding and Catalysis by Ubiquitin C-Terminal Hydrolases: Identification of Two Active Site Residues. *Biochemistry* **35**, 6735–6744 (1996).

220. Popp, M. W., Artavanis-Tsakonas, K. & Ploegh, H. L. Substrate filtering by the active site crossover loop in UCHL3 revealed by sortagging and gain-of-function mutations. *J. Biol. Chem.* **284**, 3593–3602 (2009).

221. Wilkinson, K. D. *et al.* The binding site for UCH-L3 on ubiquitin: mutagenesis and NMR studies on the complex between ubiquitin and UCH-L3. *J. Mol. Biol.* **291**, 1067–1077 (1999).

222. Semenova, E., Wang, X., Jablonski, M. M., Levorse, J. & Tilghman, S. M. An engineered 800 kilobase deletion of Uchl3 and Lmo7 on mouse chromosome 14 causes defects in viability, postnatal growth and degeneration of muscle and retina. *Hum. Mol. Genet.* **12**, 1301–1312 (2003).

223. Wood, M. A., Kaplan, M. P., Brensinger, C. M., Guo, W. & Abel, T. Ubiquitin C-terminal hydrolase L3 (Uchl3) is involved in working memory. *Hippocampus* **15**, 610–621 (2005).

224. Suzuki, M., Setsuie, R. & Wada, K. Ubiquitin carboxyl-terminal hydrolase l3 promotes insulin signaling and adipogenesis. *Endocrinology* **150**, 5230–5239 (2009).

225. Setsuie, R. *et al.* Ubiquitin C-terminal hydrolase-L3-knockout mice are resistant to diet-induced obesity and show increased activation of AMP-activated protein kinase in skeletal muscle. *FASEB J. Off. Publ. Fed. Am. Soc. Exp. Biol.* **23**, 4148–4157 (2009).

226. Nishi, R. *et al.* The deubiquitylating enzyme UCHL3 regulates Ku80 retention at sites of DNA damage. *Sci. Rep.* **8**, 17891 (2018).

227. Miyoshi, Y. *et al.* High expression of ubiquitin carboxy-terminal hydrolase-L1 and -L3 mRNA predicts early recurrence in patients with invasive breast cancer. *Cancer Sci.* **97**, 523–529 (2006).

228. Rolén, U. *et al.* Activity profiling of deubiquitinating enzymes in cervical carcinoma biopsies and cell lines. *Mol. Carcinog.* **45**, 260–269 (2006).

229. Song, H. M., Lee, J. E. & Kim, J. H. Ubiquitin C-terminal hydrolase-L3 regulates EMT process and cancer metastasis in prostate cell lines. *Biochem. Biophys. Res. Commun.* **452**, 722–727 (2014).

230. Butterworth, M. B. *et al.* The deubiquitinating enzyme UCH-L3 regulates the apical membrane recycling of the epithelial sodium channel. *J. Biol. Chem.* **282**, 37885–37893 (2007).

231. Mtango, N. R., Sutovsky, M., Vandevoort, C. A., Latham, K. E. & Sutovsky, P. Essential role of ubiquitin C-terminal hydrolases UCHL1 and UCHL3 in mammalian oocyte maturation. *J. Cell. Physiol.* **227**, 2022–2029 (2012).

232. Earnshaw, W. C. Discovering centromere proteins: from cold white hands to the A, B, C of CENPs. *Nat. Rev. Mol. Cell Biol.* **16**, 443–449 (2015).

233. Dickins, R. A. *et al.* Probing tumor phenotypes using stable and regulated synthetic microRNA precursors. *Nat. Genet.* **37**, 1289–1295 (2005).

234. Measurement — CellProfiler 3.0.0 documentation. Available at: http://cellprofiler-manual.s3.amazonaws.com/CellProfiler-3.0.0/modules/measurement.html. (Accessed: 11th June 2019)

235. Orr, B. & Maiato, H. No chromosome left behind: The importance of metaphase alignment for mitotic fidelity. *J. Cell Biol.* **218**, 1086–1088 (2019).

236. Fonseca, C. L. *et al. Mitotic chromosome alignment is required for proper nuclear envelope reassembly*. (Cell Biology, 2018). doi:10.1101/343475

237. Chung, H. J., Park, J. E., Lee, N. S., Kim, H. & Jang, C.-Y. Phosphorylation of Astrin Regulates Its Kinetochore Function. *J. Biol. Chem.* **291**, 17579–17592 (2016).

238. Holland, A. J. & Cleveland, D. W. The deubiquitinase USP44 is a tumor suppressor that protects against chromosome missegregation. *J. Clin. Invest.* **122**, 4325–4328 (2012).

239. Bhattacharya, S., Chakraborty, D., Basu, M. & Ghosh, M. K. Emerging insights into HAUSP (USP7) in physiology, cancer and other diseases. *Signal Transduct. Target. Ther.* **3**, (2018).

240. Palazzo, L., Della Monica, R., Visconti, R., Costanzo, V. & Grieco, D. ATM controls proper mitotic spindle structure. *Cell Cycle Georget. Tex* **13**, 1091–1100 (2014).

241. Deng, C. X. Tumorigenesis as a consequence of genetic instability in Brca1 mutant mice. *Mutat. Res.* **477**, 183–189 (2001).

242. Jullien, D., Vagnarelli, P., Earnshaw, W. C. & Adachi, Y. Kinetochore localisation of the DNA damage response component 53BP1 during mitosis. *J. Cell Sci.* **115**, 71–79 (2002).

243. Wang, H. *et al.* Aurora kinase B dependent phosphorylation of 53BP1 is required for resolving merotelic kinetochore-microtubule attachment errors during mitosis. *Oncotarget* **8**, 48671–48687 (2017).

244. GDS5408 / 204616_at. Available at: https://www.ncbi.nlm.nih.gov/geo/tools/profileGraph.cgi?ID=GDS5408:204616_at. (Accessed: 16th July 2019)

245. Kurihara, L. J., Semenova, E., Levorse, J. M. & Tilghman, S. M. Expression and Functional Analysis of Uch-L3 during Mouse Development. *Mol. Cell. Biol.* **20**, 2498–2504 (2000).

246. Kapoor, T. M. *et al.* Chromosomes Can Congress to the Metaphase Plate Before Biorientation. *Science* **311**, 388–391 (2006).

247. Barisic, M., Aguiar, P., Geley, S. & Maiato, H. Kinetochore motors drive congression of peripheral polar chromosomes by overcoming random arm-ejection forces. *Nat. Cell Biol.* **16**, 1249–1256 (2014).

248. Gudimchuk, N. *et al.* Kinetochore kinesin CENP-E is a processive bi-directional tracker of dynamic microtubule tips. *Nat. Cell Biol.* **15**, 1079–1088 (2013).

249. Yucel, J. K. *et al.* CENP-meta, an Essential Kinetochore Kinesin Required for the Maintenance of Metaphase Chromosome Alignment in Drosophila. *J. Cell Biol.* **150**, 1–12 (2000).

250. Johnson, V. L., Scott, M. I. F., Holt, S. V., Hussein, D. & Taylor, S. S. Bub1 is required for kinetochore localization of BubR1, Cenp-E, Cenp-F and Mad2, and chromosome congression. *J. Cell Sci.* **117**, 1577–1589 (2004).

251. Yao, X., Abrieu, A., Zheng, Y., Sullivan, K. F. & Cleveland, D. W. CENP-E forms a link between attachment of spindle microtubules to kinetochores and the mitotic checkpoint. *Nat. Cell Biol.* **2**, 484 (2000).

252. Gruber, J., Harborth, J., Schnabel, J., Weber, K. & Hatzfeld, M. The mitotic-spindle-associated protein astrin is essential for progression through mitosis. *J. Cell Sci.* **115**, 4053–4059 (2002).

253. Kern, D. M., Monda, J. K., Su, K.-C., Wilson-Kubalek, E. M. & Cheeseman, I. M. Astrin-SKAP complex reconstitution reveals its kinetochore interaction with microtubule-bound Ndc80. *eLife* **6**, (2017).

254. Schmidt, J. C. *et al.* Aurora B kinase controls the targeting of the Astrin–SKAP complex to bioriented kinetochores. *J. Cell Biol.* **191**, 269–280 (2010).

255. Dunsch, A. K., Linnane, E., Barr, F. A. & Gruneberg, U. The astrin–kinastrin/SKAP complex localizes to microtubule plus ends and facilitates chromosome alignment. *J. Cell Biol.* **192**, 959–968 (2011).

256. Polak, B., Risteski, P., Lesjak, S. & Tolić, I. M. PRC1-labeled microtubule bundles and kinetochore pairs show one-to-one association in metaphase. *EMBO Rep.* **18**, 217–230 (2017).

257. Chen, J. & Liu, J. Spindle Size Scaling Contributes to Robust Silencing of Mitotic Spindle Assembly Checkpoint. *Biophys. J.* **111**, 1064–1077 (2016).

258. Nunes Bastos, R. *et al.* Aurora B suppresses microtubule dynamics and limits central spindle size by locally activating KIF4A. *J. Cell Biol.* **202**, 605–621 (2013).

259. Bird, A. W. & Hyman, A. A. Building a spindle of the correct length in human cells requires the interaction between TPX2 and Aurora A. *J. Cell Biol.* **182**, 289–300 (2008).

260. Young, S., Besson, S. & Welburn, J. P. I. Length-dependent anisotropic scaling of spindle shape. *Biol. Open* **3**, 1217–1223 (2014).

261. Shrestha, R. L. & Draviam, V. M. Lateral to end-on conversion of chromosome-microtubule attachment requires kinesins CENP-E and MCAK. *Curr. Biol. CB* **23**, 1514–1526 (2013).

262. Shrestha, R. L. *et al.* Aurora-B kinase pathway controls the lateral to end-on conversion of kinetochore-microtubule attachments in human cells. *Nat. Commun.* **8**, (2017).

263. Cimini, D., Cameron, L. A. & Salmon, E. D. Anaphase spindle mechanics prevent mis-segregation of merotelically oriented chromosomes. *Curr. Biol. CB* **14**, 2149–2155 (2004).

264. Cimini, D., Fioravanti, D., Salmon, E. D. & Degrassi, F. Merotelic kinetochore orientation versus chromosome mono-orientation in the origin of lagging chromosomes in human primary cells. *J. Cell Sci.* **115**, 507–515 (2002).

265. Ma, H. T., Chan, Y. Y., Chen, X., On, K. F. & Poon, R. Y. C. Depletion of p31comet protein promotes sensitivity to antimitotic drugs. *J. Biol. Chem.* **287**, 21561–21569 (2012).

266. Wang, K. *et al.* Thyroid hormone receptor interacting protein 13 (TRIP13) AAA-ATPase is a novel mitotic checkpoint-silencing protein. *J. Biol. Chem.* **289**, 23928–23937 (2014).

267. Sear, R. P. & Howard, M. Modeling dual pathways for the metazoan spindle assembly checkpoint. *Proc. Natl. Acad. Sci. U. S. A.* **103**, 16758–16763 (2006).

268. Luo, X. & Yu, H. Protein Metamorphosis: The Two-State Behavior of Mad2. *Struct. Lond. Engl. 1993* **16**, 1616 (2008).

269. Lohel, M., Ibrahim, B., Diekmann, S. & Dittrich, P. The role of localization in the operation of the mitotic spindle assembly checkpoint. *Cell Cycle* **8**, 2650–2660 (2009).

270. Rieder, C. L., Schultz, A., Cole, R. & Sluder, G. Anaphase onset in vertebrate somatic cells is controlled by a checkpoint that monitors sister kinetochore attachment to the spindle. *J. Cell Biol.* **127**, 1301–1310 (1994).

271. Rieder, C. L., Cole, R. W., Khodjakov, A. & Sluder, G. The checkpoint delaying anaphase in response to chromosome monoorientation is mediated by an inhibitory signal produced by unattached kinetochores. *J. Cell Biol.* **130**, 941–948 (1995).

272. Rieder, C. L. *et al.* Mitosis in vertebrate somatic cells with two spindles: implications for the metaphase/anaphase transition checkpoint and cleavage. *Proc. Natl. Acad. Sci. U. S. A.* **94**, 5107–5112 (1997).

273. Griffis, E. R., Stuurman, N. & Vale, R. D. Spindly, a novel protein essential for silencing the spindle assembly checkpoint, recruits dynein to the kinetochore. *J. Cell Biol.* **177**, 1005–1015 (2007).

274. Westhorpe, F. G., Tighe, A., Lara-Gonzalez, P. & Taylor, S. S. p31comet-mediated extraction of Mad2 from the MCC promotes efficient mitotic exit. *J. Cell Sci.* **124**, 3905–3916 (2011).

275. Habu, T. & Matsumoto, T. p31(comet) inactivates the chemically induced Mad2-dependent spindle assembly checkpoint and leads to resistance to anti-mitotic drugs. *SpringerPlus* **2**, 562 (2013).

276. Knowlton, A. L., Lan, W. & Stukenberg, P. T. Aurora B is enriched at merotelic attachment sites, where it regulates MCAK. *Curr. Biol. CB* **16**, 1705–1710 (2006).

277. Santaguida, S., Tighe, A., D'Alise, A. M., Taylor, S. S. & Musacchio, A. Dissecting the role of MPS1 in chromosome biorientation and the spindle checkpoint through the small molecule inhibitor reversine. *J. Cell Biol.* **190**, 73–87 (2010).

278. Weaver, B. A. A. & Cleveland, D. W. Does aneuploidy cause cancer? *Curr. Opin. Cell Biol.* **18**, 658–667 (2006).

279. Fang, Y. & Shen, X. Ubiquitin carboxyl-terminal hydrolases: involvement in cancer progression and clinical implications. *Cancer Metastasis Rev.* **36**, 669–682 (2017).

280. Expression of UCHL3 in cancer - Summary - The Human Protein Atlas. Available at: https://www.proteinatlas.org/ENSG00000118939-UCHL3/pathology. (Accessed: 17th July 2019)

281. Song, Z. *et al.* A novel UCHL3 inhibitor, perifosine, enhances PARP inhibitor cytotoxicity through inhibition of homologous recombination-mediated DNA double strand break repair. *Cell Death Dis.* **10**, (2019).

282. Meroni, G. & Diez-Roux, G. TRIM/RBCC, a novel class of 'single protein RING finger' E3 ubiquitin ligases. *BioEssays* **27**, 1147–1157 (2005).

283. Koliopoulos, M. G., Esposito, D., Christodoulou, E., Taylor, I. A. & Rittinger, K. Functional role of TRIM E3 ligase oligomerization and regulation of catalytic activity. *EMBO J.* **35**, 1204–1218 (2016).

284. Borden, K. L. *et al.* In vivo and in vitro characterization of the B1 and B2 zinc-binding domains from the acute promyelocytic leukemia protooncoprotein PML. *Proc. Natl. Acad. Sci.* **93**, 1601–1606 (1996).

285. Versteeg, G. A. *et al.* The E3-Ligase TRIM Family of Proteins Regulates Signaling Pathways Triggered by Innate Immune Pattern-Recognition Receptors. *Immunity* **38**, 384–398 (2013).

286. Kano, S., Miyajima, N., Fukuda, S. & Hatakeyama, S. Tripartite Motif Protein 32 Facilitates Cell Growth and Migration via Degradation of Abl-Interactor 2. *Cancer Res.* **68**, 5572–5580 (2008).

287. Watanabe, M., Tsukiyama, T. & Hatakeyama, S. TRIM31 interacts with p52Shc and inhibits Src-induced anchorage-independent growth. *Biochem. Biophys. Res. Commun.* **388**, 422–427 (2009).

288. Masuda, Y. *et al.* TRIM29 regulates the assembly of DNA repair proteins into damaged chromatin. *Nat. Commun.* **6**, 7299 (2015).

289. Sato, T., Okumura, F., Ariga, T. & Hatakeyama, S. TRIM6 interacts with Myc and maintains the pluripotency of mouse embryonic stem cells. *J. Cell Sci.* **125**, 1544–1555 (2012).

290. Jensen, K., Shiels, C. & Freemont, P. S. PML protein isoforms and the RBCC/TRIM motif. *Oncogene* **20**, 7223–7233 (2001).

291. Uchil, P. D., Quinlan, B. D., Chan, W.-T., Luna, J. M. & Mothes, W. TRIM E3 Ligases Interfere with Early and Late Stages of the Retroviral Life Cycle. *PLoS Pathog.* **4**, e16 (2008).

292. Stremlau, M. *et al.* The cytoplasmic body component TRIM5α restricts HIV-1 infection in Old World monkeys. *Nature* **427**, 848–853 (2004).

293. Chen, S. N. *et al.* Human Molecular Genetic and Functional Studies Identify *TRIM63* , Encoding Muscle RING Finger Protein 1, as a Novel Gene for Human Hypertrophic Cardiomyopathy. *Circ. Res.* **111**, 907–919 (2012).

294. Arra, M. *et al.* The M694V Variant of the Familial Mediterranean Fever Gene Is Associated with Sporadic Early-Onset Alzheimer's Disease in an Italian Population Sample. *Dement. Geriatr. Cogn. Disord.* **23**, 55–59 (2007).

295. Trockenbacher, A. *et al.* MID1, mutated in Opitz syndrome, encodes an ubiquitin ligase that targets phosphatase 2A for degradation. *Nat. Genet.* **29**, 287–294 (2001).

296. Tsai, W.-W. *et al.* TRIM24 links a non-canonical histone signature to breast cancer. *Nature* **468**, 927–932 (2010).

297. Herquel, B. *et al.* Transcription cofactors TRIM24, TRIM28, and TRIM33 associate to form regulatory complexes that suppress murine hepatocellular carcinoma. *Proc. Natl. Acad. Sci.* **108**, 8212–8217 (2011).

298. Sardiello, M., Cairo, S., Fontanella, B., Ballabio, A. & Meroni, G. Genomic analysis of the TRIM family reveals two groups of genes with distinct evolutionary properties. *BMC Evol. Biol.* **8**, 225 (2008).

299. Meroni, G. Genomics and Evolution of the TRIM Gene Family. in *TRIM/RBCC Proteins* (ed. Meroni, G.) **770**, 1–9 (Springer New York, 2012).

300. Short, K. M. & Cox, T. C. Subclassification of the RBCC/TRIM Superfamily Reveals a Novel Motif Necessary for Microtubule Binding. *J. Biol. Chem.* **281**, 8970–8980 (2006).

301. Massiah, M. A., Simmons, B. N., Short, K. M. & Cox, T. C. Solution Structure of the RBCC/TRIM B-box1 Domain of Human MID1: B-box with a RING. *J. Mol. Biol.* **358**, 532–545 (2006).

302. Napolitano, L. M. & Meroni, G. TRIM family: Pleiotropy and diversification through homomultimer and heteromultimer formation. *IUBMB Life* **64**, 64–71 (2012).

303. Ozato, K., Shin, D.-M., Chang, T.-H. & Morse, H. C. TRIM family proteins and their emerging roles in innate immunity. *Nat. Rev. Immunol.* **8**, 849–860 (2008).

304. Woo, J.-S. *et al.* Structural and functional insights into the B30.2/SPRY domain. *EMBO J.* **25**, 1353–1363 (2006).

305. Li, X., Yeung, D. F., Fiegen, A. M. & Sodroski, J. Determinants of the Higher Order Association of the Restriction Factor TRIM5α and Other Tripartite Motif (TRIM) Proteins. *J. Biol. Chem.* **286**, 27959–27970 (2011).

306. Reymond, A. The tripartite motif family identifies cell compartments. *EMBO J.* **20**, 2140–2151 (2001).

307. Napolitano, L. M., Jaffray, E. G., Hay, R. T. & Meroni, G. Functional interactions between ubiquitin E2 enzymes and TRIM proteins. *Biochem. J.* **434**, 309–319 (2011).

308. McEwan, W. A. *et al.* Intracellular antibody-bound pathogens stimulate immune signaling via the Fc receptor TRIM21. *Nat. Immunol.* **14**, 327–336 (2013).

309. Lee, H.-J. The Role of Tripartite Motif Family Proteins in TGF-β Signaling Pathway and Cancer. *J. Cancer Prev.* **23**, 162–169 (2018).

310. Wilkinson, K. A. & Henley, J. M. Mechanisms, regulation and consequences of protein SUMOylation. *Biochem. J.* **428**, 133–145 (2010).

311. Yuan, Z. *et al.* The ATDC (TRIM29) Protein Binds p53 and Antagonizes p53-Mediated Functions. *Mol. Cell. Biol.* **30**, 3004–3015 (2010).

312. Venuto & Merla. E3 Ubiquitin Ligase TRIM Proteins, Cell Cycle and Mitosis. *Cells* **8**, 510 (2019).

313. Recio, C. *et al.* Signal transducer and activator of transcription (STAT)-5: an opportunity for drug development in oncohematology. *Oncogene* (2019). doi:10.1038/s41388-019-0752-3

314. Caratozzolo, M. F. *et al.* TRIM8 modulates p53 activity to dictate cell cycle arrest. *Cell Cycle* **11**, 511–523 (2012).

315. Xu, G. *et al.* TRIM14 regulates cell proliferation and invasion in osteosarcoma via promotion of the AKT signaling pathway. *Sci. Rep.* **7**, 42411 (2017).

316. Mu, X., Li, H., Zhou, L. & Xu, W. TRIM52 regulates the proliferation and invasiveness of lung cancer cells via the Wnt/β-catenin pathway. *Oncol. Rep.* (2019). doi:10.3892/or.2019.7110

317. Gack, M. U. *et al.* TRIM25 RING-finger E3 ubiquitin ligase is essential for RIG-I-mediated antiviral activity. *Nature* **446**, 916–920 (2007).

318. Gack, M. U. *et al.* Influenza A Virus NS1 Targets the Ubiquitin Ligase TRIM25 to Evade Recognition by the Host Viral RNA Sensor RIG-I. *Cell Host Microbe* **5**, 439–449 (2009).

319. Grütter, M. G. & Luban, J. TRIM5 structure, HIV-1 capsid recognition, and innate immune signaling. *Curr. Opin. Virol.* **2**, 142–150 (2012).

320. Tissot, C. & Mechti, N. Molecular Cloning of a New Interferon-induced Factor That Represses Human Immunodeficiency Virus Type 1 Long Terminal Repeat Expression. *J. Biol. Chem.* **270**, 14891–14898 (1995).

321. Allouch, A. *et al.* The TRIM Family Protein KAP1 Inhibits HIV-1 Integration. *Cell Host Microbe* **9**, 484–495 (2011).

322. Watanabe, M. & Hatakeyama, S. TRIM proteins and diseases. *J. Biochem. (Tokyo)* mvw087 (2017). doi:10.1093/jb/mvw087

323. Shieh, P. B., Kudryashova, E. & Spencer, M. J. Limb-girdle muscular dystrophy 2H and the role of TRIM32. in *Handbook of Clinical Neurology* **101**, 125–133 (Elsevier, 2011).

324. Zhang, Z. *et al.* TRIM11 Upregulation Contributes to Proliferation, Invasion, and EMT of Hepatocellular Carcinoma Cells. *Oncol. Res. Featur. Preclin. Clin. Cancer Ther.* **25**, 691–699 (2017).

325. Czerwińska, P., Mazurek, S. & Wiznerowicz, M. The complexity of TRIM28 contribution to cancer. *J. Biomed. Sci.* **24**, 63 (2017).

326. Caratozzolo, M. F. *et al.* TRIM8 anti-proliferative action against chemo-resistant renal cell carcinoma. *Oncotarget* **5**, (2014).

327. Roche, J. The Epithelial-to-Mesenchymal Transition in Cancer. *Cancers* **10**, 52 (2018).

328. Feng, S. *et al.* Tripartite motif-containing 14 (TRIM14) promotes epithelial-mesenchymal transition via ZEB2 in glioblastoma cells. *J. Exp. Clin. Cancer Res.* **38**, 57 (2019).

329. Moh, M. C. & Shen, S. The roles of cell adhesion molecules in tumor suppression and cell migration: a new paradox. *Cell Adhes. Migr.* **3**, 334–336 (2009).

330. Zhu, Z. *et al.* TRIM25 blockade by RNA interference inhibited migration and invasion of gastric cancer cells through TGF-β signaling. *Sci. Rep.* **6**, 19070 (2016).

331. Jin, Z. *et al.* TRIM14 promotes colorectal cancer cell migration and invasion through the SPHK1/STAT3 pathway. *Cancer Cell Int.* **18**, 202 (2018).

332. Wang, S. *et al.* The ubiquitin ligase TRIM25 targets ERG for degradation in prostate cancer. *Oncotarget* **7**, (2016).

333. Guo, P. *et al.* TRIM31 is upregulated in hepatocellular carcinoma and promotes disease progression by inducing ubiquitination of TSC1–TSC2 complex. *Oncogene* **37**, 478–488 (2018).

334. Zhang, J. *et al.* TRIM45 functions as a tumor suppressor in the brain via its E3 ligase activity by stabilizing p53 through K63-linked ubiquitination. *Cell Death Dis.* **8**, e2831–e2831 (2017).

335. Shi, H. *et al.* Analysis of Genome-Wide Association Study (GWAS) data looking for replicating signals in Alzheimer's disease (AD). *Int. J. Mol. Epidemiol. Genet.* **1**, 53–66 (2010).

336. Uchil, P. D. *et al.* TRIM protein-mediated regulation of inflammatory and innate immune signaling and its association with antiretroviral activity. *J. Virol.* **87**, 257–272 (2013).

337. Uchil, P. D. *et al.* TRIM15 is a focal adhesion protein that regulates focal adhesion disassembly. *J. Cell Sci.* **127**, 3928–3942 (2014).

338. Chen, W., Lu, C. & Hong, J. TRIM15 Exerts Anti-Tumor Effects Through Suppressing Cancer Cell Invasion in Gastric Adenocarcinoma. *Med. Sci. Monit.* **24**, 8033–8041 (2018).

339. Lee, O.-H. *et al.* Role of the focal adhesion protein TRIM15 in colon cancer development. *Biochim. Biophys. Acta BBA - Mol. Cell Res.* **1853**, 409–421 (2015).

340. Doyle, E. L. *et al.* TAL Effector-Nucleotide Targeter (TALE-NT) 2.0: tools for TAL effector design and target prediction. *Nucleic Acids Res.* **40**, W117–W122 (2012).

341. ATCC Cell Lines. Available at: http://www.lgcstandards-atcc.org/Products/Cells_and_Microorganisms/Cell_Lines.aspx?geo_country=fr. (Accessed: 16th July 2019)

342. Shibata, H. *et al.* Rapid colorectal adenoma formation initiated by conditional targeting of the Apc gene. *Science* **278**, 120–123 (1997).

343. De Robertis, M. *et al.* The AOM/DSS murine model for the study of colon carcinogenesis: From pathways to diagnosis and therapy studies. *J. Carcinog.* **10**, 9 (2011).

344. Uchil, P. D. *et al.* TRIM15 is a focal adhesion protein that regulates focal adhesion disassembly. *J. Cell Sci.* **127**, 3928–3942 (2014).

345. Uchil, P. D. *et al.* TRIM15 is a focal adhesion protein that regulates focal adhesion disassembly. *J. Cell Sci.* **127**, 3928–3942 (2014).

346. Lee, O.-H. *et al.* Role of the focal adhesion protein TRIM15 in colon cancer development. *Biochim. Biophys. Acta BBA - Mol. Cell Res.* **1853**, 409–421 (2015).

347. Svingen, T., Letting, H., Hadrup, N., Hass, U. & Vinggaard, A. M. Selection of reference genes for quantitative RT-PCR (RT-qPCR) analysis of rat tissues under physiological and toxicological conditions. *PeerJ* **3**, e855 (2015).

348. Horazna, M. *et al.* Msx1 loss suppresses formation of the ectopic crypts developed in the Apc-deficient small intestinal epithelium. *Sci. Rep.* **9**, 1629 (2019).

349. Chen, W., Lu, C. & Hong, J. TRIM15 Exerts Anti-Tumor Effects Through Suppressing Cancer Cell Invasion in Gastric Adenocarcinoma. *Med. Sci. Monit.* **24**, 8033–8041 (2018).

350. Cavallaro, U. & Christofori, G. Cell adhesion in tumor invasion and metastasis: loss of the glue is not enough. *Biochim. Biophys. Acta* **1552**, 39–45 (2001).

351. Moh, M. C. & Shen, S. The roles of cell adhesion molecules in tumor suppression and cell migration: a new paradox. *Cell Adhes. Migr.* **3**, 334–336 (2009).

352. Seki, N. *et al.* in a Mouse Mammary Epithelial Cell Line NMuMG by Using cDNA Microarray DEK and Proto-oncogene Cyclin B 1-regulated Genes that Include ING 1 Identification of the p 33 Updated. in (2002).

353. U-2 OS ATCC ® HTB-96™ Homo sapiens bone osteosarcoma. Available at: http://www.lgcstandards-atcc.org/Products/All/HTB-96.aspx?geo_country=fr#characteristics. (Accessed: 23rd July 2019)

# NOTES

# NOTES

# NOTES

# NOTES

# NOTES

# NOTES

# NOTES

# NOTES

# NOTES

# NOTES